Absorption of CO₂ from the air using polyamines: experiments, modelling and design

Nuria Serrano Barthe









Absorption of CO₂ from the air using polyamines: experiments, modelling and design

By

Nuria Serrano Barthe

in partial fulfilment of the requirements for the degree of

Master of Science in Mechanical Engineering

at the Delft University of Technology, to be defended publicly on Friday, June 28, 2019, at 13:30 PM.

Daily supervisor: Ir. Jan van Kranendonk ZEF

Thesis committee: Prof. dr. Ir. Earl Goetheer TU Delft (Chair)

Prof. dr. Carlos Infante Ferreira

TU Delft

Prof. dr. Rene Delfos

TU Delft

This thesis is confidential and cannot be made public until December 31, 2021.

An electronic version of this thesis is available at http://repository.tudelft.nl/.



Abstract

CO₂ concentration in the atmosphere is increasing leading to global warming and thus, climate change. Moreover, current renewable technologies such as wind or solar energy only cover the electricity market. A big part of the global energy market is still based on fossil fuels and difficult to electrify. Hence, there is an urgent need to produce renewable liquid hydrocarbons to replace fossil fuels. Zero Emission Fuels (ZEF) is a start-up that aims to develop a small-scale chemical plant to convert carbon dioxide (CO₂) and water (H₂O) from the air into methanol (MeOH) using photovoltaic energy. In this work, the absorption of CO₂ using bulk polyamines was characterized experimentally, as well as through numerical modelling. In addition to this, guidelines for the design of the absorber, part of the Direct Air Capture (DAC) unit of ZEF's microplant, are given. The focus of the study is placed on the kinetics and loading of CO₂.

To be able to model the absorption process an experimental approach has been developed regarding the uptake of CO_2 and H_2O . Firstly, pure H_2O absorption experiments were performed in a climate chamber in order to obtain the H_2O loadings using polyamines for different H_2O content in the air. Secondly, air capture experiments were performed at lab conditions in order to obtain both H_2O and CO_2 loadings for different process conditions. Thirdly, constants relevant for the modelling part (reaction rate constant and Henry constant) were obtained experimentally. An absorption model, developed in MATLAB, was used to estimate the diffusion coefficient of both H_2O and CO_2 using the experimental H_2O and CO_2 loadings.

Two main conclusions are obtained from the absorption model of CO_2 : the absorption of CO_2 on polyamines is diffusion-limited and the diffusion coefficient of CO_2 is two orders of magnitude lower than the diffusion coefficient of H_2O . Based on the fact that the CO_2 absorption process is diffusion-limited the mixing patterns should be introduced in the design of the continuous absorber. However, due to the fact that viscosity could influence the flowing behaviour of polyamines, more research is needed.

Acknowledgments

I would like to thank Jonah, Tom and Kristin for teaching me the meaning of true friendship. I would like to give special thanks to Jonah for giving feedback of the report.

I would like to thank Arjen for all the time he spent helping me while I was doing the experiments at TNO and also for always being there in case I had a problem.

I would like to thank Jan for helping me during the whole thesis. Without you this work would not even be half of what it is.

I would like to thank Earl for his guidance during the thesis. Thank you for sharing your knowledge.

I would like to thank Ulrich for giving me his hand when I needed it the most. You are a true inspiration to me.

I would like to thank Hessel for encouraging me to fight till the end.

I would like to thank every single student who has been part of ZEF. Knowing that you would be around gave me energy.

I would like to thank my dad and my mom. I love you more than anything in the world. I am so lucky and proud to have you as my parents.

Me gustaría dar las gracias a mi padre y a mi madre. Os quiero más que a nada en este mundo. Tengo muchísima suerte y estoy tremendamente orgullosa de que seáis mis padres.

Contents

	t	
Ackno	vledgmentsv	⁄ii
	claturex	
Symbo	lsx	ίij
Abbre	iationsx	ίi
List of	ables x	V
List of	iguresxv	iii
1 Intro	ductionduction	
1.1.	Climate change	
1.1.	. Increase of CO ₂ concentration in the atmosphere	2
1.1.		
1.2.	CO ₂ capture technologies from the air	4
1.3.	Carbon management	7
1.4.	Zero Emission Fuels	
1.4.	. Starting calculations	9
1.5.	TNO	
1.6.	Aim of this thesis	9
2 Ove	view of Direct Air Capture (DAC)1	
2.1.	Introduction1	
2.1.	 	
2.2.	Sorbent1	
2.2.	·	5
2.2.	·	
2.3.	Previous work at ZEF in the DAC unit2	0
2.4.	Selection2	
3 Mate	rials and methods2	
3.1.	Achieving a homogeneous layer thickness2	
3.2.	Experimental plan2	
3.2.	- I	
3.2.		
3.3.	Properties measurement3	
3.3.		
3.3.	•	
3.3.	·	
3.3.		
3.3.		
•	rimental results and discussion3	
4.1.	Plate experiments3	
4.1.	- · ·	
4.1.		
	Constants needed for modelling5	
4.2.		
4.2.	,	
4.2.	——————————————————————————————————————	
4.2.		
4.3.	Reaction mechanism5	
	egies for modelling6	
	Theory of the model6	
5.1.	. Conditions 6	5
5.2.	H₂O absorption model6	7

5.3. CO ₂ absorption model	72
5.3.1. Equilibrium CO ₂ loading of the polyamine	73
5.3.2. Diffusion coefficient of CO ₂ assuming kinematic diameter relation	73
5.3.3. Theoretical approach and discussion related to the Hatta number	74
5.3.4. Hildebrand solubility parameter	
6 Strategies for designing	
6.1. Effect of preloading H2O in polyamines in stagnant and flowing layers of	
polyamine	
6.2. Design of the absorber	
6.2.1. Design of stagnant layer system	
6.2.2. Velocity calculation	
6.2.3. Design of flowing layer system	87
6.3. Optimization	
6.4. Cost of the sorbent	
6.5. Final design	
7 Conclusions and recommendations	
7.1. Conclusions	
7.2. Recommendations	
7.2.1. Experiments	
7.2.2. Modelling	
7.2.3. Design	
Appendices	
A. Calculations of the stream volumes	
B. Calculation to obtain the layer thickness equation	
C. Arduino codes and wiring	
Measurement of relative humidity and temperature	
Measurement of relative humidity, temperature and CO ₂ concentration	
D. H ₂ O duplos E. 756 coulometric FK titrator measurement error	
F. PEI is a Newtonian fluid	
G. CO ₂ duplos	
·	
H. Film theory	
Finding steady state of CO ₂ and H ₂ O absorption	
Changing the air velocity	
TEPA in contact with air containing different concentrations of CO ₂	
TEPA premixed with H ₂ O in contact with air containing different concentration	
CO ₂	
J. Subtraction of the H ₂ O content in MeOH	
K. Calibration of CO ₂ ppm	
L. Spectrometers	
PEI	
TEPA	
M. MATLAB codes	
H ₂ O model	
CO ₂ model assuming a high Hatta number	
Bibliography	125

Nomenclature

Symbols

Area Α Capacity α

β C Angle of inclination

Cost

D Diffusion coefficient

DR Dilution rate Gibbs free energy ΔG Ε Enhancement factor Second law efficiency η g Acceleration of gravity

Layer thickness h Henry constant Н На Hatta number k Reaction constant

L Length M Mass Mol n Ν Number μ Ρ Viscosity Price Density ρ

RT Residence time

Spacing s Т Temperature th **Thickness**

Diffusion time constant τ

Velocity u ٧ Volume Width W W Work

Abbreviations

Ar

ATR Attenuated Total Reflectance

CAPEX Capital Expenditure Calcium carbonate CaCO₃ CaO Calcium oxide Ca(OH)₂ Calcium hydroxide

Carbon Capture and Reuse CCR Carbon Capture and Storage CCS Carbon Capture and Utilization CCU

CF Concentration Factor

CH₄ Methane

 CO_2 Carbon dioxide

CTA **Covalently Tethered Amine** DAC Direct Air Capture

Fe₂O₃ Iron oxide

GHG Greenhouse gases

HAS Hyperbranched aminosilica

HCO₋₃ Bicarbonate anion

He Helium

HMW High molecular weight

H₂ Hydrogen Carbonic acid

H₂O Water

H₂S Hydrogen sulfide H₃PO₄ Phosphoric acid H⁺ Hydrogen anion

KIT-6 Korea Institute of Science and Technology No. 6

KOH Potassium hydroxide LMW Low molecular weight

MCM-41 Mobil Composition of Matter No. 41

MeOH Methanol

MFC Mass flow controller MgO Magnesium oxide MW Molecular weight NaOH Sodium hydroxide Na₂CO₃ Sodium carbonate

Ne Neon

NO_x Nitrogen oxides

N₂ Nitrogen N₂O Nitrous oxide

OPEX Operating Expenses

O₂ Oxygen

PEI Polyethylenimine
PLA Polylactide
ppm Parts per million

PMMA Poly(methyl methacrylate)
ppmv Parts per million volume

PS Polystyrene RH Relative humidity

SAS Supported amine sorbents

SBA-15 Santa Barbara Amorphous No. 15

SO_x Sulphur oxides

TEPA Tetraethylenepentamine

TNO Nederlandse Organisatie voor Toegepast

Natuurwetenschappelijk Onderzoek

wt% Weight percentage ZEF Zero Emission Fuels

List of tables

Table 1: Composition of flue gas vs dry air	12
Table 2: Input to calculate the free energy of sorption	13
Table 3: Amine types	17
Table 4: Chemical structure of the sorbents studied	
Table 5: Aminosilane types	
Table 6: Input to calculate average layer thickness	
Table 7: Experimental plan followed during the thesis	
Table 8: H ₂ O content in PEI, TEPA and MeOH	31
Table 9: Input to calculate the solubility constant of N ₂ O	34
Table 10: Lab conditions and CO ₂ and H ₂ O loadings of layer thickness experiments	
Table 11: Lab conditions and CO ₂ and H2O loading of blend experiments	
Table 12: Lab conditions and CO ₂ and H ₂ O loadings of solution experiments	
Table 13: Comparison pure polyamine vs polyamine preloaded with H ₂ O	
Table 14: Lab conditions and ${ m CO_2}$ and ${ m H_2O}$ loadings of PEI in contact with higher ${ m CO_2}$	
concentrations	49
Table 15: Lab conditions and CO ₂ and H ₂ O loadings of PEI premixed with H ₂ O in	
contact with higher CO ₂ concentrations	
Table 16: CO ₂ loading in premixed PEI with H ₂ O and pure PEI	
Table 17: Viscosity measurements	
Table 18: Input for the van't Hoff equation	
Table 19: Solubility constant of CO ₂ at 20 °C	57
Table 20: Reaction rate constants for a solution of 30 and 70 wt% TEPA and H2O a	
20 °C	
Table 21: Input for a rough estimation of the diffusion coefficient	
Table 22: Diffusion coefficients of CO ₂ in amine impregnated SBA-15 (64)	
Table 23: Relevant peaks for amine compounds	
Table 24: Relevant peaks for carbamate and bicarbonate	
Table 25: Input for the equations used in the model	
Table 26: Input for left boundary condition	
Table 27: Input for right boundary condition	
Table 28: Input for the initial condition	
Table 29: Input for Einstein-Stokes equation to calculate the diffusion coefficient of in PEI	
Table 30: Calculated diffusivity coefficients of H ₂ O in PEI	
Table 31. Calculated diffusion coefficients of H ₂ O in TEPA Table 32: Loadings of CO ₂ in TEPA impregnated silica and polymeric support (73)	
Table 33: Loadings of CO ₂ in PEI impregnated silica and polymeric support (73) Table 34: Input to calculate the diffusion coefficient of CO ₂ considering only the	/ 3
kinematic diameter influence	71
Table 35: Diffusivity coefficients of CO ₂ in TEPA and PEI considering only the kinen	/ 4 natic
diameter influence	
Table 36: Input for dimensionless numbers	
Table 30: Input for difficulties frumbers	
Table 37. Values of Flatta Humber and emilancement factor for an infinitely fast reac	
Table 38: Comparison of diffusion coefficients of CO ₂	
Table 38: Comparison of diffusion coefficients of CO ₂	
Table 39. Input to calculate the Hildebrand solubility parameter	
Table 40. Findebrand parameter for 1120 and 1EFA	
Table 41: Sorberts used in the absorber design	
Table 42: Area needed per sorbent to absorb the CO ₂ target yield	
Table 43: Input to calculate the velocity distribution	
Table 45: Dimensions of the vertical absorber	

Table 46: Dimensions of the inclined absorber	90
Table 47: Price of PEI and TEPA	91
Table 48: Sorbents mass and cost	91
Table 49: Dimensions of the inclined absorber	91
Table 50: Dimensions of the inclined absorber (proposed design)	94
Table 51: Input to calculate CO ₂ density	100
Table 52: Input to calculate CO ₂ concentration in flue gas and air streams	100
Table 53: Input to calculate the volume of flue gas and air streams needed	l to capture
CO_2	
Table 54: Input to calculate average layer thickness	101
Table 55: Duplos of the H₂O measurements	104
Table 56: H ₂ O contents of the same sample	105
Table 57: H ₂ O content of a sample, knowing its H ₂ O content, using the 756	6 coulometric
KF titrator	105
Table 58: Rotational speed vs. PEI viscosity	
Table 59: Error of CO ₂ measurement (1st batch, PEI)	106
Table 60: Error of CO ₂ measurement (1st batch, TEPA)	106
Table 61: Error of CO ₂ measurement (2 nd batch)	106
Table 62: Error of CO ₂ measurement (3 rd batch, PEI)	
Table 63: Error of CO ₂ measurement (3 rd batch, TEPA)	107
Table 64: Error of CO ₂ measurement (4 th batch)	
Table 65: Parameters of the steady mass transfer equation without chemic	
Table 66: Parameters of the boundary conditions	
Table 67: Parameters of CO ₂ flux equation and Henry's law	108
Table 68: Parameters of simplified CO ₂ flux in film theory	
Table 69: Lab conditions and CO ₂ and H ₂ O loadings of finding steady-state	е
experiments	111
Table 70: Lab conditions and CO₂ and H₂O loading for different air velocity	experiments
	113
Table 71: Lab conditions and CO_2 and H_2O loading of TEPA in contact with	
concentrations	
Table 72: CO ₂ loading and ratio of TEPA mixed with water in contact with	-
concentrations	
Table 73: CO ₂ ppm distribution for 800 ppm	
Table 74: CO ₂ ppm distribution for 1200 ppm	116

List of figures

Figure 1: Separating human and natural influences on climate change (1)	1
Figure 2: Global greenhouse gas emissions per type of gas and source (4)	2
Figure 3: Atmospheric CO ₂ levels in three different scenarios (1)	3
Figure 4: Correlation between CO ₂ concentration and temperature increase. Adapted	
from (1)	
Figure 5: Global CO ₂ emissions by sector (6)	
Figure 6: CO ₂ capture technologies (7)	
Figure 7: ZEF process	
Figure 8: ZEF micro-plant concept (29)	
Figure 9: Procedure followed to answer the research questions	
Figure 10: Minimum work required for CO ₂ capture vs. CO ₂ concentration	
Figure 11: CF vs. η of industrial separation processes (34)	
Figure 12: Process of CO ₂ capture from the air using the Na/ Ca cycle (16)	
Figure 13: Reaction of silane with silica (38)	
Figure 14: DAC prototype done by ZEF Team 1 (46)	
Figure 15: DAC prototype done by ZEF Team 2 (48)	
Figure 16: Side view of the DAC prototype done by ZEF Team 3	
Figure 17: Front view of the DAC prototype done by ZEF Team 3	22
Figure 18: Plate with the paper, top tank and COM attached	
Figure 19: Homogeneous layer thickness of polyamine	
Figure 20: Plate, paper and polyamine thicknesses	
Figure 21: Working principle of the climate chamber (50)	
Figure 22: Sample inside the climate chamber	
Figure 23: Setup used to measure the CO ₂ and H ₂ O absorption from the air	
Figure 24: Schematic diagram of the setup used to measure the CO ₂ and H ₂ O	. 23
absorption from the air	. 29
Figure 25: Setup used to measure the CO ₂ and H ₂ O absorption from the air when	. 23
varying the CO ₂ ppm	. 30
Figure 26: Schematic diagram of the setup used to measure the CO ₂ and H ₂ O	.00
absorption from the air when varying the CO ₂ ppm	30
Figure 27: Phosphoric acid titration setup in TNO	
Figure 28: Diagram of the phosphoric acid titration setup	
Figure 29: Physisorption and kinetics setup in TNO	
Figure 30: Diagram of the physisorption and kinetics setup	
Figure 31: Nicolet 6700 spectrometer	.36
Figure 32: H₂O loading in PEI at 40 °C (varying relative humidity) in the climate	. 50
chamber	30
Figure 33: H₂O loading in PEI at 30 °C (varying relative humidity) in the climate	. 00
chamber	30
Figure 34: H₂O loading in PEI at 20 °C (varying relative humidity) in the climate	. 33
chamber	30
Figure 35: H₂O loading in PEI at 10 °C (varying relative humidity) in the climate	. 55
chamber	30
Figure 36: H ₂ O loading in PEI vs. H ₂ O in the air (climate chamber experiments)	
Figure 37: H ₂ O loading in FEI vs. H ₂ O in the all (climate chamber experiments)	. 40
chamber	∕ 1∩
Figure 38: Layer of TEPA displaced by the fan	
Figure 39: Loading of H ₂ O and CO ₂ in TEPA (layer thickness of 0.25 mm) in contact	
with air	
Figure 40: Loading of H ₂ O and CO ₂ in PEI (layer thickness of 0.25 mm) in contact w	
air	
uii	. TL

Figure 41: Loading of H ₂ O and CO ₂ in TEPA (layer thickness of 0.50 mm) in contact with air	:t 42
Figure 42: Loading of H ₂ O and CO ₂ in PEI (layer thickness of 0.50 mm) in contact vair	
Figure 43: Loading of H ₂ O and CO ₂ in TEPA (layer thickness of 0.75 mm) in contact with air	t
Figure 44: Loading of H ₂ O and CO ₂ in PEI (layer thickness of 0.75 mm) in contact vair	vith
Figure 45: CO ₂ mass absorbed in three different layer thicknesses of PEI	
Figure 46: CO ₂ mass absorbed in three different layer thicknesses of TEPA	43
Figure 47: CO ₂ mass absorbed in three different layer thickness if the Hatta numbe high	r is
Figure 48: Loading of H₂O and CO₂ in 25/75 wt% PEI/TEPA in contact with air	43 15
Figure 49: Loading of H ₂ O and CO ₂ in 50/50 wt% PEI/TEPA in contact with air	
Figure 50: Loading of H ₂ O and CO ₂ in 75/25 wt% PEI/TEPA in contact with air	
Figure 51: Loading of H ₂ O and CO ₂ in 10/ 90 wt% H ₂ O/ TEPA in contact with air	
Figure 52: Loading of H ₂ O and CO ₂ in 10/ 90 wt% H ₂ O/ PEI in contact with air	
Figure 53: Loading of H ₂ O and CO ₂ in 20/ 80 wt% H ₂ O/ TEPA in contact with air	
Figure 54: Loading of H ₂ O and CO ₂ in 20/80 wt% H ₂ O/PEI in contact with air	
Figure 55: Loading of H ₂ O and CO ₂ in 30/70 wt% H ₂ O/TEPA in contact with air	
Figure 56: Loading of H ₂ O and CO ₂ in 30/70 wt% H ₂ O/PEI in contact with air	
Figure 57: Loading of H ₂ O and CO ₂ in PEI in contact with air (800 ppm of CO ₂)	
Figure 58: Loading of H ₂ O and CO ₂ in PEI in contact with air (1200 ppm of CO ₂)	49
Figure 59: H ₂ O and CO2 loading in PEI compared to CO ₂ concentration in the air	50
Figure 60: TEPA solution dried on the plate	
Figure 61: Loading of H ₂ O and CO ₂ in 40/60 wt% H ₂ O/PEI in contact with air (800 p	
	51
Figure 62: Loading of H_2O and CO_2 in 40/60 wt% H_2O/PEI in contact with air (1200	
ppm)	
Figure 63: Comparison of CO ₂ loading in pure PEI and PEI preloaded with H ₂ O	
Figure 64: PEI viscosity vs. H ₂ O content	
Figure 65: TEPA viscosity vs. H ₂ O content	
Figure 66: Water saturation pressure vs. temperature	
Figure 68: Solubility constant of PEI at 20 °C	
Figure 69: Solubility constant of PEI at 30 °C	
Figure 70: Solubility constant of PEI at 40 °C	
Figure 71: Solubility constant of TEPA at 20 °C	
Figure 72: Henry constant vs. temperature (experimental data compared to van't H	off
equation)	
Figure 73: Solubility constant of N ₂ O at 20°C (30 wt% TEPA, 70 wt% H2O)	57
Figure 74: Observed reaction rate at 20 °C (30 wt% TEPA, 70 wt% H ₂ O)	
Figure 75: Spectrometer of pure PEI	
Figure 76: Spectrometer of pure TEPA	
Figure 77: Subtracted absorbance spectrometer between PEI loaded with CO2 and	
pure PEI	
Figure 78: Subtracted absorbance spectrometer between TEPA loaded with CO2 a	nd
pure TEPA	62
Figure 79: CO ₂ absorption by a polyamine (70)	
Figure 80: Simplified CO ₂ model	
Figure 81: Experimental vs. calculated H2O loading using diffusion coefficient obtain	
from Einstein-Stokes equation	69
Figure 82: Comparison between the calculated and experimental (70% relative	
humidity and 20 °C) H2O loading in PEI	
Figure 83: H2O diffusion through the layer of PEI	69

Figure 84: Diffusion coefficient of H ₂ O in PEI vs. H ₂ O content in the air	70
Figure 85: Diffusion coefficient of H ₂ O vs. temperature	
Figure 86: Diffusion coefficient of H ₂ O in PEI vs. viscosity of PEI	
Figure 87: Comparison between the calculated and experimental H ₂ O loading in TE	
Tigaro or . Companion bottoon the dalediated and experimental rigo leading in TE	
Figure 88: H ₂ O diffusion through the layer of TEPA	
Figure 89: Correlation between experimental (TEPA 0.5 mm) and calculated CO ₂	1 2
	77
loadings using the diffusion coefficient of CO ₂ from the kinematic relation	/ /
Figure 90: Correlation between experimental (PEI 0.5 mm) and calculated CO ₂	
loadings using the diffusion coefficient of CO ₂ from the kinematic relation	
Figure 91: Comparison between the calculated and experimental ${\rm CO_2}$ loading in TE	
Figure 92: CO ₂ loading in TEPA after 9 hours	
Figure 93: CO ₂ diffusion through the layer of TEPA	
Figure 94: CO ₂ diffusion through the layer of TEPA after 9 hours	
Figure 95: Comparison between the calculated and experimental CO ₂ loading in PE	
Figure 96: Calculated CO ₂ loading in PEI achieving equilibrium after 5 hours	79
Figure 97: CO ₂ diffusion through the layer of PEI	
Figure 98: CO ₂ diffusion through the layer of PEI after 5 hours	79
Figure 99: CO2 and H ₂ O diffusing into pure polyamine	80
Figure 100: CO2 and H2O loadings of pure PEI and preloaded with H2O	83
Figure 101: CO2 and H2O loadings of pure TEPA and preloaded with H2O	
Figure 102: Flowing layer of polyamine at t=t ₀	
Figure 103: Flowing layer of polyamine at t=t ₁	
Figure 104: Laminar flow of a fluid layer falling down an inclined plate (81)	
Figure 105: Possible designs of the absorber	
Figure 106: Width and height of absorber and fan	
Figure 107: Plate height and spacing	
Figure 108: Vertical design	
Figure 109: Inclined design	
Figure 110: Inclined absorber design	
Figure 111: Wiring between RH & T sensor and Arduino	
Figure 112: Wiring between RH & T sensor, CO ₂ sensor and Arduino	
Figure 113: Comparison of water content in samples taken at 70% RH and 20 °C us	
Hydranal AG in both titrators	
Figure 114: Comparison of water content in samples taken at 70% RH and 20 °C us	
Hydranal AF in both titrators	105
Figure 115: Loading of H ₂ O and CO ₂ in PEI in contact with air for 60 min	
Figure 116: Loading of H ₂ O and CO ₂ in TEPA in contact with air for 60 min	
Figure 117: Loading of H ₂ O and CO ₂ in PEI in contact with air for 120 min	
Figure 118: Loading of H ₂ O and CO ₂ in TEPA in contact with air for 120 min	
Figure 119: Loading of H ₂ O and CO ₂ in PEI in contact with a uniform flow of air	111
Figure 120: Loading of H ₂ O and CO ₂ in TEPA in contact with a uniform flow of air	111
Figure 121: H ₂ O loading in PEI depending on the type of air flow	112
Figure 122: H ₂ O loading in TEPA depending on the type of air flow	112
Figure 123: CO ₂ loading in PEI depending on the type of air flow	112
Figure 124: CO ₂ loading in TEPA depending on the type of air flow	
Figure 125: Loading of H ₂ O and CO ₂ in TEPA in contact with air (800 ppm)	
Figure 126: Loading of H ₂ O and CO ₂ in TEPA in contact with air (1200 ppm)	
Figure 127: Loading of H_2O and CO_2 in 30/70 wt% H_2O /TEPA in contact with air (80	
ppm)	
Figure 128: Loading of H ₂ O and CO ₂ in 30/70 wt% H ₂ O/TEPA in contact with air (12	
ppm)	
Figure 129: Comparison of water content in a sample considering the H ₂ O content of	 ∖f
methanol (grey) and not considering it (blue)	
THOUSENING THE VITAL HOLD CONTROL OF THE LANGE OF THE LAN	110

Figure 131: Spectrometer of PEI mixed with H ₂ O	Figure 130: CO ₂ ppm distribution	.116
Figure 133: Spectrometer of PEI mixed with H ₂ O blown by air with different CO ₂ concentrations		
concentrations	Figure 132: Spectrometer of PEI blown by air with different CO ₂ concentrations	118
Figure 134: Spectrometer of TEPA mixed with H ₂ O	Figure 133: Spectrometer of PEI mixed with H ₂ O blown by air with different CO ₂	
Figure 137: Spectrometer of TEPA blown by air with different CO ₂ concentrations 120 Figure 138: Spectrometer of TEPA mixed with H ₂ O blown by air with different CO ₂	concentrations	118
Figure 138: Spectrometer of TEPA mixed with H ₂ O blown by air with different CO ₂	Figure 134: Spectrometer of TEPA mixed with H ₂ O	119
	Figure 137: Spectrometer of TEPA blown by air with different CO ₂ concentrations	120
concentrations120	Figure 138: Spectrometer of TEPA mixed with H ₂ O blown by air with different CO ₂	
	concentrations	120

1 Introduction

In this Chapter the environmental consequences resulting from climate change are introduced. CO_2 emissions are one of the main drivers of global warming and, in consequence, climate change. Therefore, CO_2 concentration in the atmosphere, as well as its sources are introduced. Then, different technologies that can capture CO_2 from the air are compared. Finally, the research questions that motivated this thesis are presented.

1.1. Climate change

Natural processes such as changes in solar energy, displacements of ocean currents and volcanic eruptions can influence the climate. However, they cannot explain the most recently observed global warming: since the start of the era of industrialization human activities have contributed substantially to climate change by adding greenhouse gases (GHG) to the atmosphere. These gases come from a wide array of human activities such as fossil fuel burning to generate heat and energy, fertilization of crops, storage of residues in dumping sites, the cattle industry and industrial manufacturing.

Figure 1 shows that simulation models that account only for the effects of natural processes cannot explain the most recent warming, as opposed to the ones that also consider the GHG emitted by human activities.

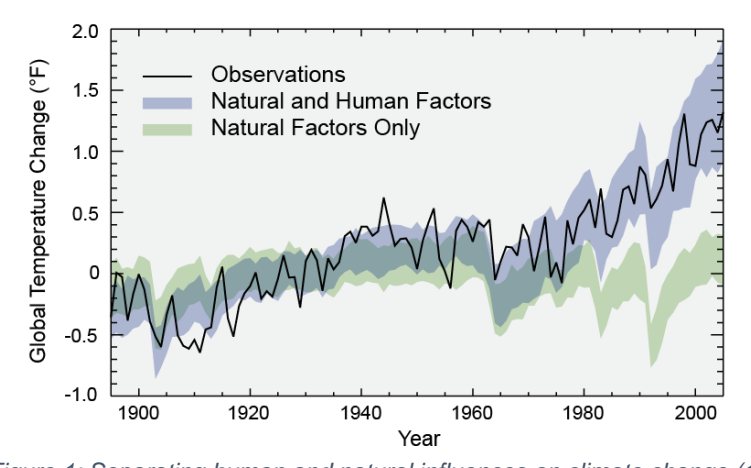


Figure 1: Separating human and natural influences on climate change (1)

The most impactful GHG directly emitted by human activity are carbon dioxide (CO_2), methane (CH_4), nitrous oxide (N_2O) and fluorinated gases (2).

Figure 2 shows that about half of cumulative anthropogenic CO₂ emissions between 1750 and 2010 have occurred in the last 40 years: human activities currently release over 30 billion tons of CO₂ into the atmosphere per year (3).

1

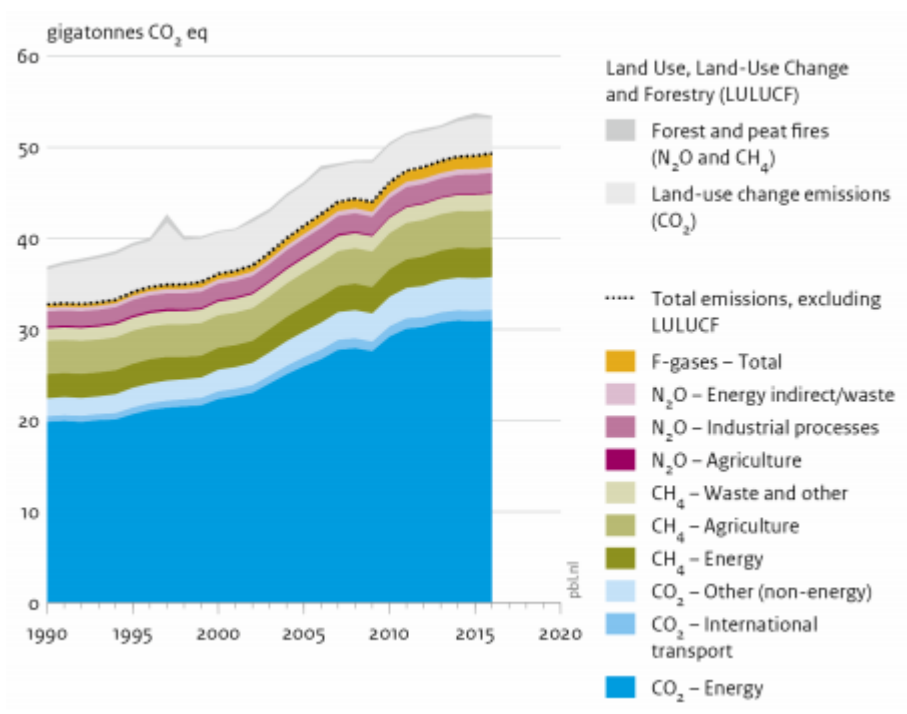


Figure 2: Global greenhouse gas emissions per type of gas and source (4)

A more detailed description of the increase of CO₂ concentration in the atmosphere, as well as the sources causing it, is given in the next two subsections since a way to mitigate its emissions is the main driver of this thesis.

1.1.1. Increase of CO₂ concentration in the atmosphere

CO₂ is the main GHG that contributes to recent climate change. Although it is absorbed and emitted naturally as a part of the carbon cycle, human activities (especially burning fossil fuels for energy generation and transportation) release huge amounts considerably increasing its concentration in the atmosphere.

Natural processes have varied atmospheric CO_2 concentrations from 170 to 300 ppmv. As a result of industrialization CO_2 levels have increased to 400 ppmv, higher than in any period in the last one million years (3). Figure 3 shows that, under a very low emissions scenario, emissions from human activities are projected to increase CO_2 concentration up to 420 ppmv in 2100 whereas for a higher emissions scenario they will reach 935 ppmv. The very low scenario would require immediate and sharp emissions reductions whereas the higher scenario assumes a continued increase in emissions.

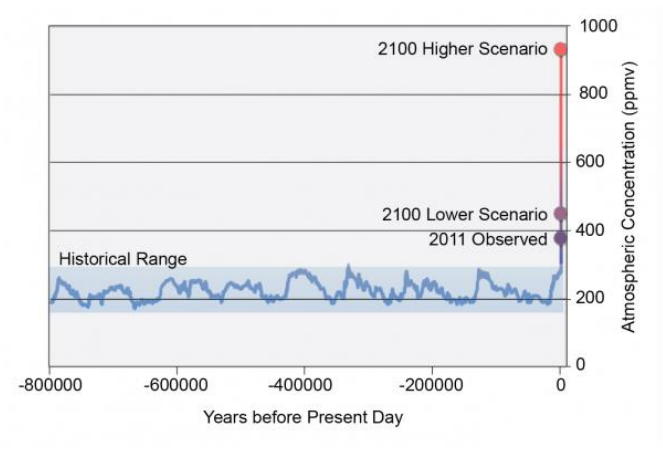


Figure 3: Atmospheric CO₂ levels in three different scenarios (1)

The average global temperature at the surface of the Earth has increased by about 0.8 °C since 1880. Two- thirds of this growth have taken place since 1975. Depending on the future emissions of CO₂ and the climate response to them, it is expected that the average temperature will increase globally from 1.43 °C to 4.57 °C (1).

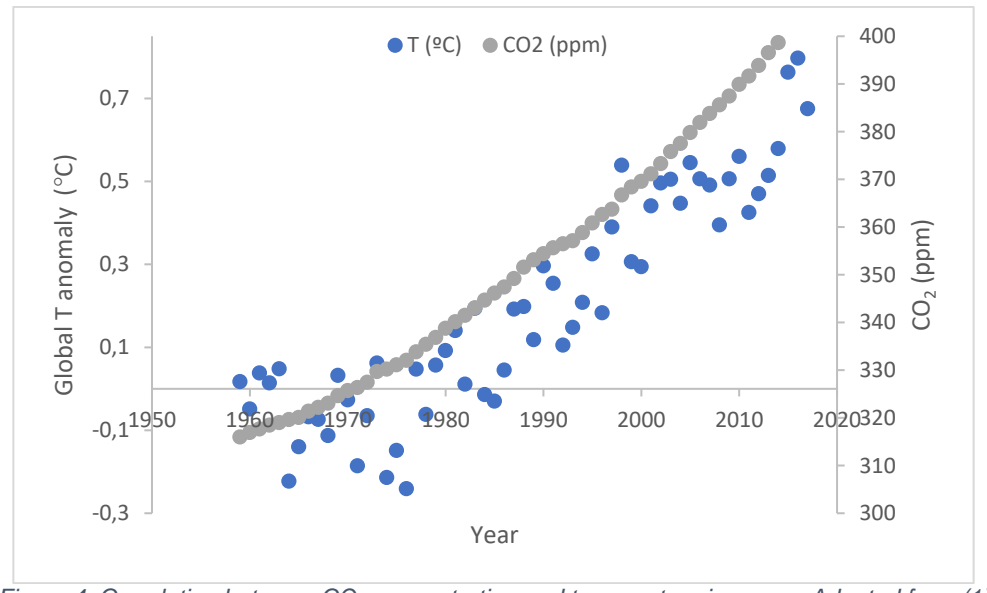


Figure 4: Correlation between CO₂ concentration and temperature increase. Adapted from (1)

In order to limit climate change, emissions of CO₂ must be substantially reduced. In order to do so, it is necessary to analyze the different sources of CO₂ emission.

1.1.2. Sources of CO₂

The main human activity that emits CO_2 is the combustion of fossil fuels (coal, natural gas and oil) for energy and transportation. In addition, certain industrial processes and land-use changes also emit CO_2 (5).

CO₂ sources can be classified as centralized or non-centralized. The first group includes energy generation and industry whereas the second group includes transportation, agriculture and residential areas. 66% of the total CO₂ emissions come from centralized point sources, where emissions are released to the atmosphere

through large flue gas stacks. Each individual non- centralized point sources emits a very small amount of CO₂. However, when added up they represent 34% of the global CO₂ emissions (6).

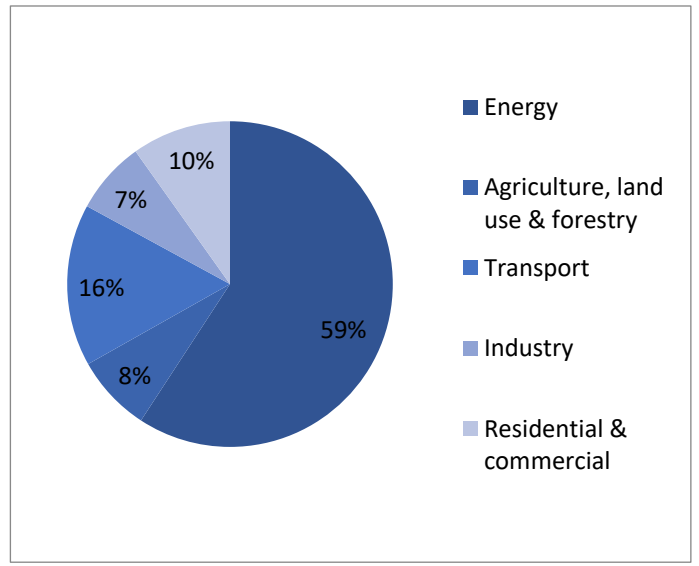


Figure 5: Global CO₂ emissions by sector (6)

1.2. CO₂ capture technologies from the air

In this subsection, each different carbon capture method is introduced and briefly explained. Then, the constraints that make Direct Air Capture (DAC) difficult will determine the viability of them.

Figure 6 summarizes all the CO₂ capture technologies:

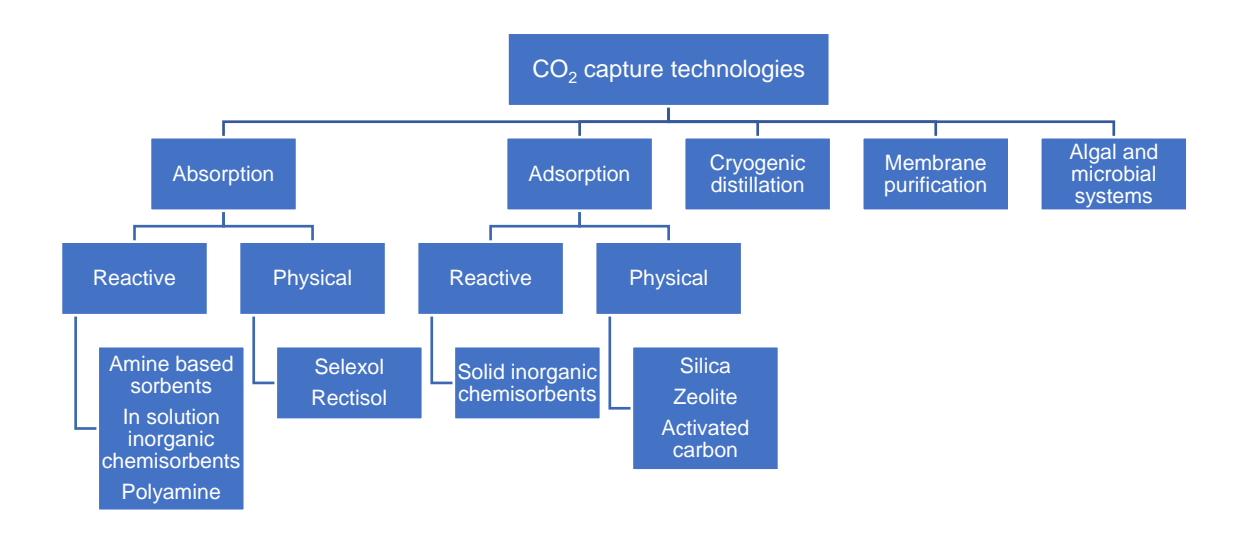


Figure 6: CO₂ capture technologies (7)

- Absorption is a phenomenon in which atoms, molecules or ions enter a bulk phase, liquid or solid. Molecules undergoing absorption are taken up by the volume (8). Absorption can be classified as physisorption or chemisorption.
 - Amine-based sorbents are the most used for CO₂ capture at low partial pressures in post-combustion processes (9). The CO₂ rich gas stream is passed through the aqueous amine solution where the CO₂ reacts, remaining in the solution, whereas the other components stay in the gas phase. Then, the CO₂ is desorbed from the solution via the addition of heat and/ or reduction in pressure such that a near pure CO₂ stream is produced (10).
 - Physical absorption can be performed, for example, by **Selexol** and **Rectisol**. They are solvents that can separate acid gases, such as hydrogen sulfide (H₂S) and CO₂ at high partial pressures, from feed gas streams (for example, synthesis gas) which makes the feed gas more suitable for combustion and/ or further processing (11). Selexol is made up of dimethyl ethers of polyethylene glycol whereas Rectisol consists of methanol (12).
- **Adsorption** is the adhesion of atoms, ions or molecules from a gas, liquid or dissolved solid (adsorbate) to a surface (adsorbent). This process creates a film of the adsorbate on the surface of the adsorbent. It is a surface phenomenon (13). Adsorption can be classified as physisorption or chemisorption.

The most relevant sorbents capable of capturing CO₂ that have been reported in literature are silica, zeolites and activated carbon. All of them are physisorbents. The forces that play a role in physical adsorption are van der Waals and electrostatic interactions. The van der Waals interaction is always present whereas the electrostatic forces are only taken into account if the sorbent has an ionic structure, like zeolites (13).

- Cryogenic distillation is a low-temperature process which operates at different boiling points of the feed components. The feed is cooled, thus condensing its impurities. The refrigeration makes the process energy and capital expensive (14).
- **Membrane purification**. The membrane performs as a filter allowing certain molecules to pass through, while blocking other specific molecules (15).
- **Algal and microbial systems**: photosynthesis captures CO₂ from the atmosphere and produces biomass using H₂O as the H₂ source, solar energy and chlorophyll as the catalyst. This biomass can be used either as a feedstock, burned to produce heat or electricity or transformed into liquid fuels such as ethanol, methanol or biodiesel.

Capturing CO₂ from the air is challenging because of its very low concentration, the presence of moisture and the requirement to operate close to ambient temperature and pressure. These three conditions exclude:

- Absorption:

• Amine-based sorbents can suffer from stability problems when they come into contact with air as well as evaporation issues due to the large volume of gas to be handled. Typically, amine sorbents, such as MEA, are used as aqueous solutions which might increase the cost of the desorption process if all the H₂O needs to be evaporated (16).

 Selexol and Rectisol, as was explained before, are only relevant for high CO₂ partial pressure streams.

- Adsorption:

- Physisorbents have low selectivity for CO₂ in the presence of other gases and very low heat of adsorption (the physical interaction will often be too weak to overcome the minimum change in free energy of adsorption), which result in low adsorption capacities (17).
- Cryogenic distillation is excluded because both the OPEX and CAPEX will increase sharply due to the fact that a huge amount of air would need to be cooled down (16).
- Membrane purification is more suited for relatively high concentrations of CO₂, such as H₂/ CO₂ separation for pre-combustion and CO₂/ N₂ separation for post-combustion (15).
- The photosynthesis performed by **algal and microbial systems** is inefficient at converting the sun's energy into chemical energy in the form of biomass. Specifically, most crop's photosynthetic efficiency is limited to 0.5- 2% which is significantly lower to the conversion of solar energy to electricity using solar cells (about 10- 20%) (16).

There are several companies involved in developing DAC units. Each of their approaches is different, but they are all based on a process in which the air contacts a sorbent/ contactor, removes the CO₂ from the sorbent/ contactor, and then regenerates the sorbent/ contactor for it to be used to collect/ capture CO₂ again. In the next paragraphs each approach is briefly described (18):

- Carbon Engineering: Air is pulled through a sodium hydroxide (NaOH) liquid solution which absorbs CO₂. The CO₂ is driven off by heating up with natural gas.
- **Climeworks**: Air is pulled through a filter material that saturates with CO₂ and then releases it through the application of low-grade heat.
- Global Thermostat: An amine-based chemical sorbent bonded to honeycomb ceramic monoliths adsorbs the CO₂. Waste heat and a steam solution are used to release the CO₂.
- Skytree: Amine functionalized polymer beats capture CO₂. They are regenerated by low- grade heat.
- **Infinitree** and **CNCE**: Moisture swing technology is used to rotate contactors through dry and wet environments to deliver CO₂ directly.

It is important to mention that Oxy Low Carbon Ventures, LLC (OLCV) and Carbon Engineering have recently announced that they are jointly proceeding with the engineering and design of the world's largest DAC unit. The facility would be able to capture 500 kilotonnes of CO₂ per year, which would be used in enhanced oil recovery (EOR) operations and subsequently stored underground permanently (19).

In addition to this, Climeworks has launched a demonstration plant as part of the Horizon 2020 research project STORE&GO (20) whereas Infinitree (21), CNCE (22)

and Skytree (23) are currently in the prototype stage and Global Thermostat has an operating demonstration plant (24).

1.3. Carbon management

Mitigation technologies must be developed and enforced to reduce the previously mentioned CO₂ emissions, since they cannot simply be banned because current transportation, energy production and many industrial processes are (and in the near future be) heavily dependent on fossil fuels (16). There are three main approaches:

- **Emitting less CO₂**: this option requires more energy-efficient technologies but will not be enough to stop the increase of atmospheric CO₂ concentration.
- Carbon capture and storage (CCS): this process consists of capturing and storing CO₂ from centralized point sources in a geological site for a long-term period of time (25).
- Carbon capture and utilization (CCU): instead of storing CO₂, it can be utilized as a resource instead. For example, it can be used for biofuel production, in greenhouses, fuel synthesis and water treatment (25).

Conventional CO₂ capture technology faces two important limitations (16):

- It is only applied at the **centralized CO₂ sources**. Hence 34% of the global CO₂ emissions from the dispersed type are missed.
- Processes that use CO₂ as a feedstock (CCU) should be **close to the large point sources**. Otherwise, additional transport costs will show up.

Direct air capture (DAC), this is, extraction of CO₂ directly from the air, gives a solution to these two challenges. Moreover, it has several advantages (16):

- It can serve as a **carbon source** of the future, replacing finite fossil fuels, when coupled with recycling to products.
- CO₂ is captured directly from the atmosphere so its capture is independent of the CO₂ sources.
- Air has a **lower concentration of contaminants** such as NO_x , SO_x and particulates compared to flue gases.

On the other hand, it has some disadvantages (26):

- It is an energy intensive process because the CO₂ concentration in the air is low. Thus, large volumes of air must be processed to collect meaningful amounts of CO₂.
- The **presence of moisture** in the air might affect the stability of the sorbent.
- It requires to operate close to ambient temperature and pressure.
- CO₂ capture from the air is **more expensive** than CO₂ capture from power plants: the cost of CO₂ captured from the atmosphere ranges between 94 and

232 \$/ ton CO₂ (27) whereas the cost of CO₂ captured from the flue gas of power plants varies from 13 to 74 \$/ ton CO₂ (28).

1.4. Zero Emission Fuels

Two-thirds of the global energy use are fossil-based and difficult to electrify whereas global warming asks for more sustainable energy technologies. Renewable liquid hydrocarbons might be the solution for these issues. However, the main challenge is to reduce their production costs.

ZEF is a start-up whose main goal is to achieve economic production of renewable methanol (MeOH) in a micro-plant. The route followed by ZEF, shown in Figure 7, produces methanol from solar energy and CO₂ and H₂O captured from the air. The H₂O is fed into an electrolyzer producing H₂. Then, CO₂ and H₂ goes into the methanol synthesis reactor which produces methanol as well as H₂O. These products are separated from each other in a distillation unit. The plant will be entirely powered by solar energy (29).

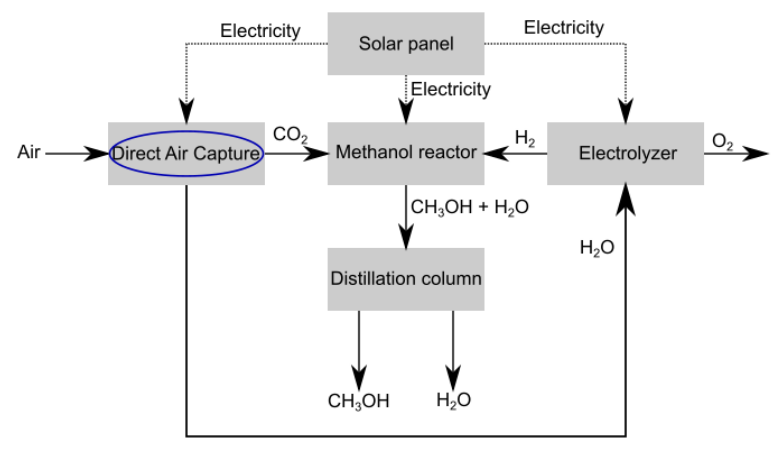


Figure 7: ZEF process

ZEF philosophy is based on numbering up, instead of scaling up which is, and was, the common practice of chemical industry: it increases the production by increasing the number of plants as opposed to increasing the size of the equipment (29).

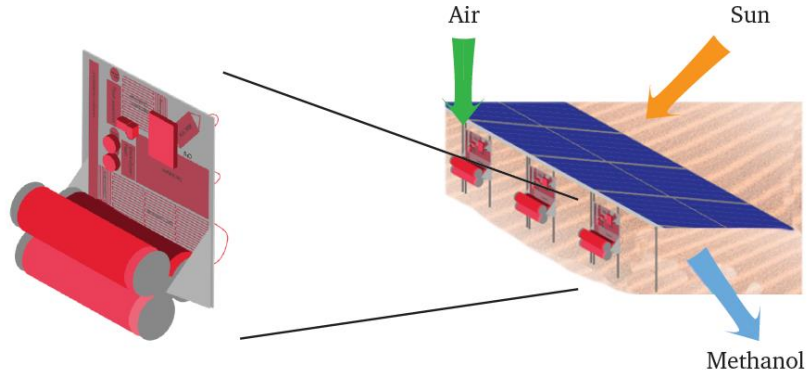


Figure 8: ZEF micro-plant concept (29)

1.4.1. Starting calculations

The absorption part is a critical area for ZEF. ZEF's goal is to produce 213 g MeOH/day per micro-plant (29). According to the stoichiometry of the MeOH production from CO₂ and H₂, it is possible to find the amount of CO₂ that the DAC system must absorb:

$$CO_2 + 3H_2 \rightarrow CH_3OH + H_2O$$
 (1-1)

Eq. (1-1) shows that on molar basis the amounts of CO_2 and MeOH are equal and taking into the molecular weights of CO_2 and MeOH it is possible to find that 213 g MeOH/ day require, at least, 293 g CO_2 / day, if the efficiency of the methanol reactor is assumed to be 100%. However, the estimated efficiency is 38% (30) which increases the CO_2 needed. In addition to this, not all the CO_2 of the air that flows through the DAC unit will be absorbed. As a rough estimation, the efficiency of the DAC unit is assumed to be 25% (31).

The design developed in this thesis is a first estimate, hence, 293 g CO₂/ day was assumed as the target yield.

1.5. TNO

TNO (Nederlandse Organisatie voor Toegepast Natuurwetenschappelijk Onderzoek) is an independent research organization in the Netherlands. TNO's strategy is based on technological innovations that develop the industry and ensure the well- being of society in a sustainable way. ZEF and TNO share the same motto which helped to develop a close relationship.

1.6. Aim of this thesis

The majority of the CO_2 capture from the air has been done with solid materials. This thesis is going to extend towards to completely fluid materials where there are a lot of unknowns. Because of that, the effects of different parameters will be studied in the thesis.

The aim of this thesis is to characterize polyamine sorbent materials that can capture CO_2 . A sorbent material has three relevant parameters that will determine if they can be used in a commercial process: capacity (g CO_2 / kg sorbent), capture rate (g CO_2 / h) and stability. Specifically, this thesis will focus on the first two.

The research questions are:

- What is the effect of varying process conditions (type of polyamine, layer thickness, H₂O content and CO₂ concentration) in the air capture?
- What is the chemical process that drives the CO₂ absorption on polyamines?
- How should be an absorber be designed in order to meet ZEF requirements?

The approach followed to answer the research questions is shown in Figure 9.

 H₂O plays an important role in the CO₂ absorption process, since it is absorbed as well. Consequently, the H₂O loading in polyamines is studied in an environment with negligible CO₂ presence (the climate chamber).

- The process conditions of air capture (layer thickness, blends and preloading polyamines with H₂O) are changed in order to study its effect on CO₂ and H₂O absorption.
- The FTIR experiments are done to find out the reaction mechanism of the CO₂ absorption in polyamines.
- The solubility constant and the reaction rate constant of CO₂ are obtained experimentally since they are needed in the modelling part. The calculation of these constants requires viscosity values.
- An absorption model is developed in MATLAB using the H₂O and CO₂ loadings in order to obtain the diffusion coefficient of both H₂O and CO₂.
- Finally, several guidelines for the design of an absorber are given.

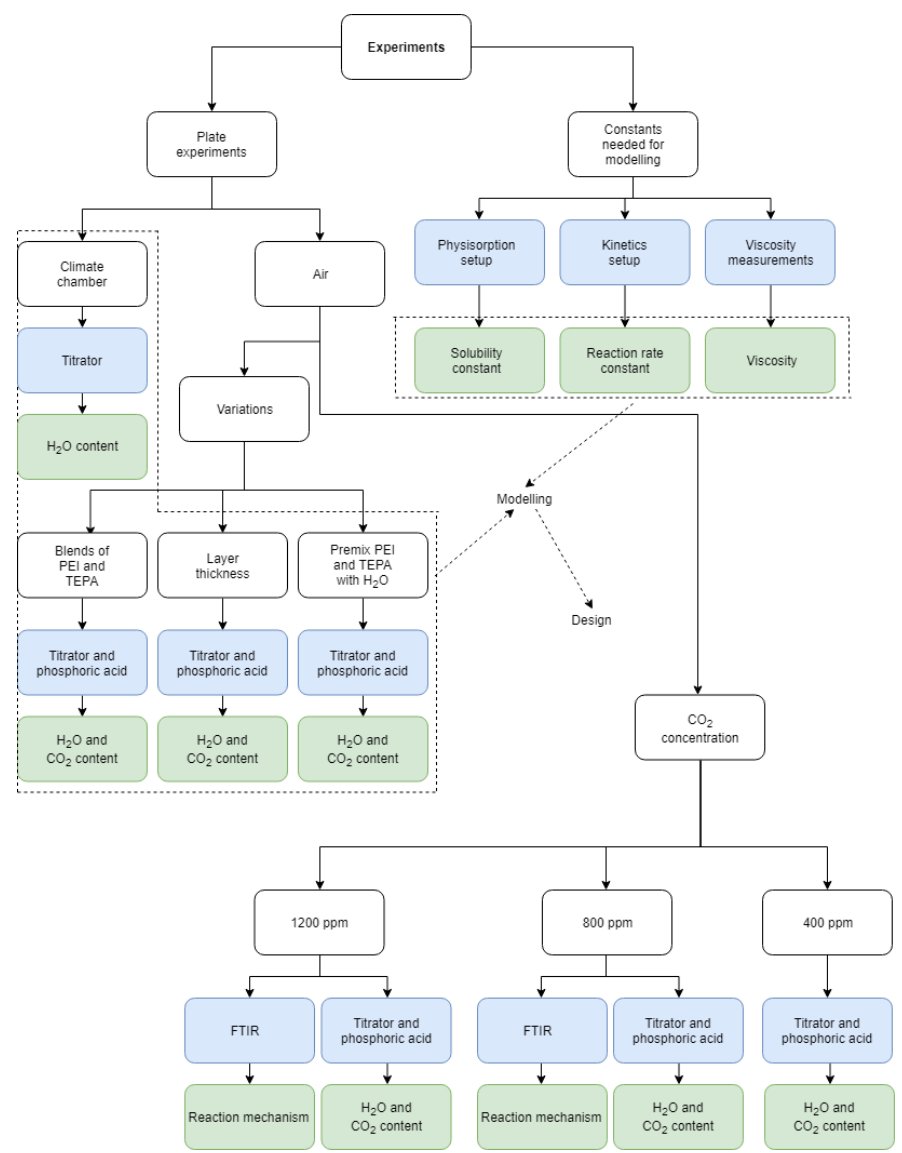


Figure 9: Procedure followed to answer the research questions

2 Overview of Direct Air Capture (DAC)

Chapter 1 indicates that DAC can be a promising technology to mitigate climate change by capturing CO₂ emissions and recycling them to obtain relevant products. In this Chapter, an in-depth explanation of different DAC technologies is given. Special attention is given to polyamines, since they are the focus of this thesis and will be further analyzed from the experimental and modelling point of view.

2.1. Introduction

The main difference between capturing CO_2 from the air and from centralized sources is the concentration of CO_2 . Although the current concentration of CO_2 in the atmosphere is higher than at any time in the last one million years, it is still 400 ppmv. The concentration of CO_2 in a conventional flue gas depends on the technology but it can vary from 4% (natural gas fired system) to 11% (coal fired system). Flue gas from coal combustion is given as an example and compared with dry air (32).

Table 1: Composition of flue gas vs dry air

Gases	Composition (vol %)		
	Coal combustion flue gas	Dry air (33)	
O_2	6	21	
N_2	76	78	
CO ₂	11	0.04	
H₂O	6	0	
Ar	1	0.93	
Other constituents (Ne, He, CH ₄)	-	0.03	

ZEF's idea is to capture CO₂ directly from the air, where H₂O is present. H₂O content in the air can vary because of different humidity and temperature.

Since the concentration of CO_2 in the air is lower than in the flue gas, the amount of volume that must be processed in DAC to capture the same amount of CO_2 will be higher. This is one of the main difficulties when it comes to DAC technology. The calculations of the stream volumes are available in Appendix A. Capturing 1 kg of CO_2 in the flue gas would require around 5 m³ of gas to be processed whereas for air the amount increases sharply up to 1366 m³ assuming 100% efficiency in both cases.

2.1.1 Thermodynamics

The theoretical minimum work required to achieve a thermodynamic change is the net change in work potential of the system. For an isothermal, isobaric and reversible process the change in work potential is minimized and reduces to the Gibbs free energy (34).

The Gibbs free energy represents the minimum energy needed by the sorbent to capture CO_2 . The higher the free energy, the more energy demanding will the process be. In this case, the free energy required to capture 1 kg of CO_2 under normal conditions (ΔG in [J/mol]) is calculated following equation (2-1).

$$\Delta G = RT \ln \frac{P}{P_0^i} \tag{2-1}$$

Where:

Table 2: Input to calculate the free energy of sorption

Symbol	Description	Value	Unit
R	Universal gas constant	8.314	[J/(K*mol)]
T	Temperature	293.1	[K]
		5	
P	CO ₂ pressure in the desorbed stream	1	[atm]
P_0^i	CO ₂ pressure	Varies	[atm]

On one hand, the need to reduce CO_2 emissions makes it desirable to capture most of the CO_2 from the flue gas of a power plant. On the other hand, an air capture system offers the possibility to freely adjust the fraction of CO_2 captured from the air trading off the energy cost of capture against the cost of moving air through the system (35). As a simplification, the CO_2 pressure in the desorbed stream is assumed to be 1 for both streams.

Using the values from Table 2 the Gibbs free energy can be calculated. It must be, at least, 19.07 kJ/ mol CO₂ if air is used as the input stream and 5.38 kJ/ mol CO₂ if flue gas is used. No real process can operate at the theoretical minimum work because achieving reversibility would require theoretical equipment of infinite size and cost (34).

It can be seen in Figure 10 that the minimum work required for CO_2 capture grows logarithmically with the CO_2 dilution: the concentration of CO_2 in the air is 275 times lower than in flue gases but theoretically, its capture would require only 3.54 times the energy as CO_2 capture from flue gases. Material candidates for DAC should have an interaction energy with CO_2 enough to overcome the thermodynamic limit and efficiently capture it.

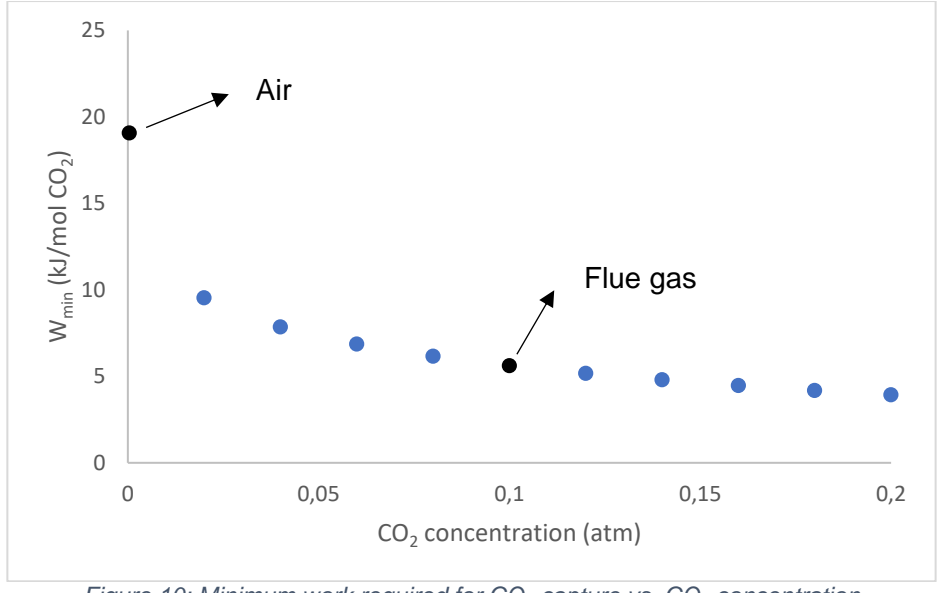


Figure 10: Minimum work required for CO₂ capture vs. CO₂ concentration

Real separation processes typically achieve 2^{nd} law efficiencies (η) in the 5- 40% range. The 2^{nd} law efficiency is defined as the ratio of the theoretical minimum work required to carry out a process (W_{min}) to the actual work required (W_{actual}):

$$\eta = \frac{W_{\min}}{W_{\text{actual}}} \tag{2-2}$$

The concentration factor (CF) is the ratio of the component's mole fraction in the product stream (c_{final}) and in the feed ($c_{initial}$):

$$CF = \frac{c_{\text{final}}}{c_{\text{initial}}} \tag{2-3}$$

Figure 11 shows the empirical relationship between the CF and the η of industrial separation processes. The data indicate that separation processes have a wide range of CF and η but they never exhibit high CF and η at the same time. This trend suggests that, for DAC, η is likely to be around 5% (unless a new technology makes a major change) (34).

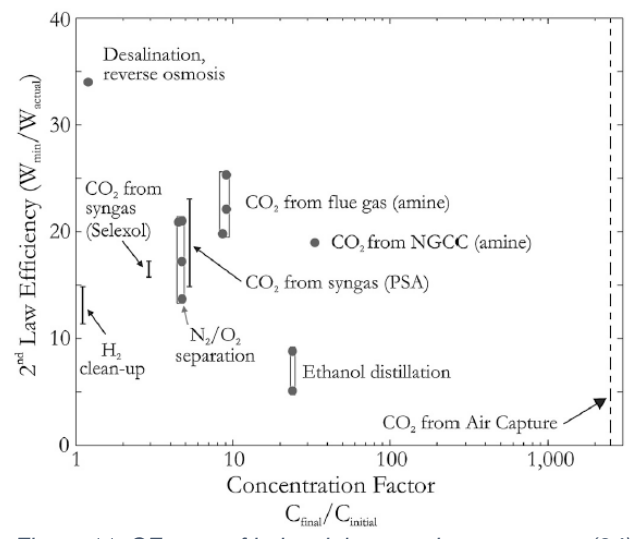


Figure 11: CF vs. η of industrial separation processes (34)

It can be concluded that the actual work for air capture systems becomes 381 kJ/mol CO₂. For a standard MEA process, the actual work is 180 kJ/ mol CO₂ (36) if the activation energy, and not the Gibbs energy, is used as the minimum work (37).

2.2. Sorbent

The sorbent is the key element in the DAC process since it is the chemical complex that will capture CO₂ from the air. Part of the requirements that the sorbent must fulfill in order to be eligible for DAC are (17) (36):

- High selectivity towards CO₂ compared to other gases present in air, since it is present at low concentrations.
- Enough binding energy.
- Stability under moisture and O₂.
- Fast kinetics at ambient conditions.
- Easy to regenerate (CO₂ should not bound too strongly).

- Scalability.
- Low energy requirement for regeneration.
- Low pressure drop.
- Cheap.
- Able to stand particles.

In the next two Sections, sorbents capable of capturing CO₂ directly from the air are divided depending if they adsorb or absorb CO₂. A special emphasis is given to polyamines, since this thesis focuses on them.

2.2.1. Adsorption

Solid inorganic chemisorbents

According to the previously mentioned definition, adsorption is defined as a surface phenomenon, but CO_2 capture will also take place in the bulk, since CO_2 can penetrate, but generally speaking solid inorganic chemisorbents are classified as adsorbents.

The acidic nature of CO₂ facilitates its adsorption on the basic sites of metal oxides (38). This group includes alkaline metal oxides and alkaline earth metal oxides.

- Alkaline earth metal oxides adsorb CO₂ according to the following reaction:

$$MO(s) + CO_2(g) \leftrightarrow MCO_3(s)$$
 (2-4)

MgO (magnesium oxides) and CaO (calcium oxides) are the most relevant oxides for CO₂ adsorption (38). A great advantage of CaO is that calcium minerals are one of the most abundant in nature. However, the adsorption rate is influenced by temperature and CO₂ partial pressure, which are extremely low in DAC, making this approach impractical. MgO has lower regeneration energy requirements than CaO but, on the other hand, their lower CO₂ adsorption capacities make them inferior to CaO (38).

Alkaline metal oxides react with CO₂ according to:

$$M_2O(s) + CO_2(g) \leftrightarrow M_2CO_3(s)$$
 (2-5)

2.2.2. Absorption

In solution inorganic chemisorbents

Strong bases such as sodium hydroxide (NaOH) and potassium hydroxide (KOH) can react with CO_2 from ambient air (16). KOH cycles are not described in this thesis since KOH is more expensive than NaOH. The technology is divided in two steps: capture the CO_2 and recover the sorbent. Depending on the pH of the solution MOH reacts with CO_2 producing carbonates (Eq. (2-6)) or bicarbonates (Eq. (2-7)) (36):

$$2MOH(1) + CO_2 \rightarrow M_2CO_3 + H_2O$$
 (2-6)

$$MOH(l) + CO_2 \rightarrow MHCO_3 \tag{2-7}$$

After the NaOH solution has been in contact with CO_2 (air contactor in Figure 12) it forms dissolved sodium carbonate (Na_2CO_3), which must be recycled back to NaOH to complete the cycle. Na_2CO_3 is highly soluble in H_2O which makes its collection difficult and energy intensive since large quantities of H_2O must be evaporated. Causticization is an interesting candidate for NaOH regeneration since it solves this issue. Na_2CO_3 reacts with calcium hydroxide ($Ca(OH)_2$) producing calcium carbonate ($CaCO_3$) and NaOH. $CaCO_3$ precipitates out of the solution and is thermally decomposed (lime kiln in Figure 12) to produce CO_2 , which can be utilized or stored, and CaO_3 , which is hydrated to form $Ca(OH)_2$ to close the cycle (lime hydration in Figure 12). The regenerated NaOH is recycled back to the air contactor (16).

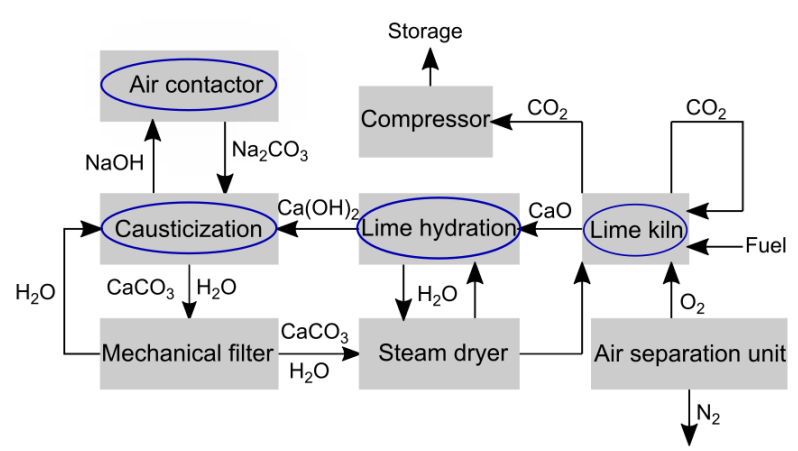


Figure 12: Process of CO₂ capture from the air using the Na/ Ca cycle (16)

The biggest disadvantage of inorganic chemisorbents is that they strongly bind CO₂, far more than needed for DAC, which requires considerable energy in the regeneration step. In addition to this, the corrosiveness of strong alkaline solutions, H₂O loss, local drying of solutions and mass transfer problems (16) add extra difficulties.

It is true that Carbon Engineering has already opened a pilot plant, which proves that absorption in inorganic chemisorbents is possible. However, natural gas is still needed for heating up (27), which releases CO₂. Therefore, this option is neglected and will not be further studied.

Polyamine sorbents

Having said that liquid amine solutions are the most used technology for CO₂ capture from centralized sources it seems interesting to see how they can be applied in DAC.

Most of the literature is focused on supported amine sorbents (SAS) rather on diluted amines. This kind of sorbents consists of two main ingredients: a solid and highly porous support and a functional amine which lays on the support.

SAS systems could be more interesting than diluted amines for DAC due to (36) (38) (39):

- Low-pressure drop.
- Easier control of the residence time.
- More compact designs and less moving parts.
- Substitution of H₂O for a support with lower heat capacity, decreasing the energy cost during desorption.
- Solid- solid contact between the support particles and other solid surface is poor. Hence, vessel corrosion is less problematic.

However, a solid sorbent makes heat integration more difficult (36).

Amines

Amines are compounds and functional groups that contain a basic nitrogen atom with a single pair of electrons. Amines are formal derivatives of ammonia, wherein one or more hydrogen atoms have been replaced by a substituent. There are three main types of amines, but it is also possible to have four organic substituents on the nitrogen (Table 3). These species are not amines but quaternary ammonium cations and have a charged nitrogen center (40).

Table 3: Amine types

Primary amine	Secondary amine	Tertiary amine	Quaternary amine
R ¹ H	R ¹ H	R ¹	R ¹

Reactions

The reactions between amines and CO₂ have been widely studied. Primary and secondary amines react with CO₂ forming carbamates where there is no, or little, steric hinderance. There is a debate in literature regarding the mechanism of formation of carbamates (41). In this case, the zwitterion mechanism is explained.

The zwitterion mechanism consists of two steps. In the first one, CO₂ reacts directly with an amine molecule forming a zwitterion molecule. After that, in the second step, another amino group deprotonates the zwitterion forming carbamate.

Two amine groups (RNH₂) are required to bind one molecule of CO₂, as it can be seen below (38):

$$RNH_2 + CO_2 \leftrightarrow RNH_2^+COO^- \tag{2-8}$$

$$RNH_2^+COO^- + RNH_2 \leftrightarrow RNHCOO^- + RNH_3^+$$
 (2-9)

Tertiary amines react differently because they form bicarbonate, which is then fixed by electrostatic forces. Bicarbonate formation only takes place at high CO_2 partial pressures or with sterically hindered amines. In the first step of the tertiary amine reaction, the tertiary amine dissociates H_2O to form a quaternary amine and OH^- (38). Then, CO_2 reacts with H_2O to form carbonic acid (H_2CO_3) which rapidly dissociates to form a bicarbonate anion (HCO_3) and a hydrogen anion (H^+) (42). Finally, the protonated amine and the bicarbonate anion associate ionically (38).

$$R_1R_2R_3N + H_2O \rightarrow R_1R_2R_3N^+H + OH^-$$
 (2-10)

$$CO_2 + H_2O \leftrightarrow H_2CO_3 \tag{2-11}$$

$$H_2CO_3 \leftrightarrow HCO_3^- + H^+$$
 (2-12)

$$R_1R_2R_3N^+H + HCO_3^- \rightarrow [R_1R_2R_3N^+H][HCO_3^-]$$
 (2-13)

The reaction between amines and CO₂ is exothermic. In general, primary amines have a higher heat of adsorption than secondary and tertiary amines whereas tertiary amines show slower reaction kinetics (31).

Supported Amine Sorbents (SAS)

SAS can be classified based on the interaction between the support and the amine and the preparation method of these materials (16). There are two main types of SAS: in the first one, the amines are physically in the support (Class 1) whereas in the second one, the amine groups are covalently bonded to the support (Class 2 and 3) (31).

Class 1 sorbents have liquid amines (active groups) dispersed in the pores of the support material so the mechanism to capture CO_2 is absorption whereas the second and third class have amine groups incorporated in the solid structure of the support (active groups and support are one) so the process is adsorption (43). However, for some reason, the researchers in this field started to call every SAS an adsorbent. It is thus more a consensus that researchers follow than something rooted in the understanding of the process itself (44).

Class 1

Impregnated amine sorbents are prepared by wet impregnation, where the amine, dissolved in a volatile solvent, is impregnated into the support. After impregnation, the solvent is evaporated leaving the amine molecules dispersed inside the pores of the support (31). Although this is the simplest method of supporting amines, the amine which is actually in the support does not have to be the same as the amine that will react with CO_2 (38).

The main drawback of Class 1 SAS is that the weak physical interaction that holds the amines onto the support surface causes the amines to leach, which leads to a loss in the absorption performance (16). Low molecular weight (LMW) amines are easier to impregnate into the support but higher MW amines suffer less from evaporation loss (31). On the other hand, additives can be added to maintain the adsorption performance over the cycles (16).

Amines commonly found in Class 1 are polyethylenimine (PEI) and tetraethylenepentamine (TEPA). The most important criteria for amine selection are the number of nitrogen atoms per amine molecule (to maximize the capacity of CO₂ capture), the adsorption heat and the sorption kinetics (31).

PEI can be a branched polymer containing a mixture of primary (1°), secondary (2°) and tertiary (3°) amines or a linear polymer of secondary amines with primary amines at the endings. PEI possesses a high amine content but the ratio of primary, secondary and tertiary amines varies depending on the molecular weight and synthesis conditions (38). Linear PEI has a higher CO₂ adsorption capacity but also a higher degree of sorbent leaching than branched PEI (16). TEPA is considered an ultra-low molecular weight PEI because it contains four repeated units of PEI (38).

The structure of both polyamines is shown in Table 4. The chemical structure of PEI is an example because PEI is a chaotic compound.

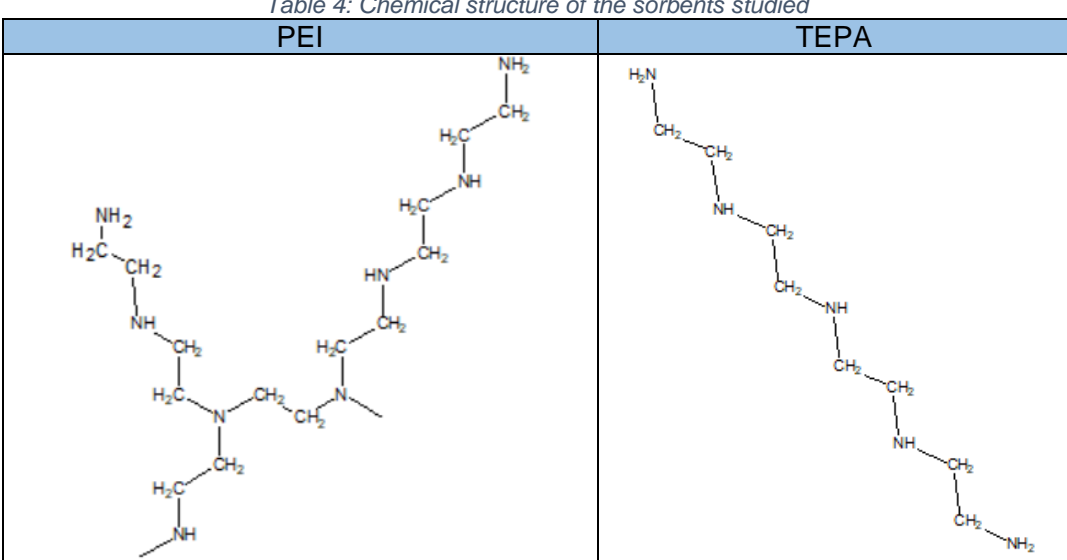


Table 4: Chemical structure of the sorbents studied

These amines have been widely studied in literature together with support material such as silicas, porous carbons, zeolites and polymers (such as poly-(methyl methacrylate) (PMMA) and polystyrene (PS)) (31).

- Silicas, although they seem to be the most promising, they are not interesting for ZEF because of their high cost.
- Porous carbon, as will be mentioned later, were already studied by ZEF Team 2. However, vacuum was not achieved so the desorption process could not be analyzed. In addition to this, achieving a good impregnation of the amines onto the support was more difficult than expected.
- Zeolites are not interesting because of their loss of capacity due to H₂O.
- Polymers, like silicas, seem promising, their main advantage being low costs.

Class 2

Class 2 sorbents are made by grafting and are commonly known as covalently tethered amine adsorbents (CTA). Grafting consists on reacting molecules with the surface of the silica support (38). As an example, aminosilanes will be considered the reacting molecules. Their main advantage with respect to Class 1 is that the chemical bonds ensure the immobilization of the sorbent, preventing rapid degradation in performance (16).

The scheme for the reaction of silane with silica is shown in Figure 13, where R¹ can either be an alkyl or aminoalkyl group and R2 is a methyl or ethyl group, depending on the type of aminosilane chosen. The amino-silane reacts with the surface in an organic solvent. Then, the alcoxysilyl groups condense with surface silanol groups to form new Si-O-Si linkages while liberating alcohols (38).

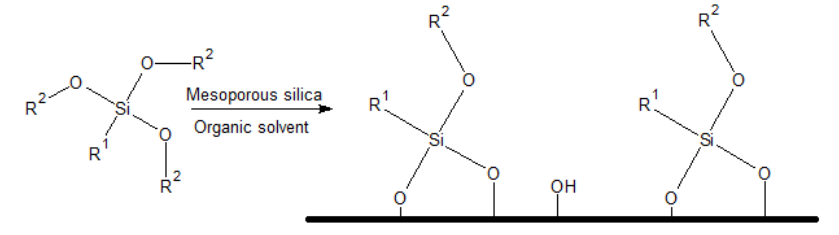


Figure 13: Reaction of silane with silica (38)

The average number of surface bonds formed depends on the density of silanols on the silica support, the R¹ and R² groups used and the reaction conditions (silane concentration, temperature and time). The best choice would be an aminosilane with high nitrogen density and accessible primary and secondary amines. However, this choice is limited to the aminosilanes that are commercially available. The three most commonly used are mono-, di- and tri-aminosilanes, which have one, two and three amines respectively (Table 5). Monoaminosilane has a primary amine as an end group whereas diaminosilane and triaminosilane have secondary amines as links and primary amines as endings (38).

Class 3

Class 3 polyamine sorbents consist of an inorganic support and a chemically grafted polyamine component that are prepared by *in situ* polymerization of amine-containing monomers. According to *Goeppert et al* (16), they combine the advantages of Class 1 (high nitrogen loading) and Class 2 (lower volatility and so higher stability).

Unfortunately, less literature has been reported for this type of sorbents. However, both *Choi et al* (38) and *Goeppert et al* (16) considered the sorbent developed by *Jones et al* (45) as promising. He prepared adsorbents through the polymerization of aziridine off of mesoporous silica surface silanols, which are known as hyperbranched aminosilica (HAS).

2.3. Previous work at ZEF in the DAC unit

In this Section, work done by three different teams in the DAC unit is briefly introduced.

The first DAC prototype, built from September until February 2018 was a proof of concept, i.e., it proved it was possible to capture CO_2 from the air. In this first design, air flowed into the system which then goes through the absorber and captures CO_2 , along with H_2O , from the air. When the sorbent is saturated, the chamber closes and the fan starts blowing air into the second chamber. The first chamber is heated and vacuumed to 0.1 bar so the CO_2 and H_2O are desorbed by temperature-vacuum swing. After desorption, the chamber is cooled back down to ambient temperature, opened and the process starts again (46).

The main conclusion made during the development of the first prototype was that a packed bed system with polyethylenimine of high molecular weight (HMW PEI) impregnated on silica (Davisil Grade 646) was not the best design to capture CO₂ due to the huge volume of the unit, as it can be seen in Figure 14. Monolithic sorbent packages were proposed as promising candidates. More specifically, due to their low costs, active carbon-based sorbent packages were considered for the next prototype (46).



Figure 14: DAC prototype done by ZEF Team 1 (46)

The second DAC prototype was built between February and July 2018. The main goal was to implement the previous recommendations. In addition to this, the behaviors of two different MW PEI (1.2K and 10K) were studied under different process conditions (47).

Figure 15 shows the 3D design of the DAC unit. It is important to note that this system was never fully functional but resembles what a working one might look like. The main difficulty, from a structural point of view, was to make the doors open and close while keeping the chambers properly leak-tight. The main difficulty, from the sorbent package point of view, was working with the active carbon to make the monolith blocks fit in the unit, as it is very brittle (47).

In addition to this, the wet impregnation was more difficult than expected. Three different techniques were tried, and the most effective one was to use a silicon "sock" which fit tightly around the monolith. The sock with the monolith inside was filled to the brim with the MeOH/ PEI solution and placed inside an oven. As the heat in the oven increased, the MeOH would evaporate, and the PEI, having a higher boiling point, remained on the monolith. However, gravity led to an inhomogeneous distribution of PEI (47).

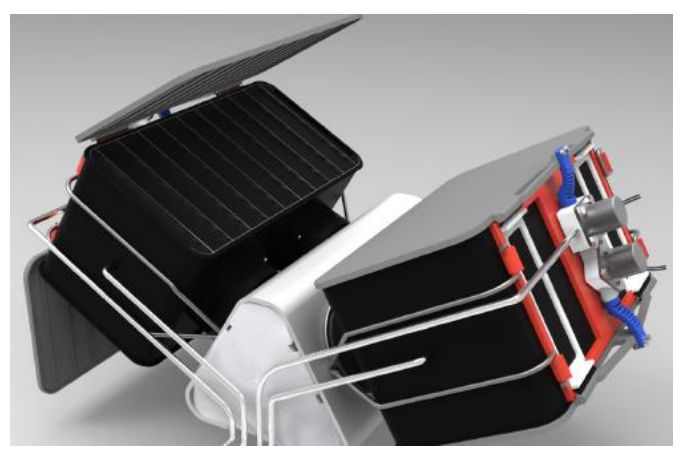


Figure 15: DAC prototype done by ZEF Team 2 (48)

ZEF Team 3 worked on the DAC system from September until December 2018. The goal of this team was to check if a continuous absorption-desorption process with bulk amines could substitute the batch system proposed by the previous team. They worked with PEI MW 600 since PEI MW 1.2K and 10K were too viscous.

The main conclusions of their work were (49):

- The time required to achieve steady state depends on the thickness of the polyamine layer.

- The direction of the air blown by the fan does not affect the overall absorption of CO₂ and H₂O.
- The more hydrophilic surface of the plate, the smaller contact angle between the sorbent and the plate and so, the thinner layer thickness. The contact angle between different types of materials and PEI MW 600 was observed. Paper and PEI MW 600 made the smallest contact angle which restricted the flow surfaces to paper-like materials.
- A heterogeneous flow was observed without manually connecting the flowing droplets of sorbent whereas a manual intervention provided a homogeneous flow.
- Pre-wetting the paper with sorbent helps to achieve a homogeneous flow.
- At the beginning of the flow, the surface tension effects are important.

The final absorption setup consists of multiple stacks of vertical plates. Figure 16 and 17 show the final design of the DAC unit proposed by this team.

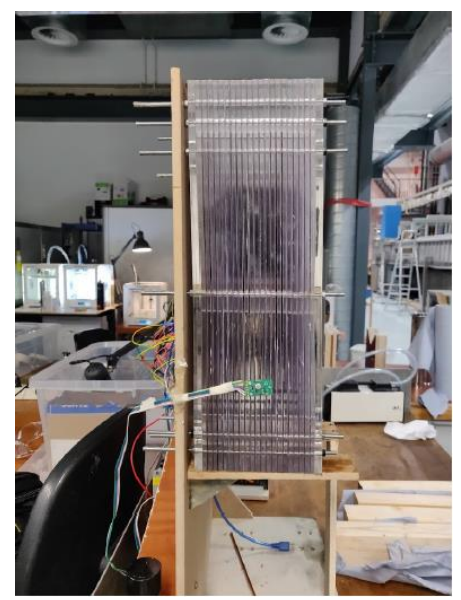


Figure 16: Side view of the DAC prototype done by ZEF Team 3

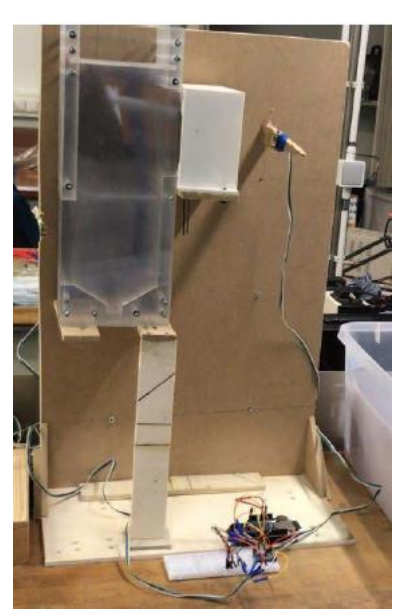


Figure 17: Front view of the DAC prototype done by ZEF Team 3

2.4 Selection

The major drawbacks of the different sorbents mentioned are:

- **Inorganic chemisorbents** require high temperatures in the regeneration step. For example, Carbon Engineering technology uses natural gas in order to have enough energy to regenerate the sorbent.
- **Physisorbents** can be considered or CO₂ capture if, and only if, they are used as support for chemisorbents.
- **SAS** are divided in three groups. Although Class 1 seems to be the easiest sorbents to prepare, the experience of ZEF Team 2 proved that it was more difficult than expected to achieve a homogeneous PEI distribution. Class 2 and Class 3 are, according to literature, already more difficult to prepare.

It is surprising to note that almost no research in bulk amines has been done. This is the reason why this thesis will focus on studying the CO₂ absorption capacities and kinetics of bulk PEI and TEPA. Since they are less or not even diluted in H₂O, the

energy penalty of desorption should be lower, just like SAS. Even amines are corrosive for metals, it would be enough to avoid them as building materials.

PEI was requested from Polyscience whereas TEPA was ordered to Sigma Aldrich.

3 Materials and methods

In the previous two chapters, the concept of direct air capture (DAC) was introduced, and it was explained how it could help mitigate climate change, what different processes and materials can be used in this technology and which one will be the main focus of in this thesis.

As it was mentioned before, the goal of this thesis is to study the capacity and the kinetics of CO₂ on bulk amines from an experimental and modeling point of view. Then, with this information, some guidelines for the absorber design can be given. This chapter explains the step-by-step procedure followed to find the CO₂ and H₂O loadings, the constants needed for modelling and the reaction mechanism.

3.1. Achieving a homogeneous layer thickness

The absorption experiments were done on horizontal plates. However, before that, a homogeneous layer of polyamine on the plate had to be achieved. This was done by preloading the plate with a uniform layer of polyamine via a flowing experiment, where the plate was inclined. Then, after some time, the plate was switched back to horizontal and the absorption experiments could begin.

The setup used to achieve a homogeneous layer thickness was already available. It consists of a top and bottom tank, a comb and a plate. The comb enhances the connection of the polyamine flow to get a homogeneous layer (49). The comb and the plate are made out of PMMA whereas the top and bottom tank are made out of PLA (polylactide).

Equation (3-1) is used to estimate the average layer thickness of the polyamine layer. The calculations followed to find Equation (3-1) are shown in Appendix B.

$$h = \frac{M}{\rho_i \times l \times B} \tag{3-1}$$

Where:

Table 6: Input to calculate average layer thickness

Symbol	Description	Value	Unit
$ ho_{TEPA}$	Density of TEPA	998	[kg/m³]
$ ho_{PEI}$	Density of PEI	1050	[kg/m³]
l	Length of the plate where the polyamine is spread	0.23	[m]
В	Width of the plate where the polyamine is spread	0.095	[m]

First, a piece of paper was placed on the plate. Then, the top tank and the comb were attached to the plate with screws (Figure 18) and the paper was pre-wetted with the polyamine, in order to enhance a homogeneous flow.

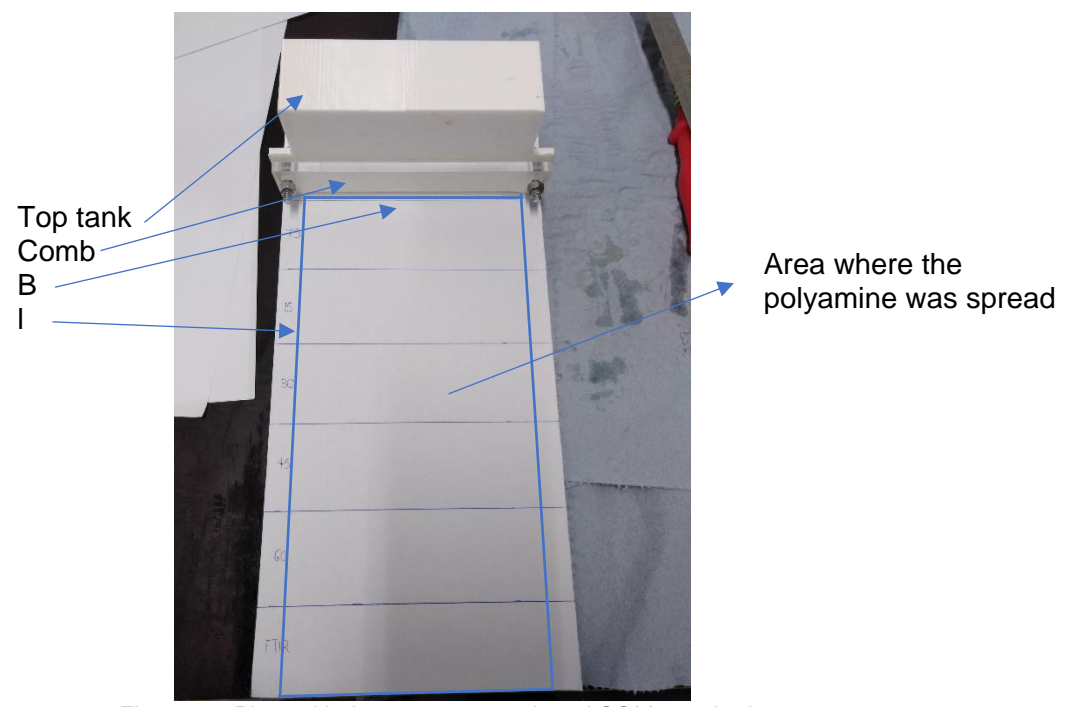


Figure 18: Plate with the paper, top tank and COM attached

After that, the plate was placed in the bottom tank whereas the polyamine was added in the top tank. Then, the polyamine flowed on the plate.

Figure 19 shows a homogeneous layer of polyamine. The layer thickness was calculated using Eq. (3-2) and once it is around 0.5 mm the absorption experiment was ready to start.



Figure 19: Homogeneous layer thickness of polyamine

Figure 20 shows the distribution of the plate, paper and polyamine layers. The polyamine might penetrate into the paper since paper is a porous material.

If the thickness of the paper is not relevant compared to the thickness of the polyamine then the system is liquid and the interface between the liquid (polyamine) and the solid (paper) can be neglected. The thickness of the paper used is 0.1 mm. The layer thickness of the polyamine varies between 0.25, 0.5 and 0.75 mm. The calculated layer

thickness of 0.25 might be smaller than the real one since this value is close to the paper layer thickness.



Figure 20: Plate, paper and polyamine thicknesses

ZEF Team 3 proved that CO₂ and H₂O absorption is negligible when there is no fan (49). This could be due to the fact that, when there is no fan, mass transfer issues in the gas phase show up.

3.2. Experimental plan

Table 7 summarizes the different experiments done in this thesis. Although ZEF Team 3 proved that the concept of a continuous absorption of CO₂ by polyamines was possible the physical process behind it was unclear.

Firstly, H₂O absorption is studied independently. Then, absorption of both CO₂ and H₂O together is studied. After that, kinetics and physisorption constans were obtained as well as material properties and reaction mechanisms. With all this information, an aborption model and an absorber design will be developed.

Experiment		Experiment cor	annig une une en	Motivation	
·	Relative humidity (%)	Temperature (°C)	Time (min)	Layer thickness (mm)	
H₂O absorption	35, 50, 70, 95	10, 20, 30, 40	60, 120	0.5	Determine the diffusion coefficient of H ₂ O
CO ₂ and H ₂ O absorption	Lab co	onditions	60	0.25, 0.5, 0.75	Determine the influence of H ₂ O in CO ₂ absorption
Kinetics & physisorption of CO ₂	0	20, 30, 40	-	-	Determine the reaction rate and solubility constants of CO ₂
Viscosity	Lab conditions		-	-	Determine the dependence of viscosity with water content
FTIR	-	-	-	-	Determine the reaction mechanism

Table 7: Experimental plan followed during the thesis

3.2.1. Experiments of H_2O absorption from the air

A climate chamber was used to study the H_2O absorption of the sorbent at different relative humidity and temperature. It was available from TNO. Figure 21 shows that the air circuit is closed so CO_2 is not regenerated after the sorbent has absorbed it.

Therefore, it is assumed that the CO₂ absorbed by the sorbent inside the climate chamber is negligible.

The model of the climate chamber is ESPEC PR- 3KPH. The temperature can be varied from -20 °C to 100 °C whereas the relative humidity range is from 20 to 98% (50). However, the minimum working relative humidity was 35%. During the experiments, samples were collected at four different times and to do so, the climate chamber was opened. At very low relative humidity, even though the climate chamber was opened for only a few seconds at a time, the increase in relative humidity inside the chamber was high enough that the time it took the chamber to get back to the original humidity was too long for the H_2O content measurements to be considered accurate. It was found that the lowest relative humidity for which the accuracy of the water content measurements was satisfactory was 35%.

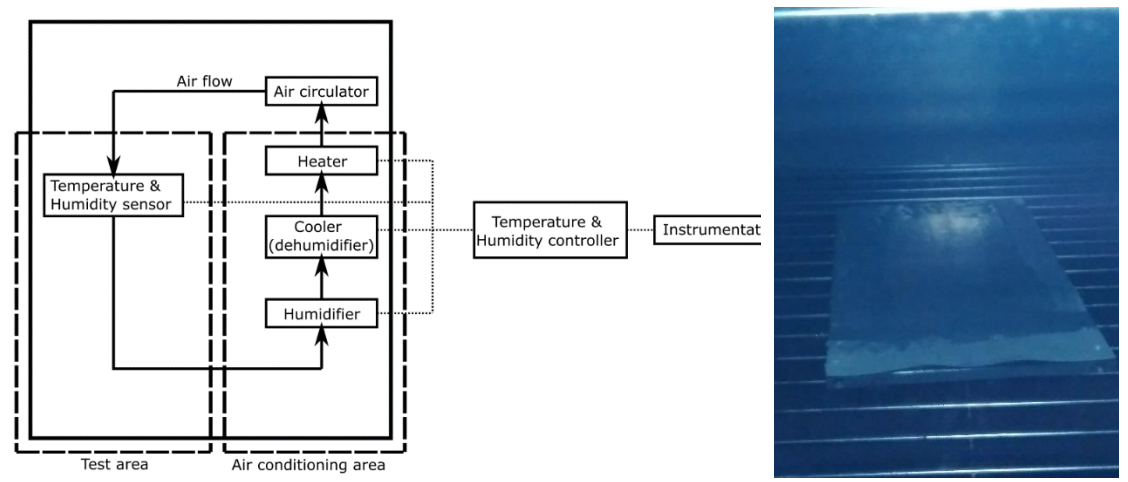


Figure 21: Working principle of the climate chamber (50)

Figure 22: Sample inside the climate chamber

Once the homogeneous layer of polyamine was achieved the sample was placed inside the climate chamber, like Figure 22 shows. In order to find out the time to achieve steady state, the samples remained inside the climate chamber for 120 minutes (1st batch). A sample was taken out after 30, 60, 90 and 120 minutes respectively. After finding out that 60 minutes was enough to achieve a stable H_2O concentration inside the PEI, the experiments were repeated by reducing the time from 120 to 60 minutes (2nd batch). A sample was removed after 15, 30, 45 and 60 minutes in order to get more data points which give more information about the increase of H_2O concentration inside the polyamine.

3.2.2. Experiments of CO₂ and H₂O absorption from the air

The next experiments done consisted on measuring the CO₂ and H₂O absorbed by the polyamine from the air. Some variations were introduced:

- The layer thickness was varied to 0.25 mm, 0.5 mm and 0.75 mm for both PEI and TEPA.
- PEI and TEPA were mixed in three different combinations: 25 wt% of PEI and 75 wt% of TEPA, 50 wt% of PEI and 50 wt% of TEPA and 75 wt% of PEI and 25 wt% of TEPA.
- 10, 20 and 30 wt% of H₂O was added to pure PEI and TEPA.
- The CO₂ content was increased from 400 to 800 and 1200 ppm.

Figure 23 shows the setup built to measure CO_2 and H_2O for the base case and for the first three variations whereas Figure 24 shows a schematic diagram of it. The components are:

- Fan SUNON (PMD1212PMB2-A) DC12V.
- Si7021 relative humidity (RH) and temperature sensor (51):
 - Precision of the relative humidity sensor: ± 3% RH (max), 0 to 80% RH.
 - o Precision of the temperature sensor: ± 0.4 °C (max), -10 to 85 °C.
- DC lab switching power supply (LABPS6005SM)

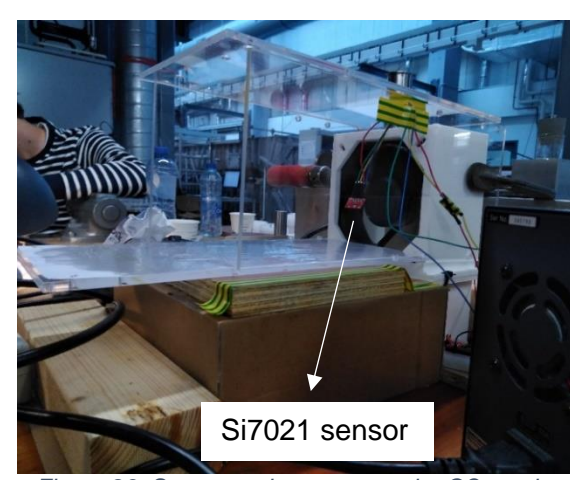


Figure 23: Setup used to measure the CO₂ and H₂O absorption from the air

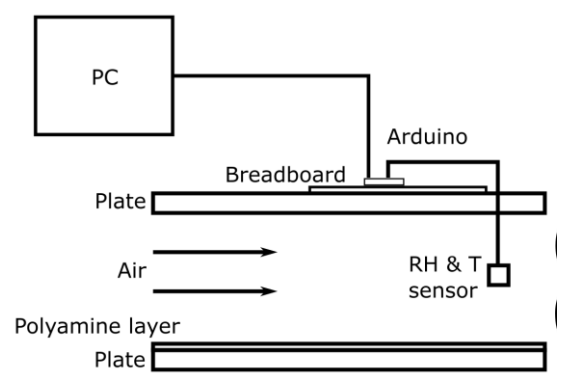


Figure 24: Schematic diagram of the setup used to measure the CO_2 and H_2O absorption from the air

Figure 25 shows the setup built to measure the CO₂ and H₂O absorbed when the CO₂ ppm in the air were varied. Figure 26 shows a schematic diagram of the setup. The components are:

- Two fans: The fan used in the previous setup was reused. Another one was added to enhance the mixing of the CO₂ coming from the bottle and the air. The other fan is a JARO (AD121HB-F93GP) DC12V.
- The previous sensor was replaced by a DHT22 sensor because it could not be used together with the CO₂ sensor since both share the same I²C address (52):
 - Precision of the relative humidity sensor: ± 2% RH (max), 0 to 100%
 - o Precision of the temperature sensor: ± 0.5 °C (max), -40 to +80 °C.
- CO₂ sensor Telaire 6703. Its specifications are (53):
 - o 400-5000 ppm ± 75 ppm or 10% of reading, whichever is greater.

- Two power supplies, one for each fan:
 - VOLTCRAFT LPS 1305
 - DIGIMESS DC POWER SUPPLY HY3003
- CO₂ MFC (Mass Flow Controller) (F-201CV-5K0-RAD-55-K) provided and calibrated for CO₂ by TNO.
- Flow bus (E-7500-RAA) provided by TNO to control the mass flow through the MFC.
- CO₂ bottle provided by TU Delft University.

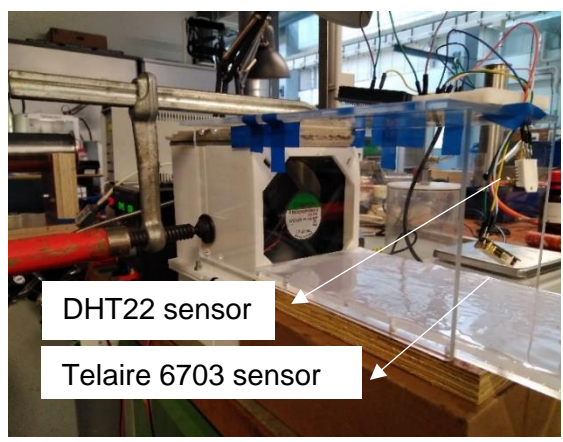


Figure 25: Setup used to measure the CO₂ and H₂O absorption from the air when varying the CO₂ ppm

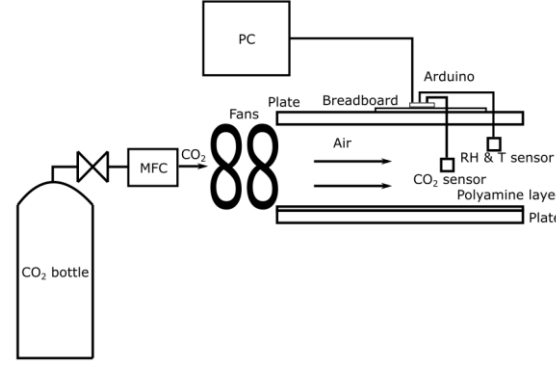


Figure 26: Schematic diagram of the setup used to measure the CO₂ and H₂O absorption from the air when varying the CO₂ ppm

The wiring between the Arduino microcontroller and the code used in the Arduino software is available in Appendix C.

3.3. Properties measurement

Different machines and setups have been used to measure the H₂O, CO₂ content of the polyamine as well as the kinetics and physisorption constants of CO₂.

- The H₂O measurements were done in a C20 coulometric KF titrator which was lent by TNO.
- Phosphoric acid titration, in the TNO office, was used to determine the loading of CO₂ in the polyamine.
- The kinetics and physisorption measurements were done in the corresponding setups in the TNO office in Delft.

3.3.1. H₂O titration

The H₂O captured by a loaded sorbent sample was measured in a C20 coulometric KF titrator.

PEI and TEPA were diluted with MeOH, before being added to the titrator. The minimum dilution rate was 5. It is important to note that the MeOH was not completely pure, which affects the H_2O measurements. Hence, the H_2O content of the MeOH is subtracted to obtain the real content of H_2O in PEI and TEPA. Also, PEI and TEPA from the bottles contain H_2O , as Table 8 shows:

Table 8: H₂O content in PEI, TEPA and MeOH

	H₂O content (ppm)
MeOH	1099
PEI	867
TEPA	1021

Duplos of H_2O measurements were done for some samples. The average error between the first and the repeated measurements is 1.70%. The H_2O content from the duplos is available in Appendix D.

At the beginning of the thesis a 756 coulometric KF titrator was used. However, the H_2O measurements were not accurate. This is why the titrator was replaced by the C20 coulometric KF titrator. More information is available in Appendix E.

3.3.2. Viscosity measurement

The viscosity was measured using a Fuengilab SMART series SMART L at the TNO office.

It was checked, and confirmed by *Sinha* (54), that PEI, although it is a long branch polymer, is Newtonian. More information about this verification is available in Appendix F.

3.3.3. Phosphoric acid titration

The polyamine loaded with CO_2 was tested in a phosphoric acid titration setup at TNO to find the CO_2 loading. The setup consisted of a round-bottom flask, which is filled with 350 mL of 85% phosphoric acid (H_3PO_4) solution, placed in a heating mantle. The heating mantle provides the required heat for the endothermic desorption of carbonated polyamines with H_3PO_4 towards CO_2 . First, H_3PO_4 reacts with the polyamine releasing the CO_2 contained in it. Then, a N_2 flow sweeps the CO_2 from the system. Finally, the CO_2/N_2 mixture goes through an infrared CO_2 analyzer to obtain the amount of CO_2 released from the polyamine. The software shows the amount of CO_2 in mg and in mol/L. The top-central opening of the set- up is fitted with a condenser to remove the H_2O before the CO_2 gets to the infrared analyzer (55) (56).

Duplos of CO₂ measurements were done for several samples. The average error between the first and the repeated measurements is 1.27%. The duplos of the CO₂ content are available in Appendix G.

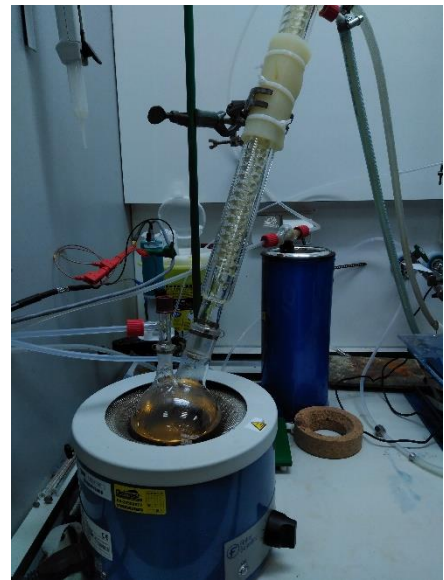


Figure 27: Phosphoric acid titration setup in TNO

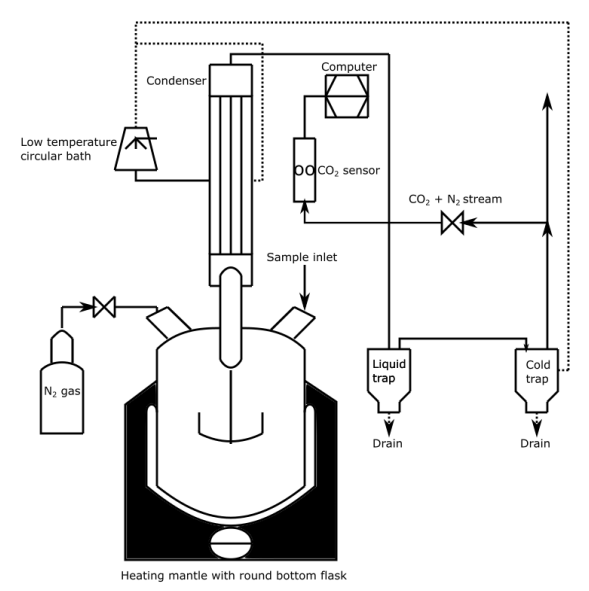


Figure 28: Diagram of the phosphoric acid titration setup

3.3.4. Physisorption and kinetics of CO₂

Unloaded polyamine was tested in the physisorption and kinetics setup at TNO to find the solubility and the reaction rate constants of the CO₂ absorption.

The setup consisted of two vessels, both filled with 0.4 L of polyamine mixed with H_2O . Because of the high viscosity of the polyamine the stirrer was not strong enough to enhance a good mixing inside the vessel. This is why H_2O was added. Both vessels are placed on two thermal plates. Also, there is a stirrer that improves the mixing of the gas inside the vessel. There are three sensors per vessel: two pressure and one temperature sensor respectively.

- Kinetics measurement: the setpoint of the pressure is changed. Then, both MFC started adding CO₂ to the reaction vessel until its pressure value matched the pressure value of the reference vessel. The pressure was changed to 5, 10, 15, 20, 17, 12, 7 mbar and the mass flow delivered by one (or both) MFC is written down. The pressure was varied in that way to check if the sorbent showed hysteresis.
- Physisorption measurement: the setpoint of the N₂O volume to be added is changed to 0.1 L so the MFC started adding N₂O to the reaction vessel. When its pressure value was stable, another N₂O pulse was given. The pressure change, as well as the N2O volume added, are collected.

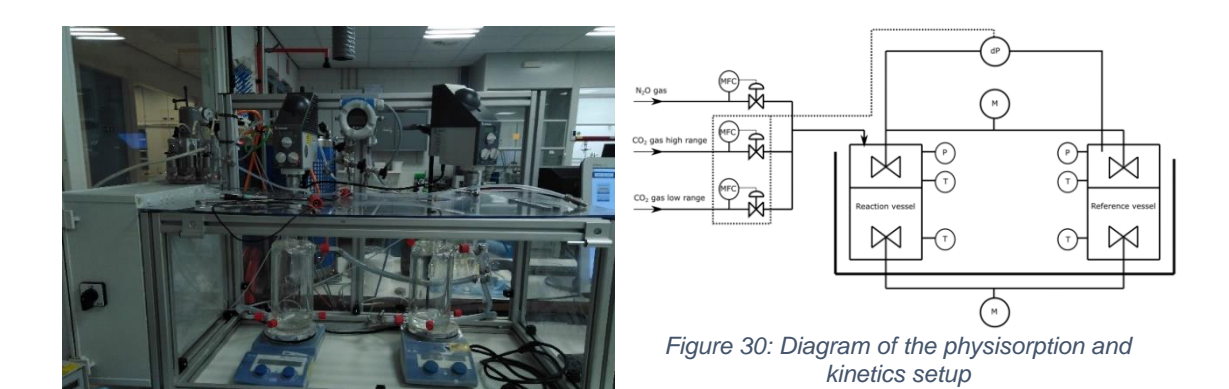


Figure 29: Physisorption and kinetics setup in

TNO

Solubility constant

Due to the fact that CO_2 reacts with amine solutions, its physical solubility cannot be measured directly. Since literature lacks of a precise model to determine the CO_2 solubility the N_2O analogy is applied. This analogy consists on determining experimentally the N_2O solubility in the amine solutions and correlate it with the CO_2 solubility in the same solution using the ratio of solubility of the two gases in water, R_H (41). The constants of Equation (3-3) were obtained from *Monteiro* (41).

$$H_{\text{CO}_2}^{\text{solution}} = \frac{H_{\text{N}_2\text{O}}^{\text{solution}}}{R_H}$$
 (3-2)

$$R_H = e^{175.7732 - \frac{4234.252}{T} - 31.28 \times \ln(T) + 0.05477 \times T}$$
(3-3)

In the methodology used, a certain known volume of N_2O was added. Because of that, the number of molecules dissolved in the liquid phase can be calculated. However, a correction factor between the temperature of the experiment and the normal temperature is needed.

$$n_{\rm N_2O} = n_{\rm N_2O,previous\,step} + p_{\rm normal} \times V_{\rm N_2O} \times \frac{\frac{T_{\rm exp}}{T_{\rm normal}}}{R \times T_{\rm normal}}$$
(3-4)

The N₂O that stayed in the gas phase is related to the pressure increase:

$$n_{N_2O,G} = \frac{p - p_{\text{step 0}}}{R \times T_{\text{exp}}} \times V_G \tag{3-5}$$

Then, the N₂O absorbed by the amine solution is the difference:

$$n_{N_2O,L} = n_{N_2O} - n_{N_2O,G} (3-6)$$

Finally, the N₂O concentration in the liquid phase is obtained:

$$c_{\rm N_2O,L} = \frac{n_{\rm N_2O,L}}{V_{\rm L}} \tag{3-7}$$

Where:

Table 9	Innut to	calculate	the	solubility	constant	of N ₂ O

Symbol	Description	Unit
n_{N_2O}	Total N₂O added	[mol]
$p_{ m normal}$	Normal pressure	[bar]
$V_{\rm N_2O}$	Normal volume of N₂O added	[nL]
$T_{\rm exp}$	Temperature of the experiment	[K]
$T_{ m normal}$	Normal temperature	[K]
$n_{N_2O,G}$	N₂O in the gas phase	[mol]
p	Pressure increase in that step	[bar]
$p_{ m step~0}$	Pressure before adding N₂O	[bar]
$V_{\rm G}$	Gas volume of the vessel	[L]
$n_{ m N_2O,L}$	N₂O in the liquid phase	[mol]
$c_{N_2O,L}$	N ₂ O concentration in the liquid phase	[mol/L]
$V_{ m L}$	Solvent volume in the vessel	[L]

The experiment was done using a solution of 30 wt% TEPA and 70 wt% H_2O at 20 $^{\circ}C$. The stirrers inside each vessel are not designed for viscous fluids. Therefore, the polyamine had to be highly diluted with H_2O , which might have consequences later on.

Reaction rate constant

The kinetic experiments performed in this thesis were conducted in a large excess of amine and H_2O . Consequently, the concentration of both species remained approximately constant throughout the reaction; and the reaction rate can be assumed to be independent on both concentrations (57). This leads to a pseudo-first order reaction, where the kinetic constant is denoted by k_1 .

$$-r_{\mathsf{CO}_2} = k_1 \times [\mathsf{CO}_2] \tag{3-8}$$

However, reactions between CO₂ and H₂O can also occur. In general, the rate of formation of carbonic acid is negligible whereas the rate of formation of bicarbonate may have to be taken into account, depending on the pH of the solution (58).

$$CO_2 + H_2O \leftrightarrow H_2CO_3 \tag{3-9}$$

$$CO_2 + OH^- \leftrightarrow HCO_3^- \tag{3-10}$$

Hence, the CO_2 reaction rate observed in the experiments results from all the reactions taking place in the system, k_{obs} .

$$-r_{\text{CO}_2} = k_2 \times [\text{CO}_2] \times [\text{Amine}] + k_{\text{OH}^-} \times [\text{OH}^-] \times [\text{CO}_2] = k_{\text{obs}} \times [\text{CO}_2]$$
(3-11)

In the pseudo-first order regime the second reaction is assumed to be negligible because it is slower than the first one. It will be explained in Section 5.3.3 why it is assumed that the reaction of CO_2 with the amine takes place in the pseudo-first order regime.

The reaction rate constant is calculated using Equation (3-12). Appendix H shows how this equation is obtained starting from the mass transfer equation using the film theory model (41).

$$k_1 = \frac{(H_{\text{CO}_2} \times k_{\text{obs}})^2}{D_{\text{CO}_2}}$$
 (3-12)

Once k_1 is known, k_2 can be easily obtained:

$$k_2 = \frac{k_1}{[\text{Amine}]} \tag{3-13}$$

There are three parameters to be determined in order to find k_1 : H_{CO_2} , k_{obs} and D_{CO_2} :

- The Henry constant of CO₂ is obtained from the physisorption experiments, as explained before. More information is available in Section 4.2.2.
- The observed reaction rate is obtained from the kinetics experiments. More information is available in Section 4.2.5.
- The diffusion coefficient of CO₂ in the polyamine solution is calculated following several steps:

The diffusivity of CO₂ and N₂O in H₂O was calculated using (59):

$$(D_{\rm CO_2})_{\rm H_2O} = 2.35 \times 10^{-6} \times e^{\frac{-2119}{T}}$$
 (3-14)

$$(D_{\rm N_2O})_{\rm H_2O} = 5.07 \times 10^{-6} \times e^{\frac{-2371}{T}}$$
 (3-15)

The diffusivity of CO₂ in aqueous alkanolamine solutions can be estimated according to a modified Stokes-Einstein type of relation (59):

$$(D_{\text{CO}_2})_{\text{Solution}} = (D_{\text{CO}_2})_{\text{H}_2\text{O}} \times (\frac{\mu_{\text{H}_2\text{O}}}{\mu_{\text{Solution}}})^{0.8}$$
 (3-16)

The experiment was done using a solution of 30 wt% TEPA and 70 wt% H_2O at 20 $^{\circ}C$. The setup was the same as the one used in the physisorption experiments. Hence, the high dilution rate of the polyamine with H_2O , might have consequences later on.

3.3.5. FTIR

These experiments were done at TNO. A Nicolet 6700 spectrometer, coupled with an Attenuated Total Reflectance (ATR) sampling accessory for liquid samples, was used (Figure 31).

As explained before, CO_2 can be absorbed by the amine by two different paths: the zwitterion and the bicarbonate path. The first one does not require H_2O whereas the second does. The objective is to find out which product is being formed: carbamate or bicarbonate.



Figure 31: Nicolet 6700 spectrometer

4 Experimental results and discussion

The purpose of this Chapter is to show and discuss the results from the experiments, which were obtained using the materials and methods described in Chapter 3. The experimental results will be further used during modelling (Chapter 5) and design (Chapter 6).

49 experiments were done and 219 samples were taken collecting 358 data points. There is a lot to be said about this data. This Chapter collects the most important lessons taken learned from the experiments. In Appendix I it is possible to find the data which is still interesting but not the most relevant.

4.1. Plate experiments

Once the layer thickness of the polyamine was around 0.50 mm (as explained in Section 3.1) the absorption experiments started. Firstly, the polyamine was placed inside the climate chamber, to study the absorption of H_2O . Secondly, the polyamine was placed in contact with the air, at lab conditions, to analyse the absorption of both CO_2 and H_2O .

4.1.1. Experiments of H₂O absorption from the air

ZEF Team 3 observed that H_2O was more absorbed than CO_2 . Therefore, it is important to gain more insight regarding H_2O absorption. These experiments were done in order to obtain the H_2O loading in the polyamines and, from that information, the diffusion coefficients of H_2O in the polyamines via modelling (Chapter 5).

The H_2O loading is measured in a titrator, where the sample is added after being diluted with MeOH (as explained in Section 3.3.1). The calculations to subtract the H_2O contained in the MeOH from the H_2O that actually is absorbed by the polyamine are shown in Appendix J.

The H_2O absorption experiments took place inside the climate chamber, where only H2O is absorbed (as explained in Section 3.3.1). PEI experiments were conducted at four different relative humidity (35, 50, 70 and 95%) and for different temperatures (10, 20, 30 and 40 $^{\circ}C$). TEPA experiments were conducted at 20 $^{\circ}C$ varying only the relative humidity.

Figure 32- 35 show the results of the experiments done with the climate chamber. The plots were grouped by the same temperature so the main driving force is the change in H_2O content in the air, and not the viscosity change of the polyamine due to the temperature increase or decrease. Although the data is quite noisy it is possible to see the first order exponential relation between the H_2O concentration and the time.

It is important to note that the solvent changes over time. As stated before (Table 8) both polyamines contain a negligible amount of water. PEI equilibrates with around 30 wt% water. The diffusivity coefficient depends on the composition of the sorbent and temperature. In this case, the dependence with temperature is negligible because all the plots summarize the data at the same temperature. However, the increase in H₂O content changes the composition of the sorbent so there will be different diffusivity

coefficients over time. Therefore, it can be concluded that the diffusivity coefficient varies in time, since the H₂O content inside the polyamine changes as well.

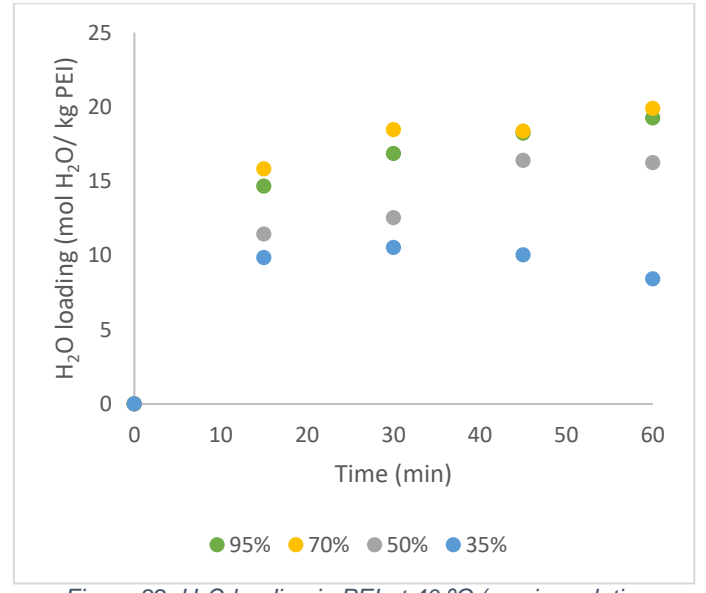


Figure 32: H₂O loading in PEI at 40 °C (varying relative humidity) in the climate chamber

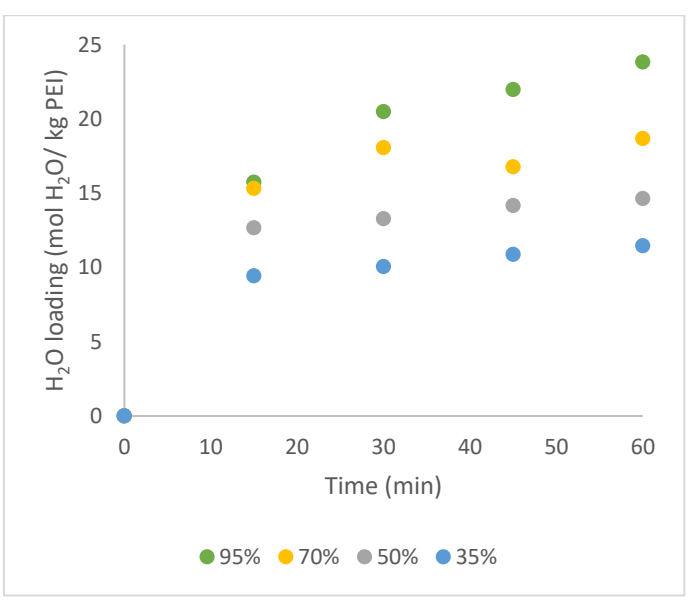


Figure 33: H₂O loading in PEI at 30 °C (varying relative humidity) in the climate chamber

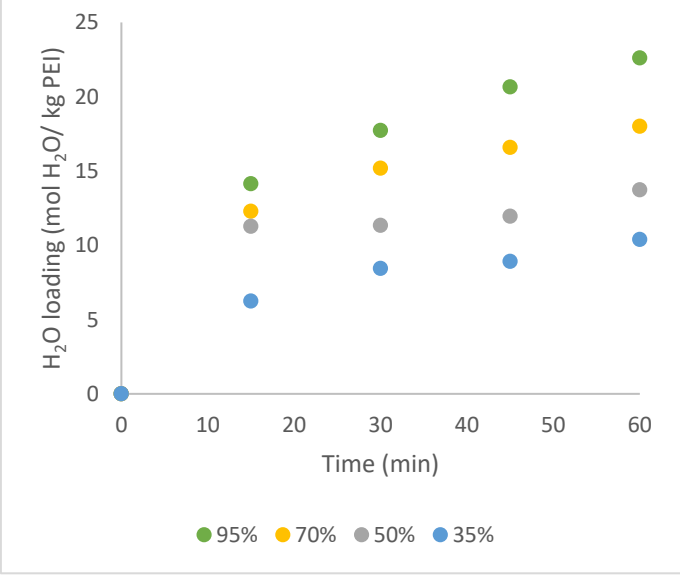


Figure 34: H₂O loading in PEI at 20 °C (varying relative humidity) in the climate chamber

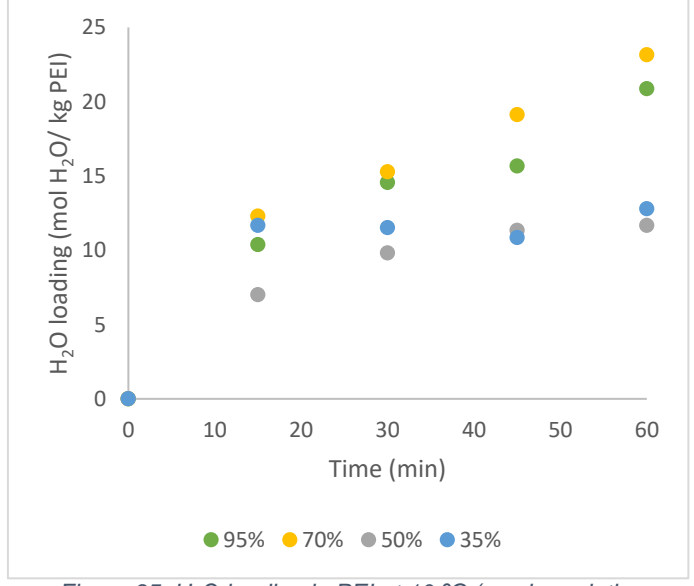


Figure 35: H₂O loading in PEI at 10 °C (varying relative humidity) in the climate chamber

The plots for 20 and 30 $^{\circ}$ C (Figure 33 and 34) show the expected behaviour: higher relative humidity, higher H₂O loading in the PEI. However, this is not the case for the plots of 10 and 40 $^{\circ}$ C (Figure 32 and 35), where the H₂O loading is higher at 70% relative humidity than at 95%. This could be due to the fact that the climate chamber was forced to work at two extreme conditions for both temperature and relative humidity and, each time the door was opened, the relative humidity and the temperature in the chamber got influenced by the outside conditions.

Figure 38 shows that the H_2O content in PEI depends on the H_2O partial pressure in the air.

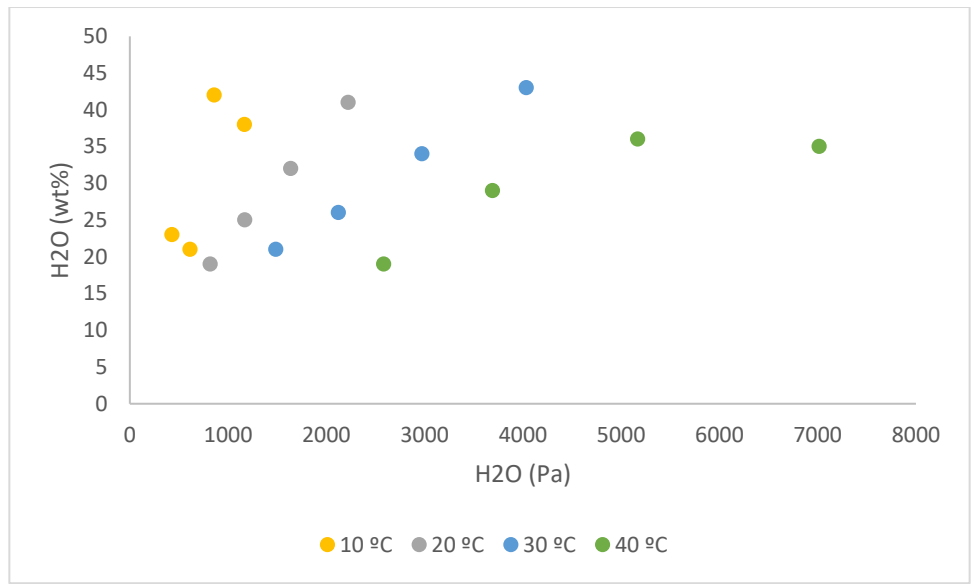


Figure 36: H₂O loading in PEI vs. H₂O in the air (climate chamber experiments)

The experimental data has an average value:

$$m_{\rm H_2O,PEI} (wt\%) = 30$$

Due to the focus in the research, TEPA behaviour was only studied at 20 $^{\circ}$ C. Figure 37 shows that the experiment done at 70% relative humidity shows unexpected results for the first two points, 15 and 30 minutes, because the H₂O is lower than at 50% relative humidity, which does not follow the expected trend of the other RH.

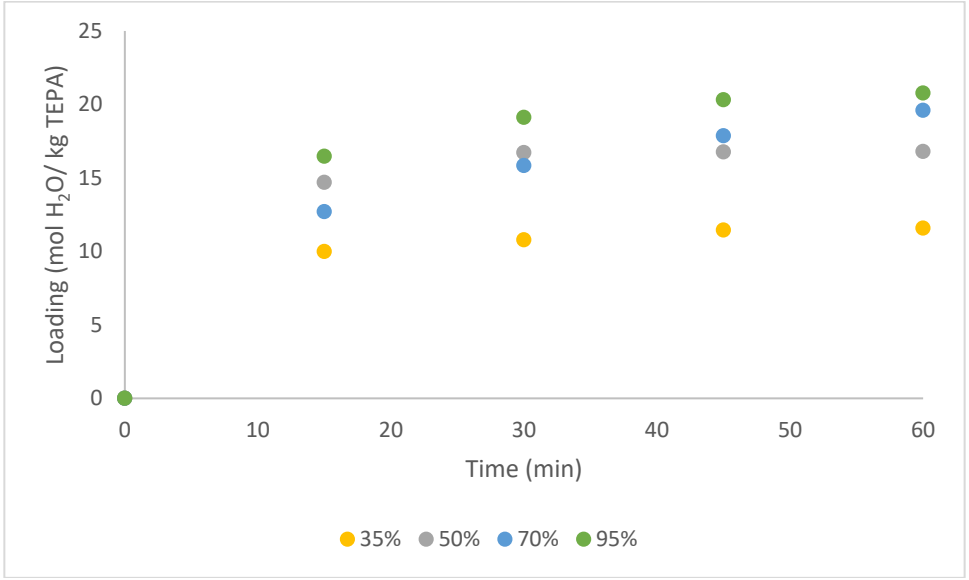


Figure 37: H₂O loading in TEPA at 20 °C (varying relative humidity) in the climate chamber

The experimental data has an average value:

$$m_{H_2O,TEPA}$$
 (wt%) = 23

The main conclusion from this Section is that, although the data is quite noisy and different trends can be identified, it is possible to find an average value of H_2O content in PEI of 30 wt% and in TEPA of 23 wt%. It might be interesting to perform more

experiments inside the climate chamber for TEPA at different temperatures, in order to find a more accurate average value.

4.1.2. Experiments of CO₂ and H₂O absorption from the air

The air capture tests were done varying different process conditions in order to get more insight on the CO_2 and H_2O loadings of the polyamines. This is why this section is divided per type of variation done: the first type corresponds to variations done in the sorbent itself, this is, changing the layer thickness of the polyamine, blending both polyamines and premixing each polyamine with H_2O . Then, the CO_2 ppm in the air were varied. Two parameters, being the main one the CO_2 loading, will be used to evaluate the performance of the sorbent in each variation:

- CO₂ loading: This parameter represents the CO₂ absorbed.
- H₂O loading: This parameter represents the H₂O absorbed. This parameter can be interesting for the desorption part, but this is not the focus of this thesis.

Variations done in the sorbent

Varying the layer thickness of the polyamine

The layer thickness of the polyamine is an important factor because it has a great influence on the residence time if the polyamine flows, which is what will be designed in Chapter 6. CO_2 and H_2O absorption experiments were done at three different layer thicknesses: 0.25, 0.50 and 0.75 mm.

Results of TEPA with a layer thickness of 0.75 mm might not be accurate enough because the fan displaced the layer of TEPA due to its low viscosity, as Figure 38 shows.



Figure 38: Layer of TEPA displaced by the fan

Figure 40, 42 and 44 show the H_2O and CO_2 loading for different layer thicknesses of PEI whereas Figure 39, 41 and 43 show the H_2O and CO_2 loading for different layer thicknesses of TEPA.

CHAPTER 4. EXPERIMENTAL RESULTS AND DISCUSSION

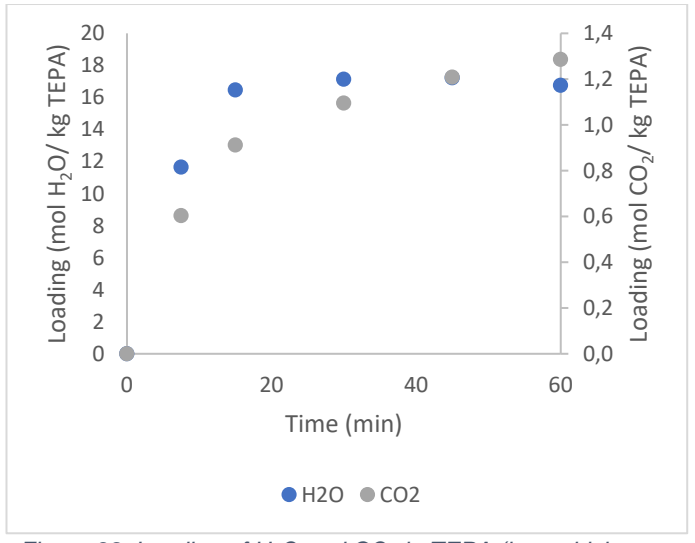


Figure 39: Loading of H₂O and CO₂ in TEPA (layer thickness of 0.25 mm) in contact with air

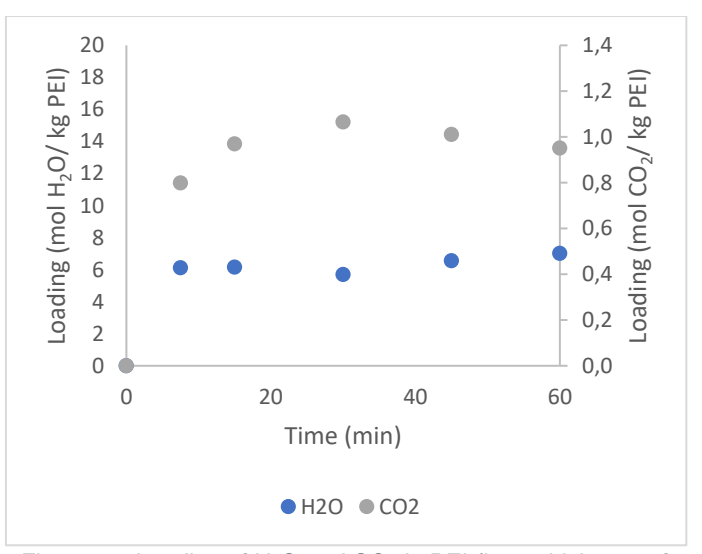


Figure 40: Loading of H₂O and CO₂ in PEI (layer thickness of 0.25 mm) in contact with air

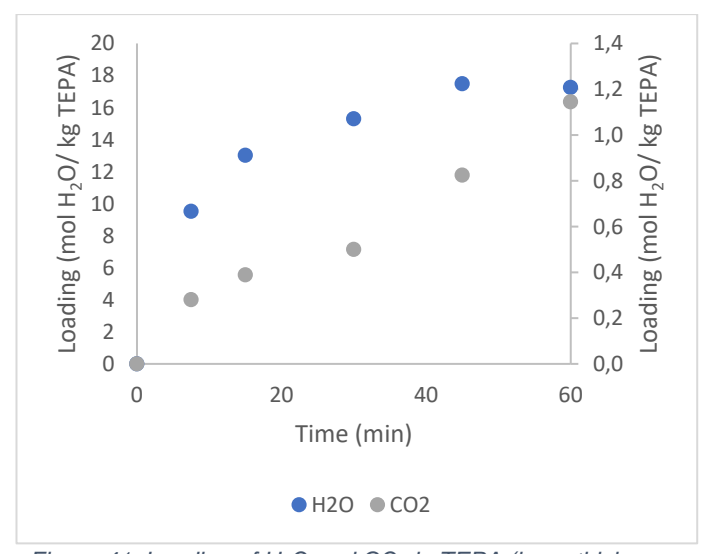


Figure 41: Loading of H_2O and CO_2 in TEPA (layer thickness of 0.50 mm) in contact with air

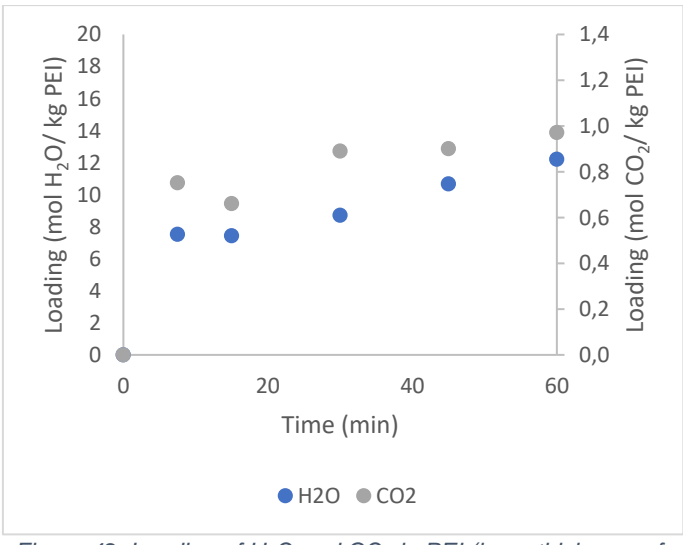


Figure 42: Loading of H₂O and CO₂ in PEI (layer thickness of 0.50 mm) in contact with air

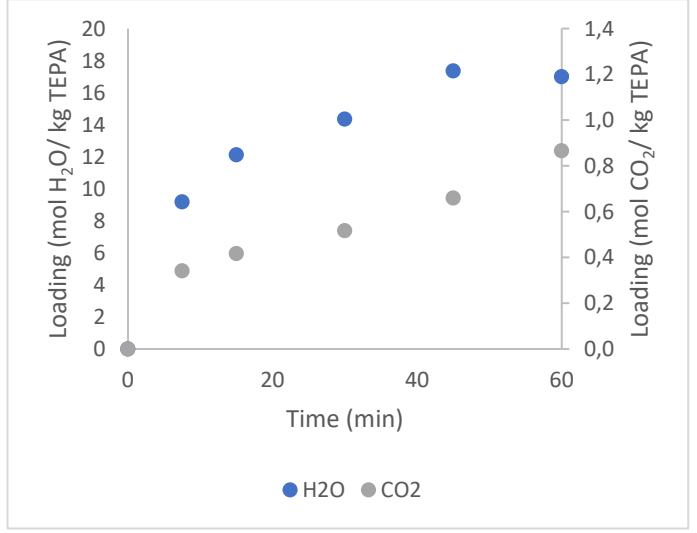


Figure 43: Loading of H₂O and CO₂ in TEPA (layer thickness of 0.75 mm) in contact with air

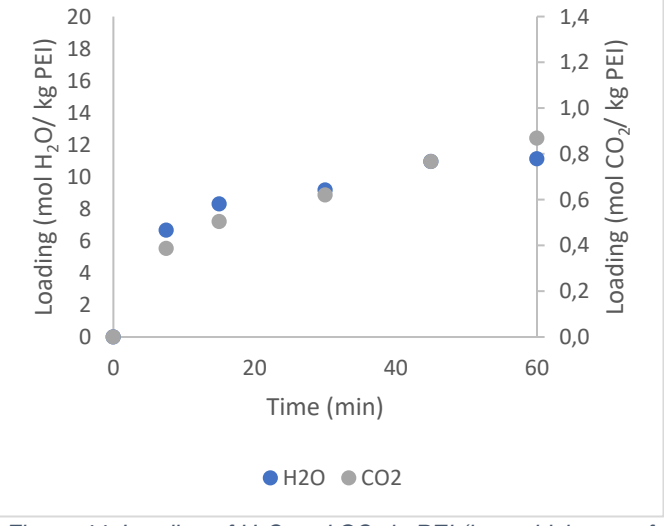
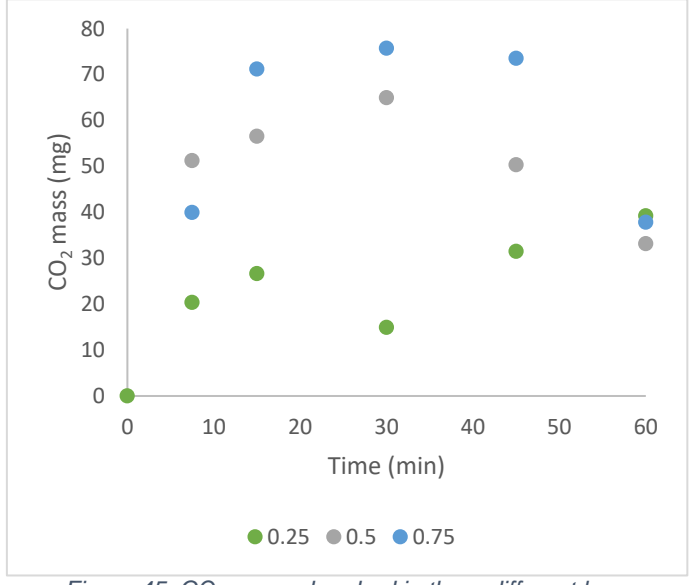


Figure 44: Loading of H₂O and CO₂ in PEI (layer thickness of 0.75 mm) in contact with air

Figures 45 and 46 show that the layer thickness becomes unimportant after 60 minutes, since the CO₂ mass absorbed becomes similar.



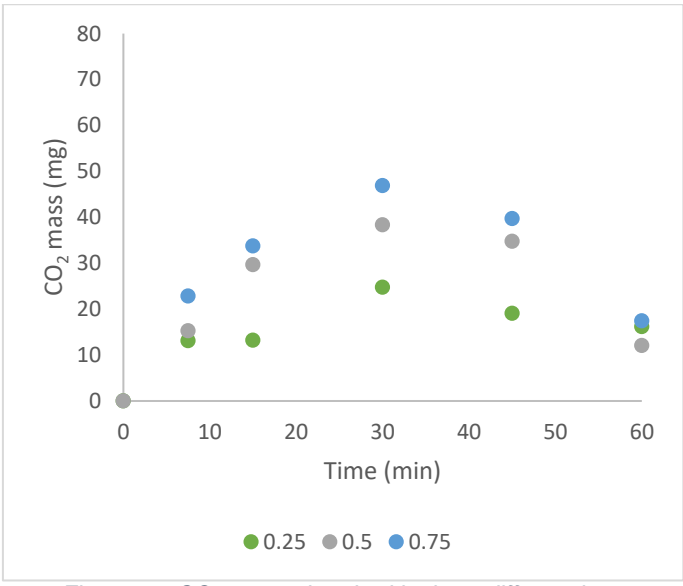


Figure 45: CO₂ mass absorbed in three different layer thicknesses of PEI

Figure 46: CO₂ mass absorbed in three different layer thicknesses of TEPA

These results are surprising. As it will be detailed explained in Section 5.3.3., the CO_2 absorption process is assumed to be diffusion limited since the Hatta number is high. According to this assumption, the CO_2 mass at the beginning of the experiments should be the same for different layer thicknesses. Hence the curves of Figures 45 and 46 should have a shape similar to Figure 47.

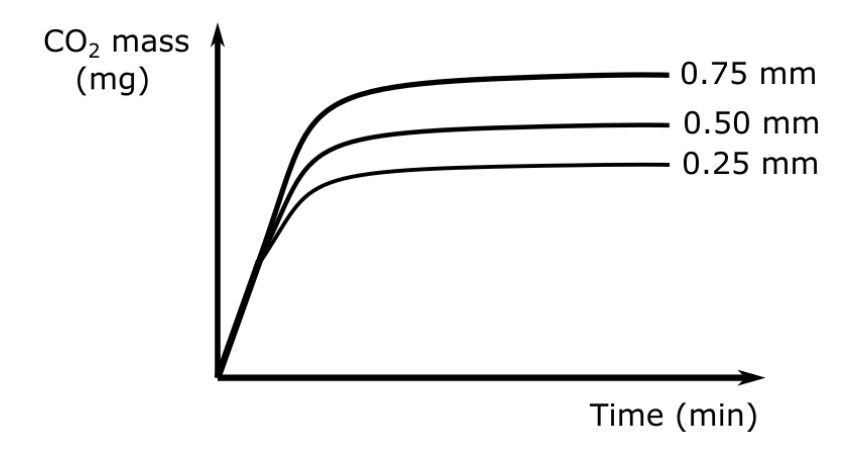


Figure 47: CO₂ mass absorbed in three different layer thickness if the Hatta number is high

This could be due to the fact that there is a missing point at the beginning of the experiment, this is, before 7.5 minutes, where actually the CO₂ mass of the different layer thicknesses is the same. Another possibility might be that the assumption made for the Hatta number is only valid until a certain loading. Then, when that loading is achieved, the Hatta number will go down and the process will become reaction limited. Kinetics will decrease because the active groups of the polyamines will get fuller and fuller. This implies that the reaction rate constant changes in time and that the Hatta number calculated in Section 5.3.3. is the highest one. However, for this thesis, given the fact that there is no kinetic data available, it is assumed that the reaction rate

constant does not depend on time. It is recommended that kinetic data should be collected at different loadings in order to check if the CO₂ absorption process varies from being diffusion to reaction-limited.

Table 10 shows the CO_2 and H_2O loadings of the different sorbents. TEPA absorbs more H_2O and CO_2 than PEI. The experiments performed with a layer thickness of 0.25 mm seem not correct since both CO_2 and H_2O loadings have different values than 0.5 and 0.75 mm. This could be due to the fact that PEI and TEPA might have penetrated into the paper.

Table 10: Lab conditions and CO₂ and H₂O loadings of layer thickness experiments

LT	0.25 mm		0.5	mm	0.75 mm	
Sorbent	TEPA	PEI	TEPA	PEI	TEPA	PEI
Relative humidity (%)	50	33	51	38	54	39
Temperature (°C)	20	19	20	20	19	19
CO ₂ loading (mol CO ₂ / kg sorbent)	1.3	1.0	1.1	1.0	0.9	0.9
H ₂ O loading (mol H ₂ O/ kg sorbent)	16.8	7.0	17.3	12.2	17.0	11.1

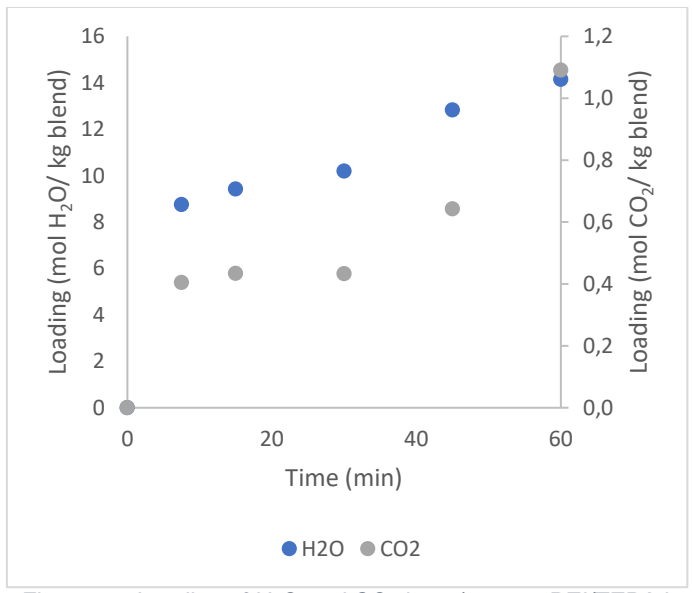
The rest of the experiments will be done with a layer thickness of 0.5 mm because a layer thickness of 0.50 mm was easier to achieve and to work with when removing the samples and also because that was the chosen layer thickness when doing the experiments in the climate chamber.

It can be concluded that the CO₂ loading and mass in both TEPA and PEI remain quite constant for different layer thicknesses after 60 minutes.

Blends of PEI and TEPA

The field of research of CO₂ absorption in bulk polyamines is quite new so it seemed interesting to blend PEI and TEPA and analyse their behaviour with respect to CO₂ and H₂O loading. These experiments were done with 25/75 wt% PEI/TEPA, 50/50 wt% PEI/TEPA and 75/25 wt% PEI/TEPA.

Figure 48- 50 show the H₂O and CO₂ loading for different blends of PEI and TEPA.



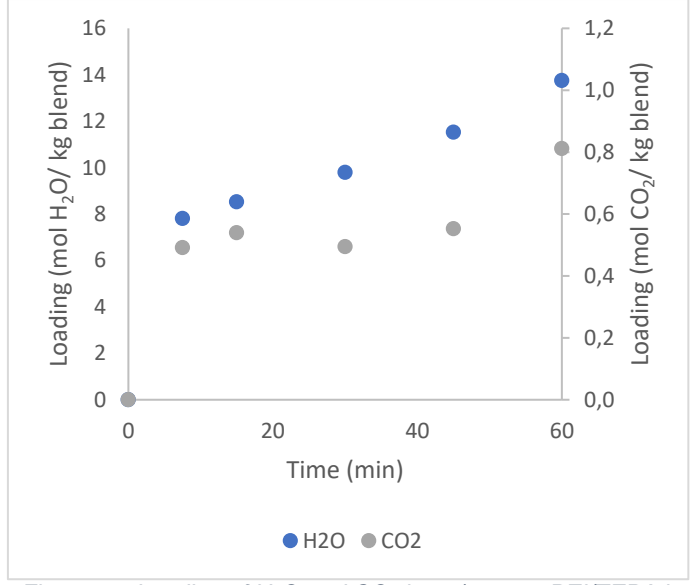


Figure 48: Loading of H₂O and CO₂ in 25/75 wt% PEI/TEPA in contact with air

Figure 49: Loading of H₂O and CO₂ in 50/50 wt% PEI/TEPA in contact with air

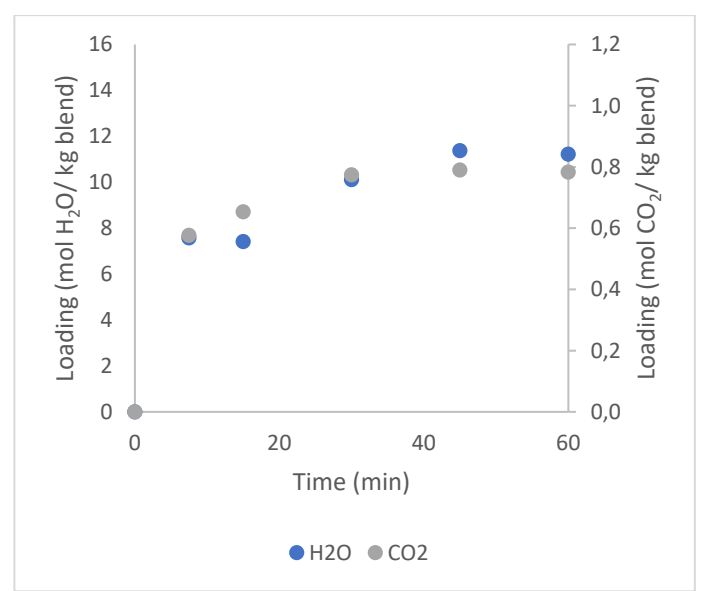


Figure 50: Loading of H₂O and CO₂ in 75/25 wt% PEI/TEPA in contact with air

Previous experiments show that TEPA has a higher CO_2 and H_2O loading than PEI. Therefore, it is expected that the blends with more content of TEPA will capture more CO_2 and H_2O , which is what Table 11 shows.

Pure TEPA and pure PEI results belong to the previous experimental variation (0.5 mm layer thickness). Pure TEPA has a higher CO₂ loading than the three blends.

Tahla 11. Lah	conditions	and CO ₂ and H.	20 Inadina	of bland	avnarimente
Table II. Lab	COHUITIONS		20 10001119	OI DIGITA	CAPCITITIONS

Sorbent	0P	25P	50P	75P	100P
Relative humidity (%)	51	42	43	43	38
Temperature (°C)	20	19	20	19	20
CO ₂ loading (mol CO ₂ / kg sorbent)	1.1	1.1	0.8	0.8	1
H ₂ O loading (mol H ₂ O/ kg sorbent)	17.3	14.1	13.8	11.2	12.2

CHAPTER 4. EXPERIMENTAL RESULTS AND DISCUSSION

The main conclusion is that blends do not seem to offer better performance than pure TEPA.

Preloaded polyamine with H₂O

This variation was done in order to test whether premixing H_2O with the polyamines influences the CO_2 capture process. H_2O was added to PEI and TEPA in three different amounts: 10, 20 and 30 wt%.

Figures 51, 53 and 55 show the CO_2 and H_2O loading of TEPA preloaded with different contents of H_2O . Figures 52, 54 and 56 show the CO_2 and H_2O loading of PEI preloaded with different contents of H_2O .

CHAPTER 4. EXPERIMENTAL RESULTS AND DISCUSSION

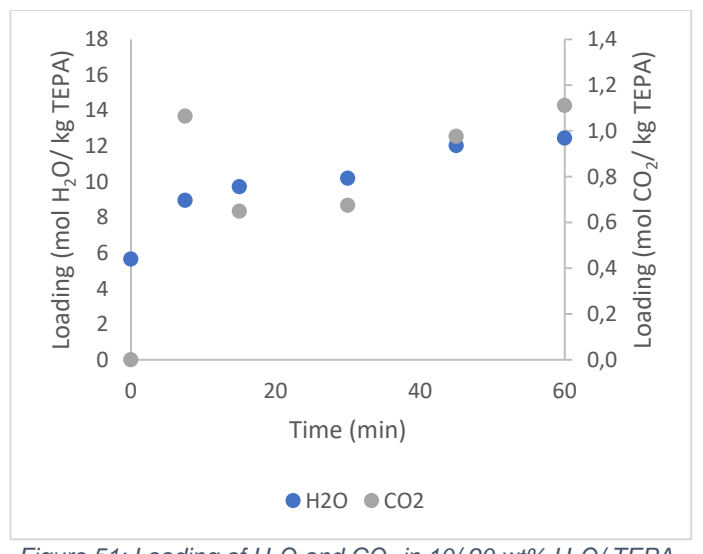


Figure 51: Loading of H₂O and CO₂ in 10/90 wt% H₂O/ TEPA in contact with air

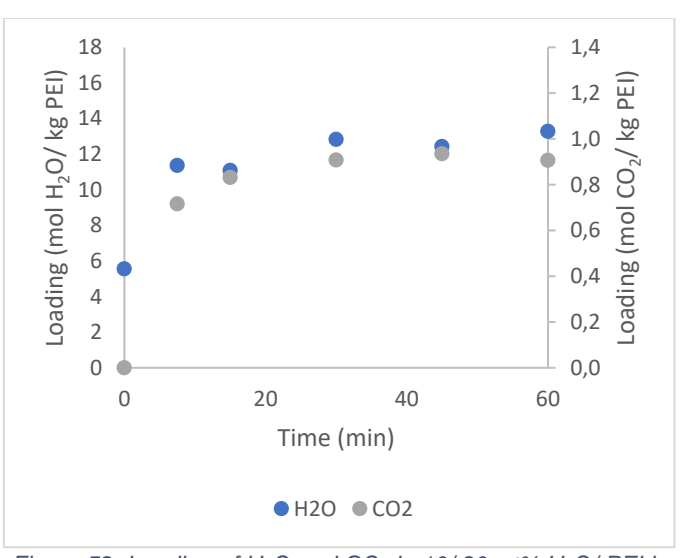


Figure 52: Loading of H₂O and CO₂ in 10/90 wt% H₂O/PEI in contact with air

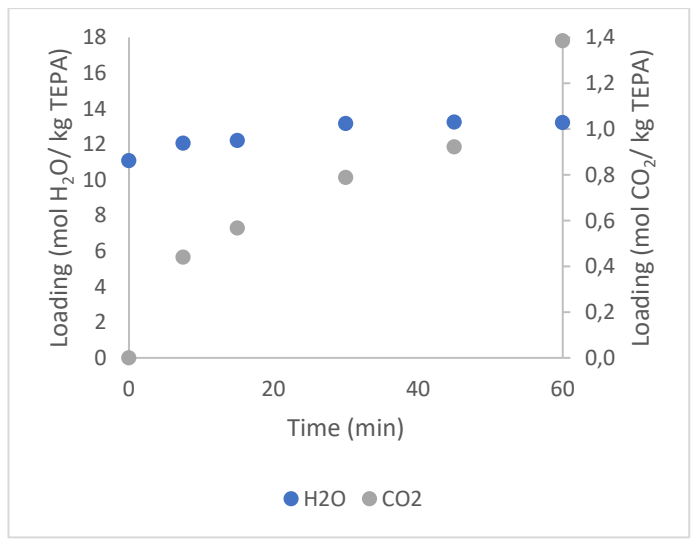


Figure 53: Loading of H₂O and CO₂ in 20/80 wt% H₂O/ TEPA in contact with air

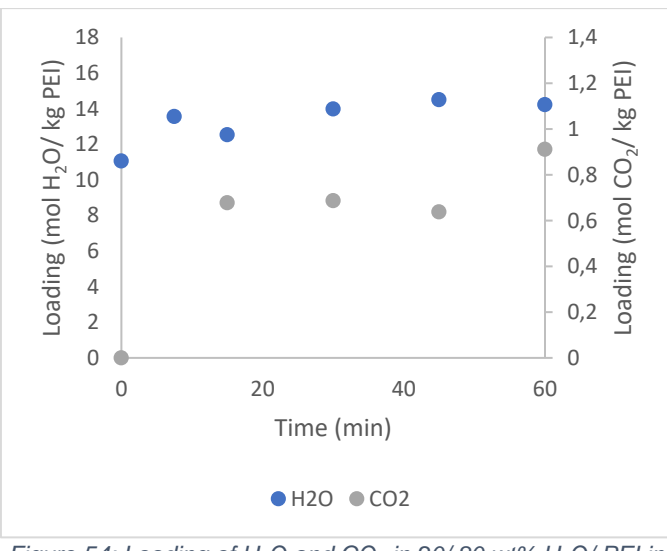


Figure 54: Loading of H₂O and CO₂ in 20/80 wt% H₂O/PEI in contact with air

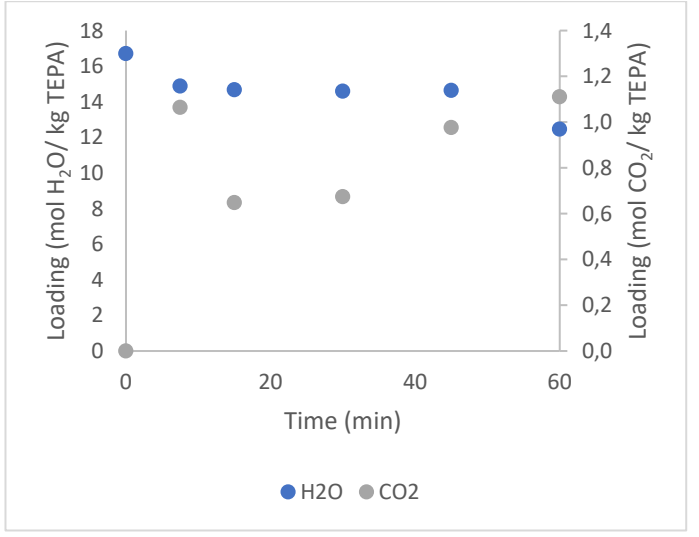


Figure 55: Loading of H₂O and CO₂ in 30/70 wt% H₂O/TEPA in contact with air

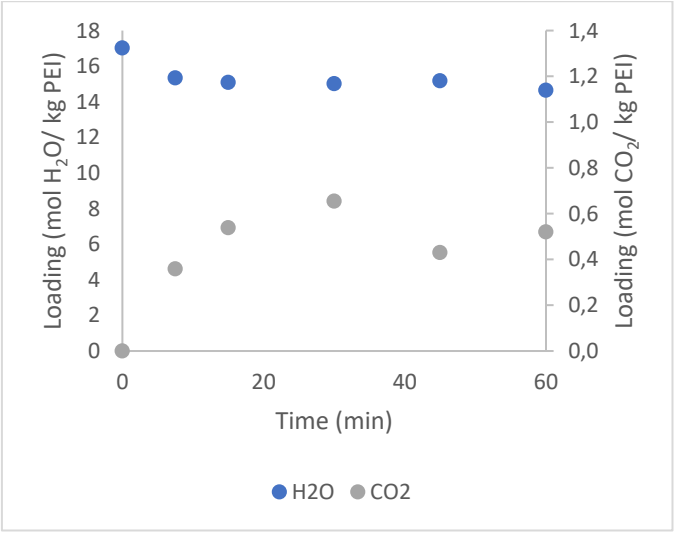


Figure 56: Loading of H₂O and CO₂ in 30/70 wt% H₂O/ PEI in contact with air

Figure 55 and 56 show that the H_2O loading in TEPA and PEI decreases. This is because H_2O was evaporating from the polyamine solution because the amount of H_2O in the gas phase is lower and not because of reactions. On the other hand, for 10 and 20 wt% of H_2O (Figure 51- 54), the polyamine kept absorbing even more H_2O .

Table 12 shows the CO_2 and H_2O loadings of TEPA and PEI preloaded with H_2O . It can be seen that TEPA solutions show better results than PEI, since the CO2 loading is higher, from the absorption point of view.

Table 12: Lab conditions and CO₂ and H₂O loadings of solution experiments

H ₂ O content (wt%)	1	10	20		30	
Sorbent	TEPA	PEI	TEPA	PEI	TEPA	PEI
Relative humidity (%)	35	43	38	44	38	45
Temperature (°C)	19	19	19	19	19	19
CO ₂ loading (mol CO ₂ / kg sorbent)	1.1	0.9	1.4	0.9	1.3	0.5
H ₂ O loading (mol H ₂ O/ kg sorbent) at the beginning	5.7	5.6	11.1	11.1	16.7	17.0
H ₂ O loading (mol H ₂ O/ kg sorbent)	12.5	13.3	13.2	14.2	12.5	14.6

Table 13 shows a comparison between the CO₂ and H₂O loadings at 60 minutes between preloaded polyamine with H₂O and pure polyamine.

Table 13: Comparison pure polyamine vs polyamine preloaded with H₂O

rable to: Companion pare polyanime ve polyanime preseased with the					
H ₂ O content (wt%)	0	20	0	30	
Sorbent	TEPA			PEI	
Relative humidity (%)	51	38	38	45	
Temperature (°C)	20	19	20	19	
CO ₂ loading (mol CO ₂ / kg sorbent)	1.1	1.4	1.0	0.5	
H ₂ O loading (mol H ₂ O/ kg sorbent) at the beginning	0	11.1	0	17.0	
H ₂ O loading (mol H ₂ O/ kg sorbent)	17.3	13.2	12.2	14.6	

The main conclusion is that if the premixed H_2O concentration is increased then the CO_2 loading is higher for TEPA and lower for PEI. This might be because PEI contains primary, secondary and tertiary amines whereas TEPA contains only primary and secondary.

Varying the CO₂ concentration of the air

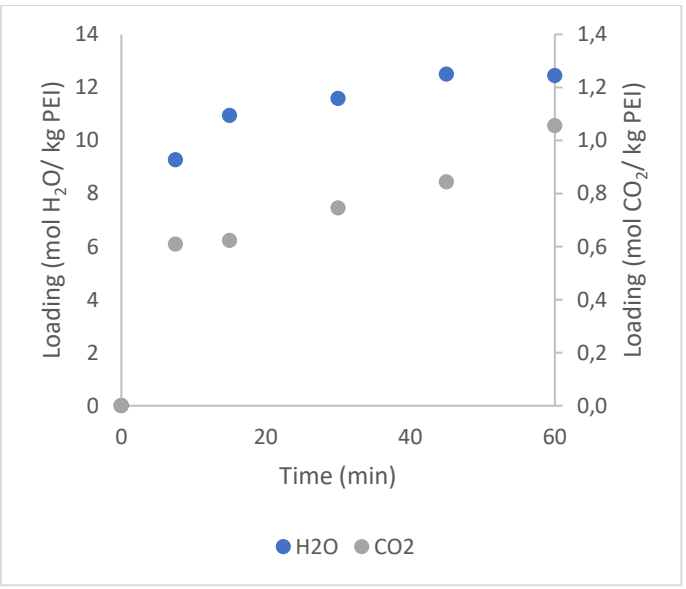
Varying the CO_2 concentration on the air is an interesting experiment since it gives more insight regarding the influence of the driving force in the CO_2 absorption process. The CO_2 concentration in the air was varied from around 400 ppm to 800 and 1200. Also, the change in the CO_2 loading was studied in pure and preloaded with H_2O polyamines.

However, before starting the experiments, it was needed to calibrate the CO₂ ppm distribution inside the setup. The calibration is shown in Appendix K.

In this batch, two fans were used, one working at 4.5 V and another at 5 V. In order to enhance the mixing of the CO₂ coming from the MFC and the air from the lab, the fans blew air over the polyamine.

Pure polyamine

Figures 57 and 58 show the H_2O and CO_2 loadings in PEI in contact with air with different CO_2 concentrations. The data obtained from the experiments done with TEPA at 800 and 1200 ppm is very inconsistent since the CO_2 loading decreased when the CO_2 ppm in the air increased. Therefore, these results are moved to Appendix I.



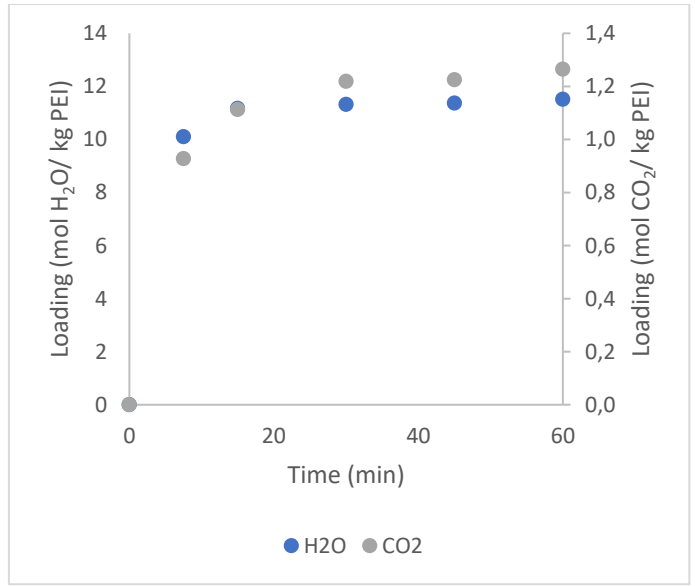


Figure 57: Loading of H₂O and CO₂ in PEI in contact with air (800 ppm of CO₂)

Figure 58: Loading of H₂O and CO₂ in PEI in contact with air (1200 ppm of CO₂)

Table 14 show that even though the CO₂ concentration in the air was doubled and tripled, the CO₂ loading in the polyamine did not increase in the same way (400 ppm results correspond to PEI with a layer thickness of 0.5 mm).

Table 14: Lab conditions and CO₂ and H₂O loadings of PEI in contact with higher CO₂ concentrations

CO ₂ concentration in the air	400	800	1200
Sorbent	PEI	PEI	PEI
Relative humidity (%)	38	42	40
Temperature (°C)	20	19	19
CO2 ppm	-	853	1124
CO ₂ loading (mol CO ₂ / kg sorbent)	1.0	1.1	1.3
H ₂ O loading (mol H ₂ O/ kg sorbent)	12.2	12.4	11.5

Figure 59 shows that the CO₂ loading does not have a huge impact on the H₂O loading, since it is quite stable.

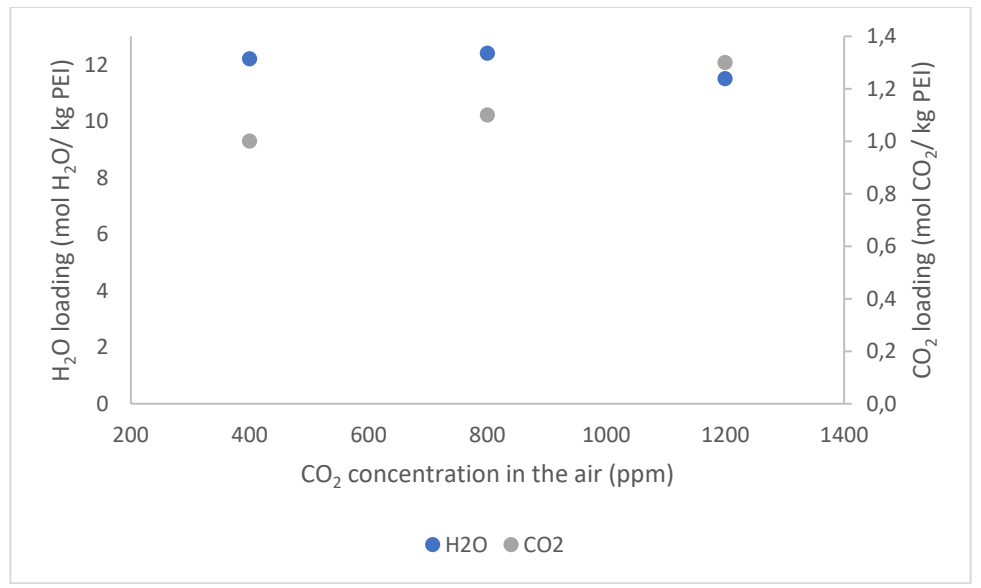


Figure 59: H₂O and CO₂ loading in PEI compared to CO₂ concentration in the air

It can be concluded that, if the CO₂ concentration in the air is increased by a factor of 2 or 3, the CO₂ loading inside the PEI only increases by a factor of 1.09 or 1.30 respectively. It is recommended to repeat this same experiment using TEPA in order to check if TEPA shows the same behaviour as PEI.

Preloaded polyamine with H₂O

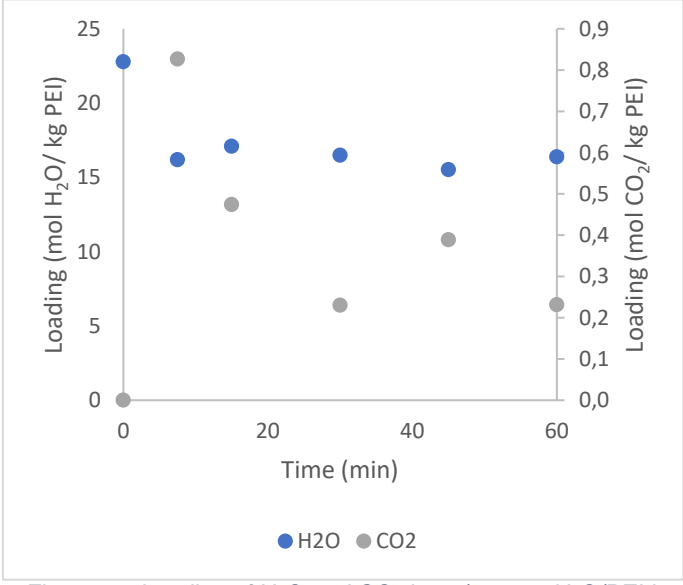
This experiment was done in order to check the effect of H₂O premixed in the polyamine in the CO₂ loading if the driving force is varied. Just like in the previous experiment the CO₂ content in the air was varied to 800 and 1200 ppm.

Since 10, 20 and 30 wt% were already tried, it was proposed to premix the polyamine with 40 wt% H_2O . An unexpected phenomenon took place while the experiment with TEPA loaded with 40 wt% of H_2O was performed. The sample crystallized after 30 minutes making it impossible to collect the sample at minute 45 (Figure 60). This phenomenon was observed by Ova (60) and Sinha (54) as well. Then, it was decided to repeat the experiment premixing the TEPA with 30 wt% of H_2O . It is surprising that 40/60 wt% H_2O / TEPA becomes a solid whereas 30/70 wt% does not.



Figure 60: TEPA solution dried on the plate

Figures 61 and 62 show that the H_2O loading inside the polyamine decreases because H_2O was evaporating from the polyamine solution. The data obtained from the experiments done with TEPA premixed with H_2O at 800 and 1200 ppm is very inconsistent since the CO_2 loading decreased when the CO_2 ppm in the air increased. Therefore, these results are moved to the Appendix I.





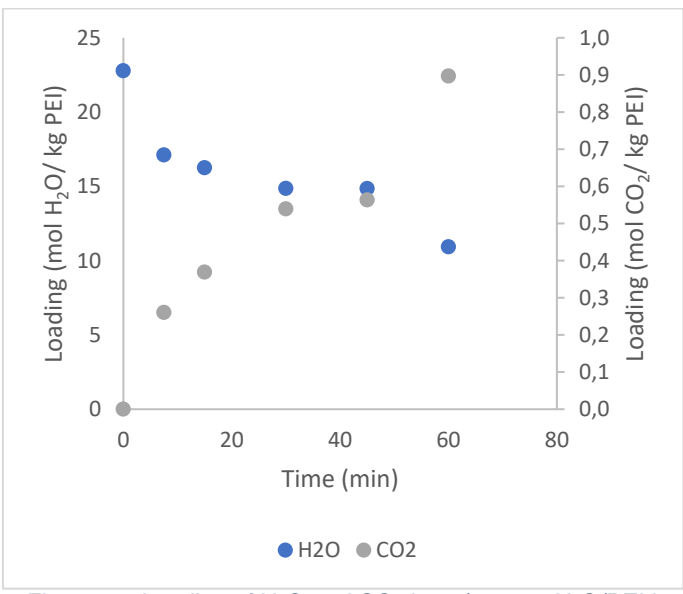


Figure 62: Loading of H₂O and CO₂ in 40/60 wt% H₂O/PEI in contact with air (1200 ppm)

Table 15 shows that the CO_2 loading increases by a factor of 3.91 from 800 to 1200 ppm for PEI. This huge increase might be due to the fact that there is a lot of noise of the data points collected at 800 ppm for PEI (Figure 61). The CO_2 loading of the base case for 400 ppm, 30/70 wt% H_2O/PEI , is higher so it is assumed that the CO_2 loading at 800 ppm is not consistent and the one at 1200 ppm is.

Table 15: Lab conditions and CO₂ and H₂O loadings of PEI premixed with H₂O in contact with higher CO₂ concentrations

CO ₂ concentration in the air	400	800	1200
H ₂ O content (wt%)	30	40	40
Sorbent		PEI	
Relative humidity (%)	45	39	39
Temperature (°C)	19	20	20
CO2 ppm	-	812	1142
CO ₂ loading (mol CO ₂ / kg sorbent)	0.5	0.2	0.9
H ₂ O loading (mol H ₂ O/ kg sorbent)	17.0	22.8	22.8
at the beginning			
H ₂ O loading (mol H ₂ O/ kg sorbent)	14.6	16.4	10.9

Table 16 shows that the kinetics of the CO₂ uptake might not be influenced by the addition of H₂O to the polyamine before starting the experiment.

1200 1200 CO₂ concentration in the air 400 400 H₂O content (wt%) 0 30 0 40 PEI Sorbent 40 Relative humidity (%) 38 44 39 Temperature (°C) 19 19 20 20 CO₂ ppm 1124 --1142 CO₂ loading (mol CO₂/ kg sorbent) 1.0 0.5 1.3 0.90 H2O loading (mol H2O/ kg sorbent) 0 0 17.0 22.8 at the beginning 12.2 H2O loading (mol H2O/ kg sorbent) 14.6 11.5 10.9

Table 16: CO₂ loading in premixed PEI with H₂O and pure PEI

Figure 63 shows that the CO_2 loading in pure PEI and PEI preloaded with H_2O follows a similar trend. However, PEI absorbs less CO_2 when premixed with H_2O , which was also observed in previous experiments.

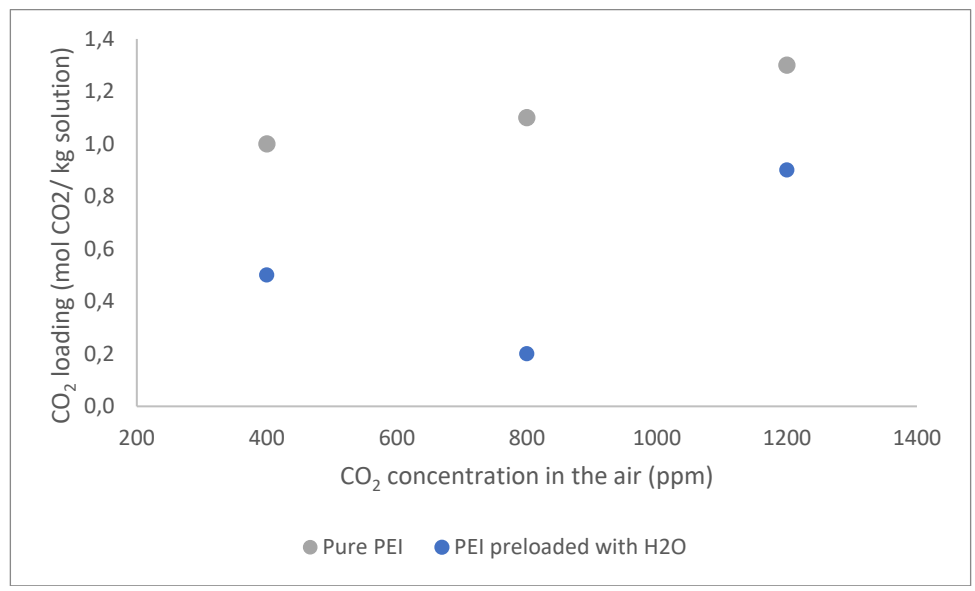


Figure 63: Comparison of CO₂ loading in pure PEI and PEI preloaded with H₂O

It can be concluded that when the CO_2 concentration in the air is increased by a factor of 3 (from 400 to 1200 ppm), the CO_2 loading inside the PEI only increases by a factor of 1.73. This behaviour is similar to the one observed when no H_2O was added to the polyamine.

The main conclusion of this section is that the layer thickness of the polyamine plays an important role for CO_2 loading and mass before 60 minutes. This is of relevance for the final design of the continuous absorber because the layer thickness influences the velocity of the polyamine. Blends do not seem to offer better CO_2 loadings than pure TEPA. Preloading TEPA with H_2O seems to increase the CO_2 loading. On the other hand, preloading PEI with H_2O does the opposite. This is of relevance for the design of the continuous absorber since not all the H_2O will be desorbed. Hence, there will be H_2O present in the polyamine.

4.2. Constants needed for modelling

The solubility and the reaction constants of CO_2 are required to develop the CO_2 absorption model. They will be measured experimentally, as explained in Section 3.3.4. The viscosity values of the polyamine solutions used in the experiments are needed as well.

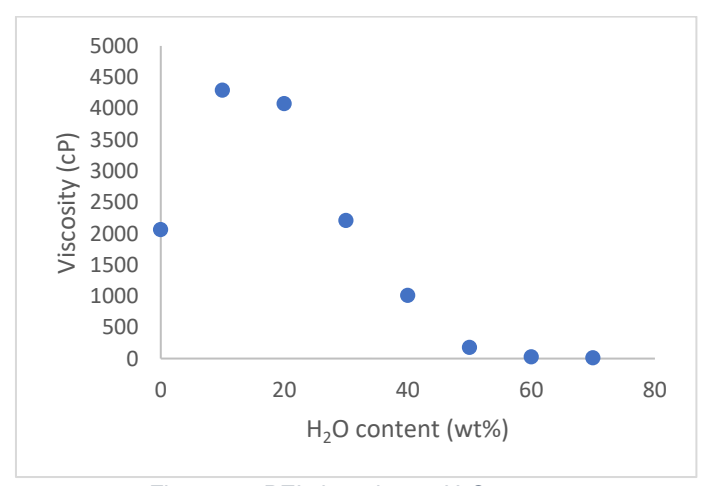
4.2.1. Viscosity

Table 17 shows the results of the viscosity measurements.

Table 17: Viscosity measurements

PEI	TEPA	H ₂ O	Viscosity at ~20 °C (cP)
100	0	0	2060.9
30	0	70	14.8
40	0	60	40.4
50	0	50	177.3
0	100	0	64.1
0	30	70	10.1
0	40	60	10.3
0	50	50	17.5

Figures 64 and 65 show the variation of the viscosity of PEI and TEPA if the H_2O content is changed. The viscosity values from 10 to 40 wt% H_2O content were measured in a Contraves low shear 40 by Sinha (54). For both polyamines, the viscosity increases till it reaches a maximum at 10 wt% H_2O for PEI and 30 wt% for TEPA respectively. Viscosity effects are a function of interactions of all kind of molecules.



450 400 350 Viscosity (cP) 300 250 200 150 100 50 0 20 40 60 80 H₂O content (wt%)

Figure 64: PEI viscosity vs. H₂O content

Figure 65: TEPA viscosity vs. H₂O content

The changes in viscosity due to H_2O addition are one of the key parameters to be taken into account when designing the continuous absorber, especially for PEI. This is because the viscosity will change while the polyamine is flowing since it will absorb H_2O .

4.2.2. Solubility constant

Henry's law states that the amount of dissolved gas in a liquid is proportional to its partial pressure above the liquid. PEI and TEPA absorb both CO₂ and H₂O, hence they will have different solubility constants.

Solubility constant of H2O

Equation (4-1) shows that the solubility constant depends on the partial pressure of H_2O in the gas phase and on the H_2O concentration in the liquid phase.

$$H_{H_2O} = \frac{p_{H_2O}}{c_{H_2O}} \tag{4-1}$$

The partial pressure of H_2O can be calculated using Equation (4-2). Both relative humidity and temperature inside the climate chamber were varied, which changes the partial pressure of H_2O .

$$p_{H_2O} = \frac{RH(\%)}{100} \times p_{H_2O,sat}$$
 (4-2)

Figure 66 shows the relationship between water saturation pressure and temperature (61).

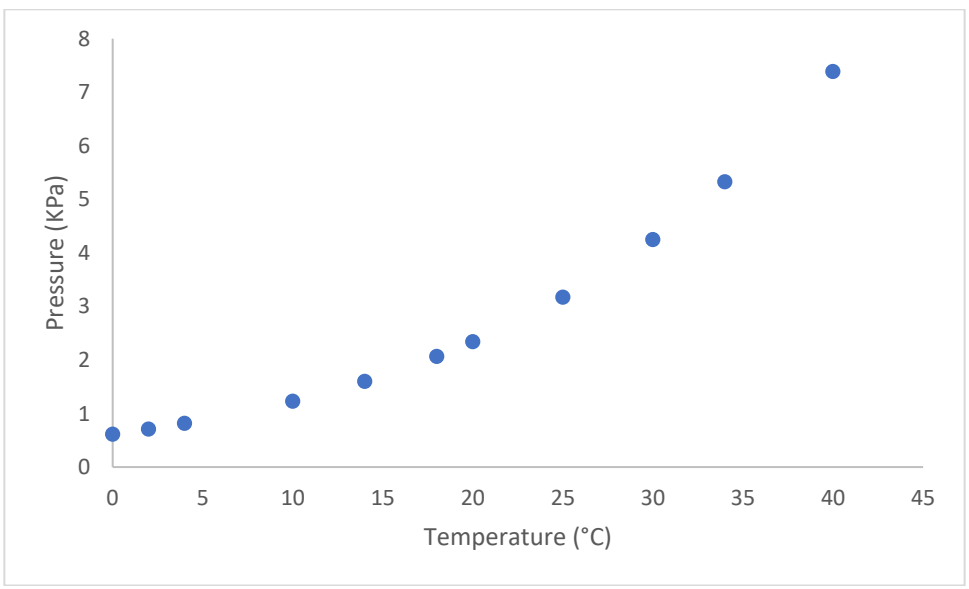
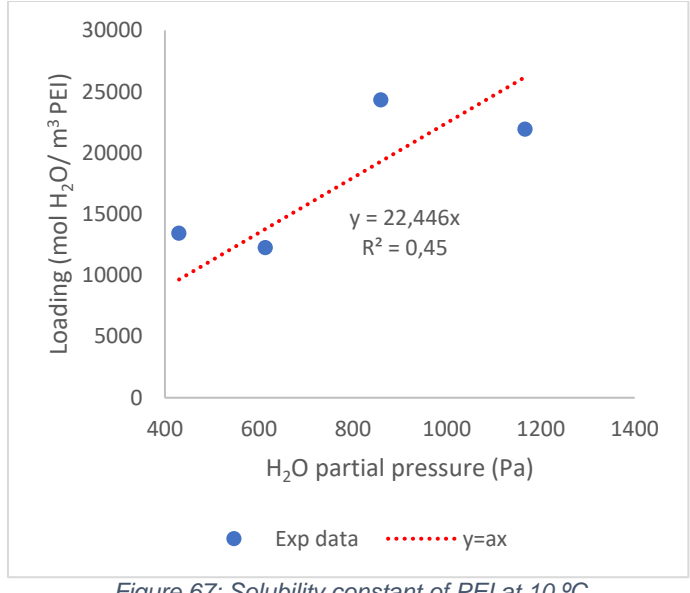


Figure 66: Water saturation pressure vs. temperature

The H_2O concentration was obtained experimentally, it is the H_2O loading measured on the titrator (Section 3.2.1). The H_2O loading used corresponds to the data point at 60 minutes from the climate chamber experiment, where pure PEI and TEPA absorb only H_2O .

With this information, the solubility constant can be obtained. The solubility constant at 10 and 40 °C (Figure 67 and 70) might not be accurate enough (R² values are quite low). This could be due to the fact that the extreme operating conditions might have affected negatively the performance of the climate chamber. However, the solubility constant at 20 and 30 °C (Figure 68 and 69) show a linear trend, as expected.

CHAPTER 4. EXPERIMENTAL RESULTS AND DISCUSSION



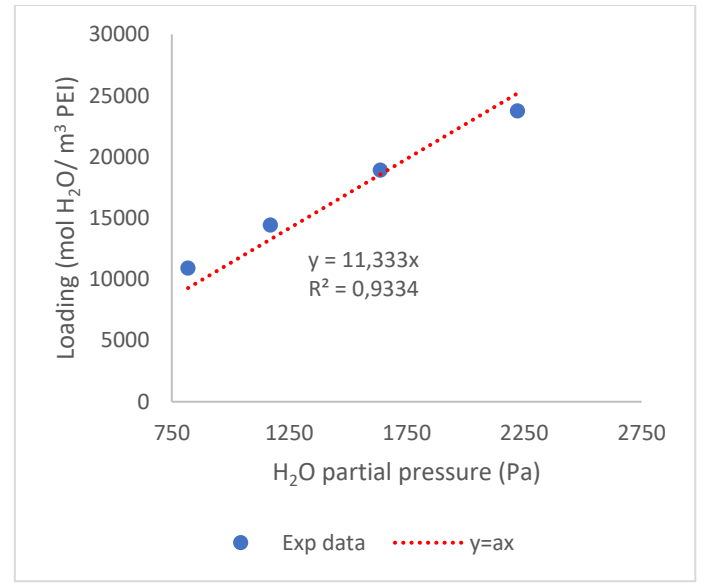
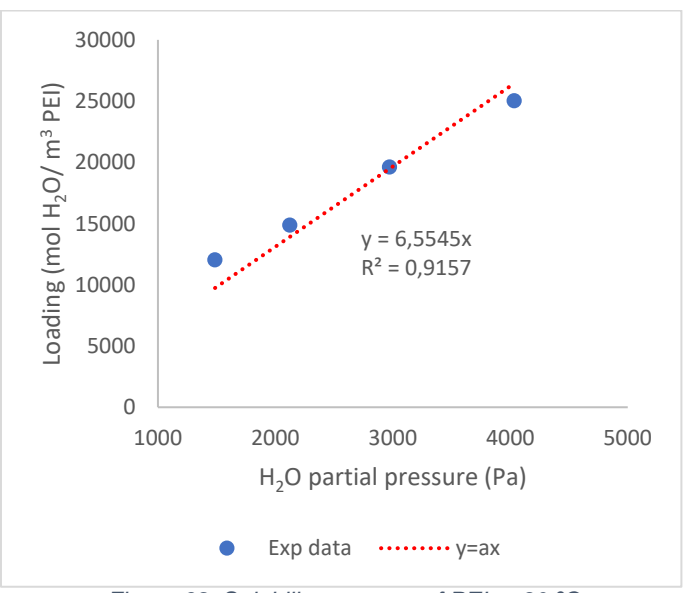


Figure 67: Solubility constant of PEI at 10 °C





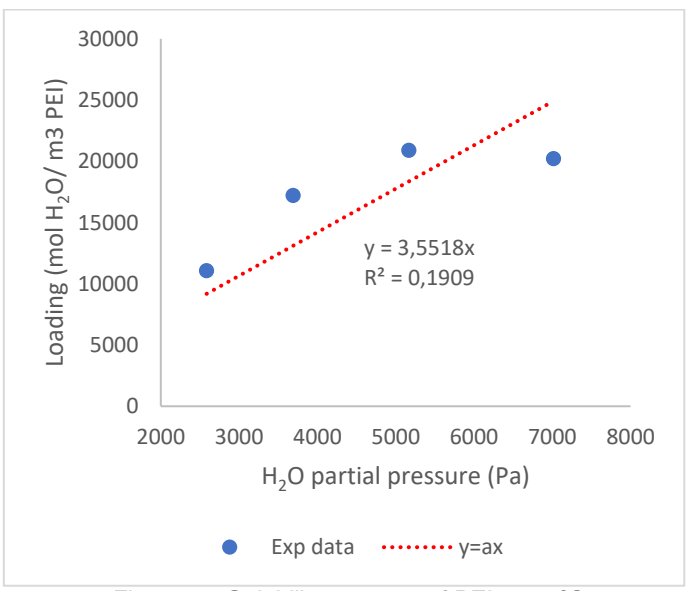


Figure 69: Solubility constant of PEI at 30 °C

Figure 70: Solubility constant of PEI at 40 °C

In the case of TEPA only the Henry constant at 20 °C can be found, since only experiments at that temperature were performed. Figure 71 shows the solubility constant. It is quite surprising that the R² value is low, since the operating conditions of the climate chamber were not extreme.

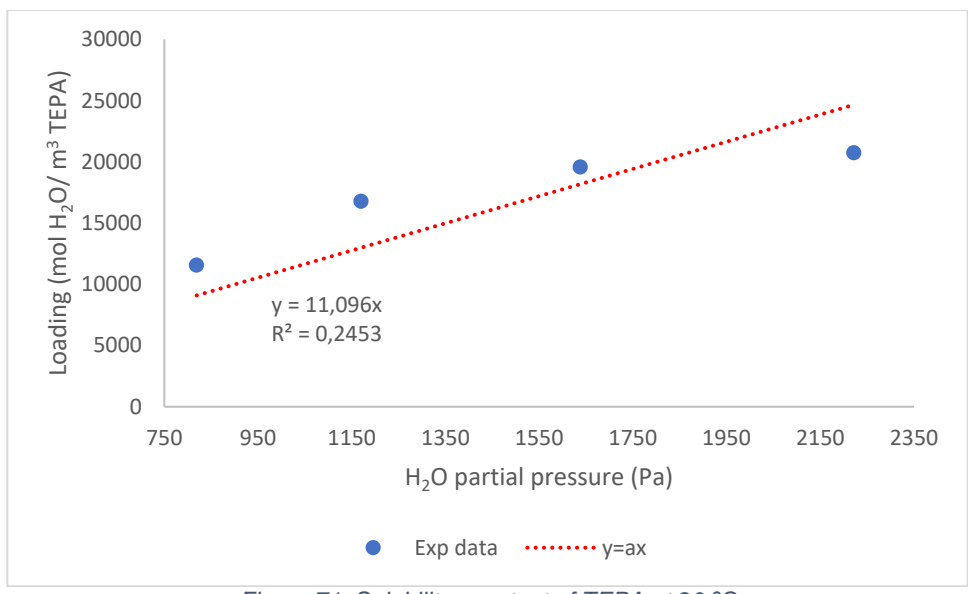


Figure 71: Solubility constant of TEPA at 20 °C

The Henry constant dependence with temperature follows the van't Hoff equation:

$$\frac{\mathrm{d}(\ln H)}{\mathrm{d}(\frac{1}{T})} = \frac{-\Delta_{\mathrm{Sol}}H}{R} \tag{4-3}$$

Where:

Table 18: Input for the van't Hoff equation

Symbol	Description
Н	Henry constant
$\Delta_{\rm sol} H$	Enthalpy of dissolution
T	Temperature
R	Universal gas constant

Figure 72 shows that the experimental Henry constant of PEI follows the solution of the van't Hoff equation, which is an exponential. It can also be seen that the solubility constant of PEI and TEPA is extremely similar at 20 °C.

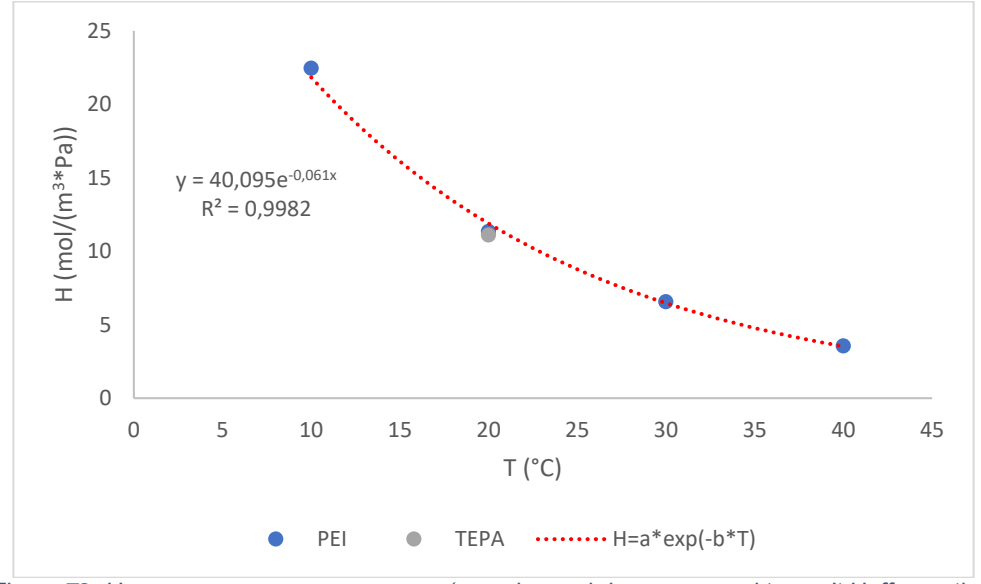


Figure 72: Henry constant vs. temperature (experimental data compared to van't Hoff equation)

It can be concluded that the Henry constant of H_2O in PEI follows a linear trend and it varies exponentially with the temperature.

Solubility constant of CO₂

The solubility constant of CO₂ cannot be calculated following the same steps as the solubility constant of H₂O because CO₂ reacts. This is why the physisorption experiment is done following the N₂O analogy, as explained in Section 3.3.4.

The solubility constant of N_2O is the slope of the pressure increase in the gas phase vs. the N_2O concentration in the liquid phase (Figure 73):

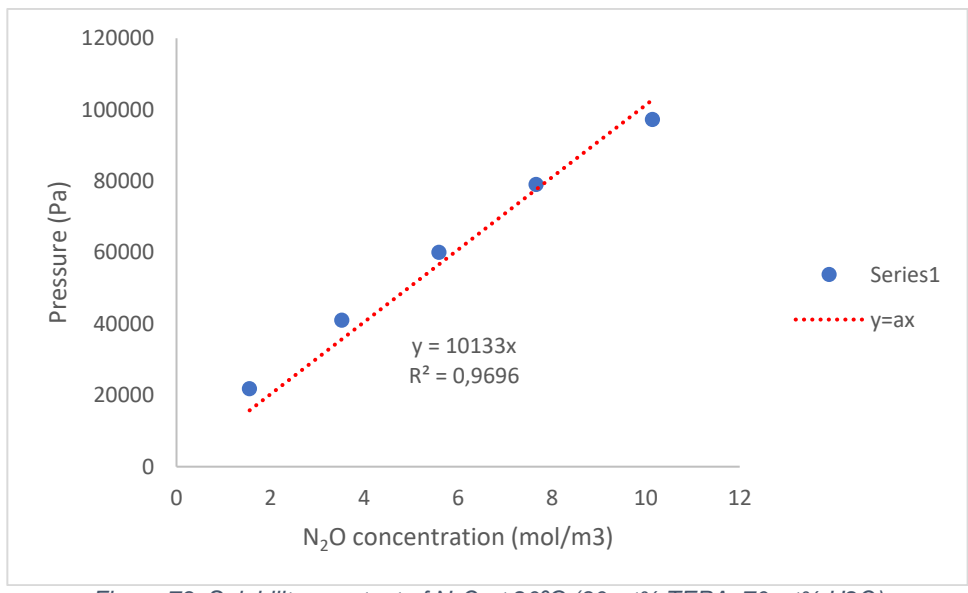


Figure 73: Solubility constant of N₂O at 20°C (30 wt% TEPA, 70 wt% H2O)

The value of the solubility constant of CO₂ is calculated using Equation (3-2). The value is shown in Table 19:

Table 19: Solubility constant of CO₂ at 20 °C

Solution	H (Pa*m³/mol) at 20 °C
30 wt% TEPA 70 wt% H ₂ O	7431

4.2.3. Reaction rate constant of CO₂

As explained in Section 3.3.4 there are two reactions taking place in the aqueous polyamine system: one where the amine reacts, and another one where the hydroxide ion is involved. The experimental reaction rate constant includes both reactions. Hence, the experimental reaction obtained is the observed reaction rate. Then, using Equations (3-12) and (3-13) it is possible to calculate the amine reaction rate constant with CO_2 .

The observed reaction rate is the slope of the CO₂ flux vs. the pressure (Figure 74):

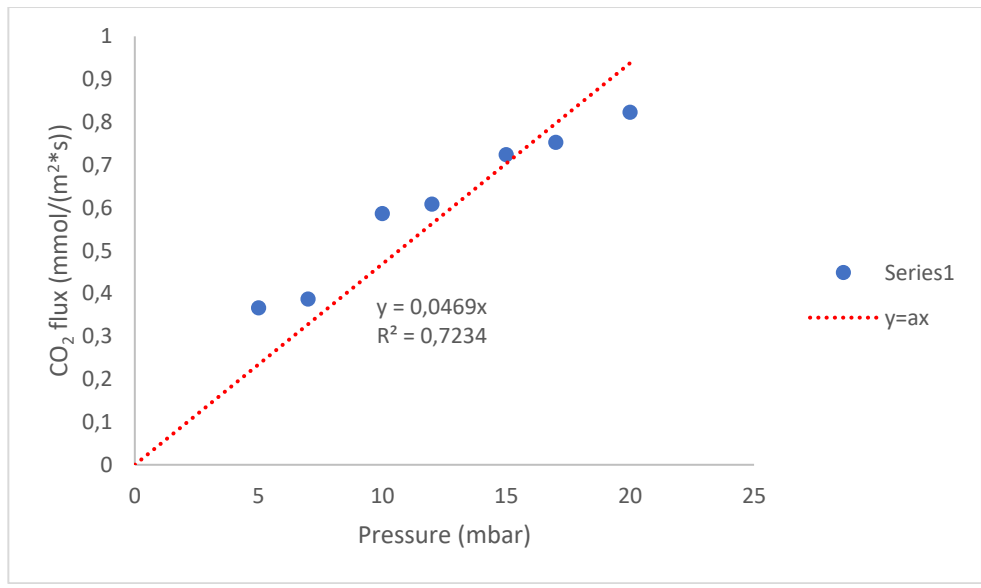


Figure 74: Observed reaction rate at 20 °C (30 wt% TEPA, 70 wt% H₂O)

The values of the reaction rate constants are shown in Table 20:

Table 20: Reaction rate constants for a solution of 30 and 70 wt% TEPA and H2O at 20 °C

Solution	k _{obs} (mol/(m ² *kPa*s)	k ₁ (1/s)	$k_2 (m^3/(mol^*s)$
30 wt% TEPA 70 wt% H2O	4.69*10-4	45230	29

The reaction rate constant of a solution of 30 wt% MEA and 70 wt% H2O at 25 °C is 6 m3/(mol*s) (62). The difference between both reaction rates is due to the fact that TEPA has more active groups available than MEA, specifically five vs one.

It can be concluded that the reaction rate constant for a solution of 30 wt% MEA and 70 wt% H2O is quite high. However, the reaction rate constant will most likely be different for H_2O concentrations closer to the experimental values, between 20 and 30 wt%.

4.2.4. Diffusion coefficient

The diffusion coefficient is another key parameter in the absorption process. In this section, a rough estimation based on the layer thickness of the polyamine and the residence time is made and then compared to the diffusion coefficients of CO₂ in SAS.

The diffusivity coefficient is correlated with viscosity, temperature and molecular interactions. Viscosity is a function of the temperature and of the concentrations of CO_2 and H_2O (54). However, due to the lack of data, for the model part, it is assumed that the diffusion coefficient is a constant.

The diffusivity coefficient of CO₂ in air at 282 K is 1.48x10⁻⁵ m²/s whereas the diffusivity coefficient of H₂O in air at 289.1 K is 2.82x10⁻⁵ m²/s (63). A rough estimation of the diffusion coefficient can be made as follows:

$$D_{\rm est} = \frac{LT^2}{t_{\rm exp}} \tag{4-4}$$

Where:

Table 21: Input for a rough estimation of the diffusion coefficient

Symbol	Description	Value	Unit
LT	Layer thickness of polyamine	0.5	mm
$t_{\rm exp}$	Experimental time	60	min

The estimated diffusion coefficient is $7x10^{-11}$ m²/s based on the assumption that, at 60 minutes, equilibrium is achieved for both CO_2 and H_2O . It can be seen that the estimated diffusion coefficient is way lower than the diffusion coefficient of CO_2 and H_2O in the air.

As mentioned before, literature has focused on supported amine sorbents. *Hahn et al.* (64) calculated the diffusion coefficients of CO₂ in amine impregnated SBA-15. The adsorption experiments were performed in a tubular reactor operated at 50 °C and a total flow of 100 nmL/ min which contained 89 vol% N₂, 10 vol% CO₂ and 1 vol% Ar tracer. The results are shown in Table 22:

Table 22: Diffusion coefficients of CO₂ in amine impregnated SBA-15 (64)

Sorbent type	9 wt% TEPA	23 wt%	5 wt% PEI MW	18 wt% PEI MW
		TEPA	800	800
D (m ² /s)	1.7*10 ⁻¹²	1.7*10 ⁻¹²	2.0*10 ⁻¹²	2.1*10 ⁻¹²

It seems that the diffusion coefficients for bulk amines are probably higher than the ones for supported amine sorbents because of the tortuosity of the support.

4.3. Reaction mechanism

The reaction of the CO₂ absorption can follow two mechanisms: the carbamate or the bicarbonate. Bicarbonates have slower kinetics but lower desorption heat whereas carbamates have faster kinetics and higher desorption heat (36).

The spectrometers of PEI and TEPA loaded with CO_2 were analysed in order to find peaks that exhibit the presence of carbamates and bicarbonates. Firstly, the spectrometers of PEI and TEPA are analysed. Then, the spectrometers of pure PEI and TEPA are subtracted from the spectrometers of loaded polyamine in order to find new peaks, this is, new compounds.

The region of the spectrometer that will be analysed goes from about 1500 to 500 cm⁻¹, which is called the fingerprint region (65). The peaks expected to be found are shown in Table 23:

Table 23: Relevant peaks for amine compounds

Group	Wavenumber (cm ⁻¹)	Reference
N-H wag	910- 665	(66)
C-N stretch	1220- 1020	(66)
C-H bend	1350- 1480	(67)

Figure 75 shows the spectrometer of pure PEI:

- N-H wag peak found at 766 cm⁻¹ with a transmitance of 0.59.
- C-N stretch peaks found at 1041 and 1123 cm⁻¹ with a transmitance of 0.72 and 0.74 respectively.
- C-H bend peaks found at 1354 and 1457 cm⁻¹ with a transmitance of 0.86 and 0.76 respectively.

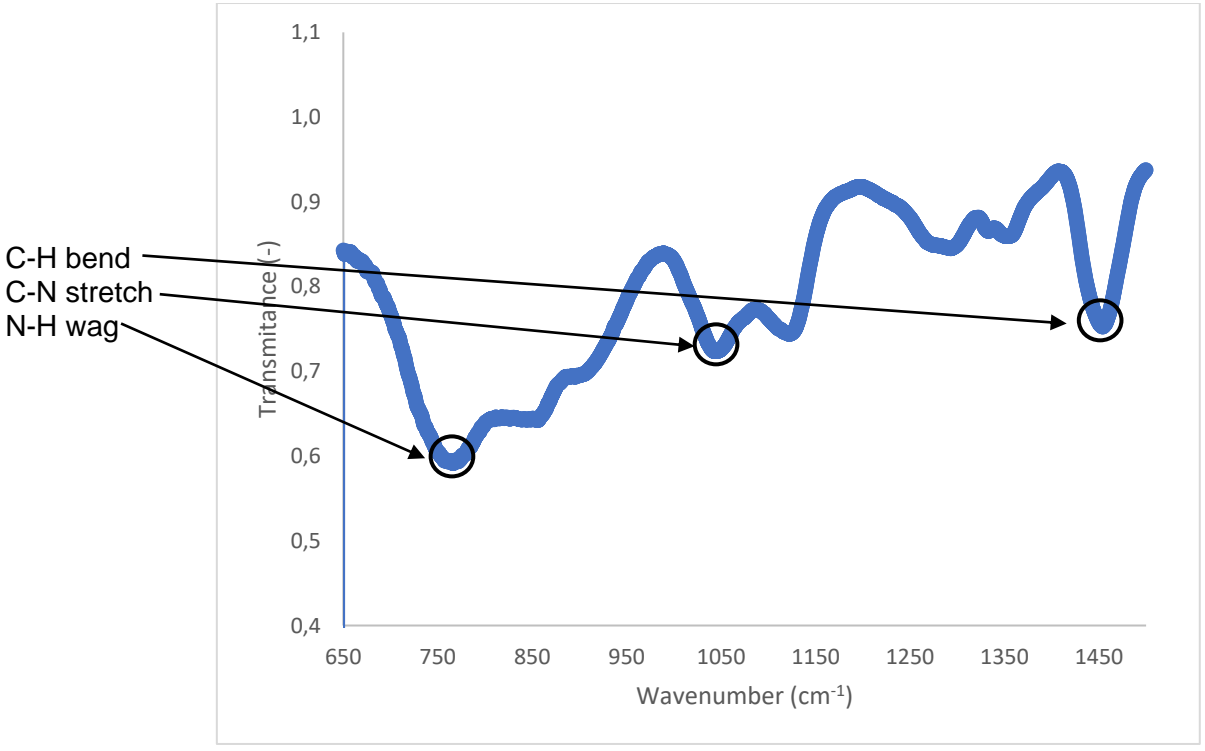


Figure 75: Spectrometer of pure PEI

Figure 76 shows the spectrometer of pure TEPA:

- N-H wag peak found at 766 cm⁻¹ with a transmitance of 0.54.
- C-N stretch peaks found at 1128 cm⁻¹ with a transmitance of 0.74.
- C-H bend peaks found at 1350 and 1456 cm⁻¹ with a transmitance of 0.88 and 0.77 respectively.

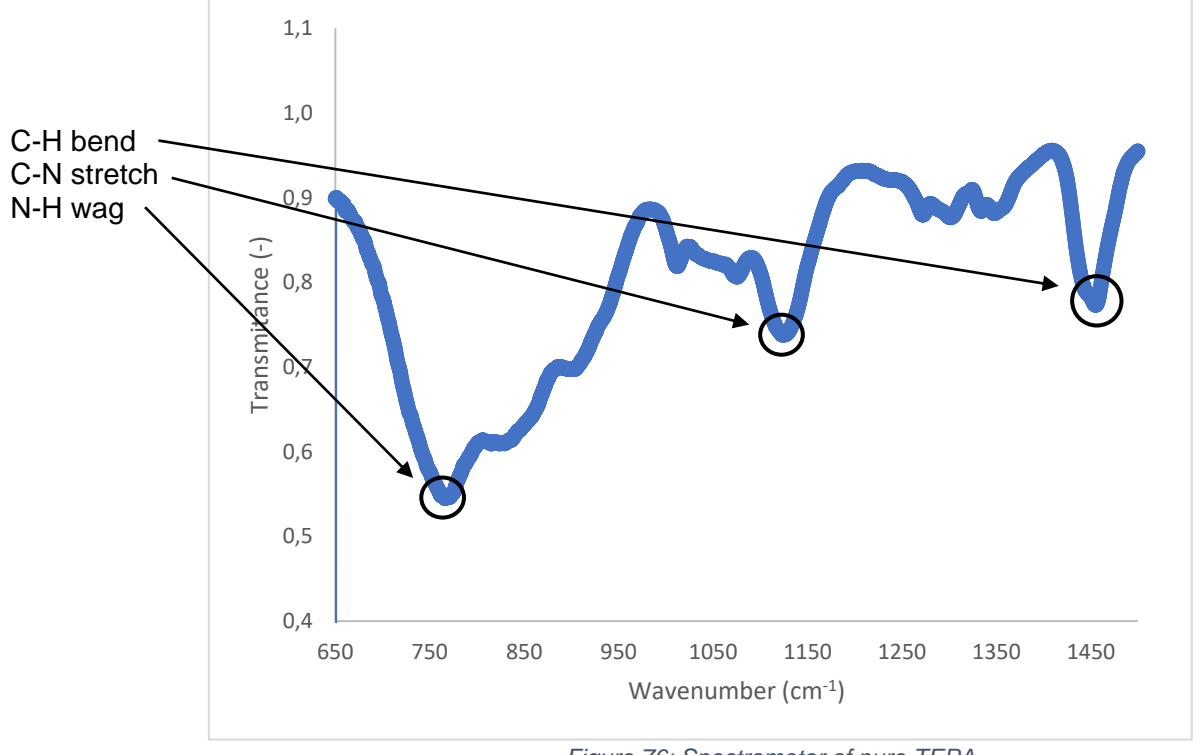


Figure 76: Spectrometer of pure TEPA

Both spectrometers are similar because PEI and TEPA are polyamines so they have the same functional groups.

As mentioned before, CO_2 is absorbed forming carbamate or bicarbonate. The spectrometer of samples loaded with CO_2 is subtracted from the pure polyamine spectrometer in order to identify carbamate and/or bicarbonate peaks, which are shown in Table 24. It can be seen that carbamate and bicarbonate presence will only alter the area between 1000 and 1500 cm⁻¹,

Table 24: Relevant peaks f	or carbamate	and bicarbonate
----------------------------	--------------	-----------------

Compound	Wavenumber (cm ⁻¹)	Reference
Carbamate	1156	(68)
	1322	, ,
Bicarbonate	1368	(68)
	1385	, ,
	1398	

TEPA is a linear molecule, so amines are not strictly hindered, and it does not contain tertiary amines. This implies that the reaction of CO_2 with TEPA will follow the carbamate pathway most likely. PEI is a branched molecule, so amines may be hindered, and it contains tertiary amines. This implies that the reaction of CO_2 with PEI can follow both the carbamate and bicarbonate pathways.

Figure 85 is the subtracted spectrometer of PEI loaded with CO₂ (4.64 wt%, PEI in contact with a CO₂ concentration of 800 ppm) and pure PEI:

- Carbamate peak found at 1311 cm⁻¹ with an absorbance of 0.12.
- The bicarbonate area goes from 1368 to 1398 cm⁻¹. However, no peaks could be found.

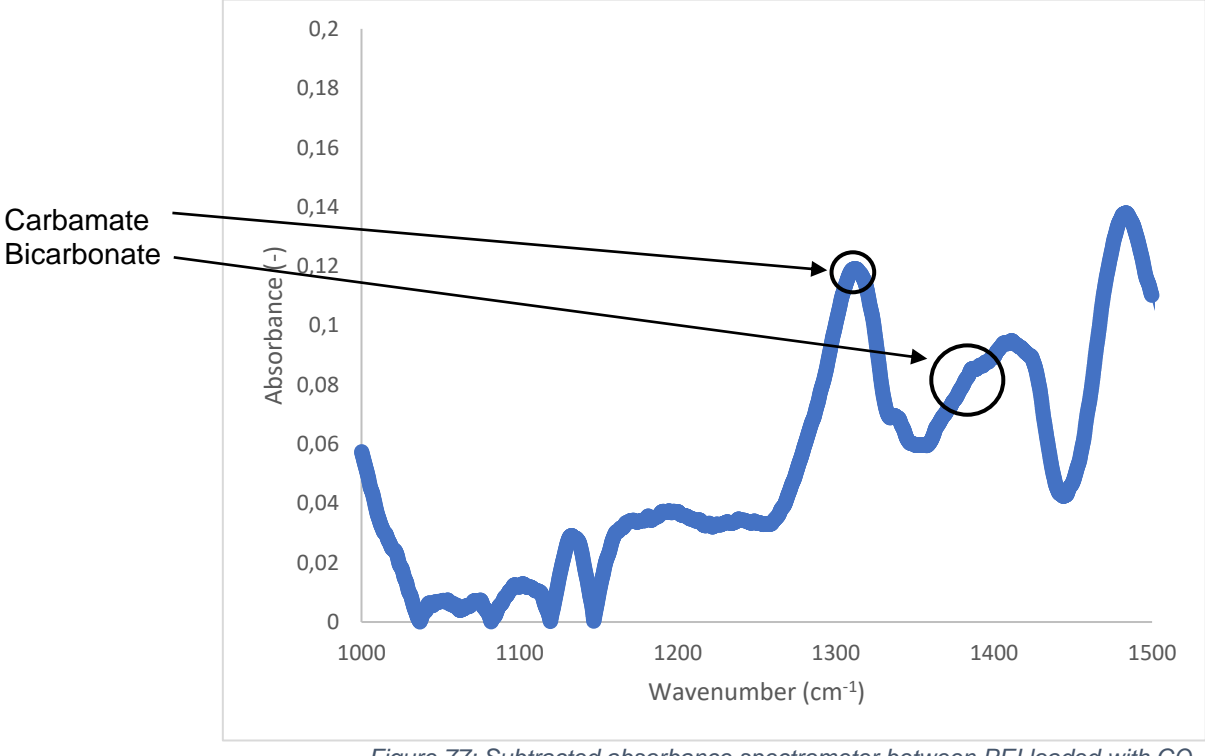


Figure 77: Subtracted absorbance spectrometer between PEI loaded with CO₂ and pure PEI

Figure 44 is the subtracted spectrometer of TEPA loaded with CO₂ (4.19 wt%, TEPA in contact with a CO₂ concentration of 800 ppm) and pure TEPA:

- Carbamate peak found at 1314 cm⁻¹ with an absorbance of 0.12.
- The bicarbonate area goes from 1368 to 1398 cm⁻¹. However, no peaks could be found.

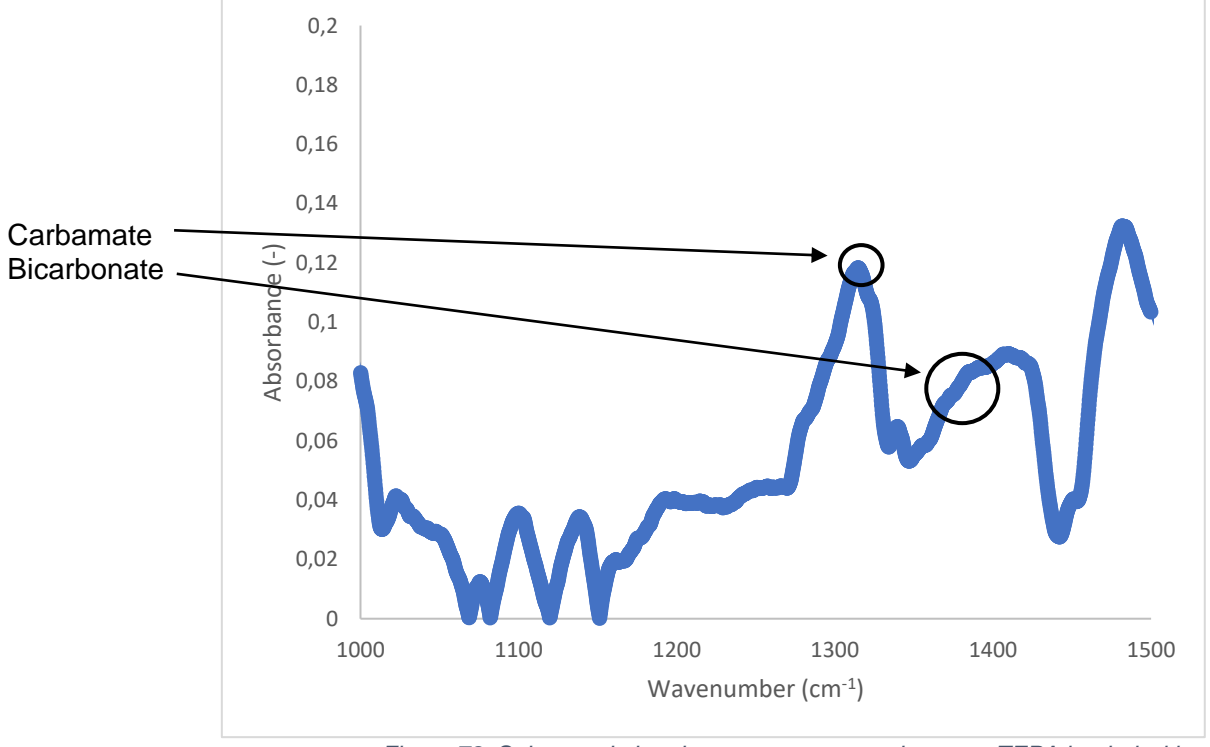


Figure 78: Subtracted absorbance spectrometer between TEPA loaded with CO₂ and pure TEPA

More spectrometers were done for solutions of PEI and TEPA with H_2O and different CO_2 concentration in the air. They are shown in Appendix L.

The main conclusion from this Section is that the reaction mechanism corresponds to the carbamate pathway. This will have consequences in the desorption part, since the desorption heat of carbamates is higher than the desorption heat of bicarbonates.

5 Strategies for modelling

The goal of this Chapter is to model the CO₂ and H₂O absorption process in polyamines in order to find the diffusion coefficient of both components. The absorption of CO₂ depends on two mechanisms: diffusion and reaction. Therefore, before diving into the model, the mechanism that limits the CO₂ diffusion will be determined.

The model for the absorption process can be built based on a 2nd order partial differential equation which is solved using a numerical method in MATLAB.

5.1. Theory of the model

In this section, some theoretical background is given in order to gain some insight regarding the equations that will be used in the model.

The convection-diffusion equation is used as the basic equation for the CO₂ and H₂O absorption model (69):

$$\frac{\partial c}{\partial t} = \nabla \cdot (D\nabla c) - \nabla \cdot (vc) + R \tag{5-1}$$

For this model, it is assumed that:

- The convection term is negligible since the polyamine does not flow.
- The CO₂ and the H₂O diffuse in only one direction, in this case, the x-direction into the layer.

Rewriting the divergence and the gradient operators and taking into account the two previous assumptions the convection-diffusion equation simplifies to:

$$\frac{\partial c}{\partial t} = D \frac{\partial^2 c}{\partial r^2} + R \tag{5-2}$$

It is assumed that H_2O does not react with the polyamine because CO_2 is absorbed via the carbamate pathway which does not mandatorily require H_2O (explained in Section 4.3).

$$\frac{\partial c_{\text{CO}_2}}{\partial t} = D_{\text{CO}_2} \frac{\partial^2 c_{\text{CO}_2}}{\partial x^2} - k_{\text{CO}_2} c_{\text{CO}_2}$$
 (5-3)

$$\frac{\partial c_{\rm H_2O}}{\partial t} = D_{\rm H_2O} \frac{\partial^2 c_{\rm H_2O}}{\partial x^2} \tag{5-4}$$

Where:

Table 25: Input for the equations used in the model

Symbol	Description	Unit
c_{CO_2}	CO ₂ concentration in the polyamine	[mol/m ³]
$c_{\mathrm{H_2O}}$	H ₂ O concentration in the polyamine	[mol/m ³]
D_{CO_2}	CO ₂ diffusion coefficient	[m ² /s]
$D_{\rm H_2O}$	H₂O diffusion coefficient	[m ² /s]
x	Diffusion direction of H ₂ O and CO ₂ diffuse	[m]
t	Experimental time	[s]

Figure 79 is a scheme of the CO_2 absorption by a polyamine using the two-film model where the reaction of the CO_2 with the amine takes place in a pseudo-first order regime. This means that the concentration of the amine is high and that the reaction fast (41). The fact that a pseudo first order regime can be assumed will be explained in Section 5.3.2.

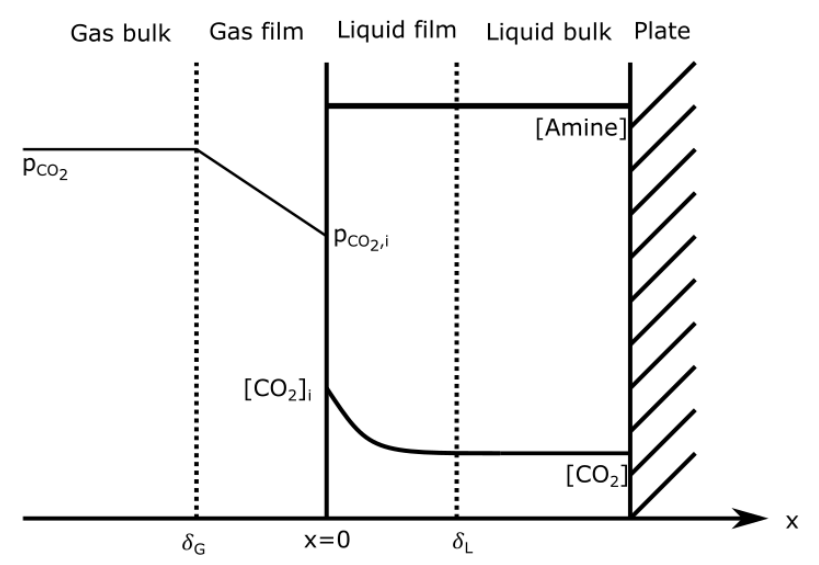


Figure 79: CO₂ absorption by a polyamine (70)

5.1.1. Conditions

Both H₂O and CO₂ models need two boundary conditions and one initial condition to be solved.

Boundary conditions

The fan used in the experiments enhanced the mixing of the gases, so the boundary layer is small, and the diffusion coefficient of CO_2 and H_2O in the gas phase is way higher than in the liquid (which makes sense since the viscosity of the air is extremely low). This is why it is assumed that the partial pressure of H_2O and CO_2 in the bulk gas is the same as the partial pressure of H_2O and CO_2 at the gas film:

$$p_{\text{CO}_2,G} = p_{\text{CO}_2,G,i}$$
 (5-5)

$$p_{\rm H_2O,G} = p_{\rm H_2O,G,i} \tag{5-6}$$

If the interface is in equilibrium Henry's law can be applied:

$$c_{\text{CO}_2}(x=0,t) = H_{\text{CO}_2} \times p_{\text{CO}_2,G}$$
 (5-7)

The CO₂ concentration in the air is assumed to be 4*10⁻⁴ atm, which is converted into Pa:

$$p_{\text{CO}_2,\text{G}} = \frac{400}{1 \times 10^6} \times 101325 \tag{5-8}$$

The Henry constant is only relevant for reactions, since the reaction depends on the physical concentration of the reactant (36). H_2O does not react. Hence:

$$c_{\text{H}_2\text{O}}(x=0,t) = c_{\text{H}_2\text{O},\text{exp}}(x=0,t=3600 \text{ s})$$
 (5-9)

Equations (5-7) and (5-9) are Dirichlet boundary condition.

Where:

Table 26: Input for left boundary condition

Symbol	Description	Unit
$p_{\mathrm{CO}_2,\mathrm{G}}$	Partial pressure of CO ₂ at the bulk gas	[Pa]
$p_{\mathrm{CO}_2,\mathrm{G,i}}$	Partial pressure of CO ₂ at the interface	[Pa]
c_{CO_2}	Concentration of CO ₂ in the polyamine	[mol/L]
H_{CO_2}	Solubility constant of CO ₂	[mol/(m ³ *Pa)]
$c_{\mathrm{H}_2\mathrm{O}}$	Concentration of H ₂ O in the polyamine	[mol/m ³]
$c_{\rm H_2O,exp}$	Experimental concentration of H ₂ O in the polyamine at minute 60.	[mol/m ³]

The end of the layer thickness of the polyamine is in touch with the plate, a solid, so the diffusion cannot go further:

$$\frac{\partial c_{\text{CO}_2}}{\partial x}(x = LT, t) = 0 \tag{5-10}$$

$$\frac{\partial c_{\rm H_2O}}{\partial x}(x=LT,t)=0 \tag{5-11}$$

Equations (5-10) and (5-11) are Neumann boundary conditions.

Where:

Table 27: Input for right boundary condition

Symbol	Description	Unit
$\partial c_{\mathrm{CO}_2}$	CO ₂ concentration gradient	[mol/m ⁴]
$\frac{\partial x}{\partial c_{\rm H_2O}}$	H ₂ O concentration gradient	[mol/m ⁴]
$\frac{\partial H_2 \partial}{\partial x}$	1120 concentration gradient	[11101/111]

Initial condition

To test whether there is CO₂ initial concentration in the PEI and TEPA extracted from the bottle a phosphoric acid titration test was done and it gave no CO₂ content.

Although the PEI and TEPA from the bottle contain some H_2O , shown in Section 3.3.1 (867 and 1021 ppm respectively), the H_2O concentration is negligible compared to the H_2O absorbed during the experiments.

Equations (5-11) and (5-12) are Dirichlet conditions.

$$c_{\text{CO}_2}(x, t = 0) = 0 (5-11)$$

$$c_{\rm H_2O}(x,t=0) = 0 {(5-12)}$$

Where:

Table 28: Input for the initial condition

Symbol	Description	Unit
c_{CO_2}	Concentration of CO ₂ at the polyamine	[mol/m ³]
$c_{\mathrm{H_2O}}$	Concentration of H ₂ O at the polyamine	[mol/m ³]
t	Experimental time	[s]
\boldsymbol{x}	Length coordinate	[m]

Figure 80 shows the simplification of the CO₂ absorption process that will be modelled taking into account Equation (5-5).

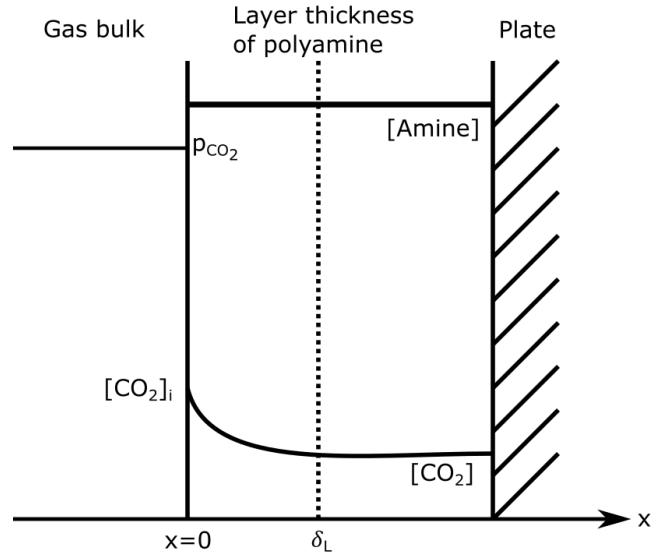


Figure 80: Simplified CO₂ model

5.2. H₂O absorption model

The equation and the boundary and initial conditions of the H_2O absorption process introduced in Section 5.1 will be used to find the diffusion coefficient of H_2O .

The H_2O loadings calculated by the model are compared with the H_2O loadings obtained experimentally during the climate chamber experiments (Section 4.1.1). Then, the diffusion coefficient is varied until both curves have a similar shape.

Equations (5-13)- (5-16) are the equations that will be solved numerically in MATLAB using the *pdepe* solver (which solves initial-boundary value problems for parabolic-elliptic PDEs in 1-D). The MATLAB code is available in Appendix M.

$$\frac{\partial c_{\rm H_2O}}{\partial t} = D_{\rm H_2O} \frac{\partial^2 c_{\rm H_2O}}{\partial x^2} \tag{5-13}$$

The boundary conditions are:

$$c_{\text{H}_2\text{O}}(x=0,t) = c_{\text{H}_2\text{O},\text{exp}}(x=0,t=3600 \text{ s})$$
 (5-14)

$$\frac{\partial c_{\text{H}_2\text{O}}}{\partial t}(x=L,t) = 0 \tag{5-15}$$

The initial condition is:

$$c_{\rm H_2O}(x,t=0) = 0 {(5-16)}$$

Einstein-Stokes equation is the most common basis for estimating diffusion coefficients in liquids even though the diffusion coefficients calculated using this equation are accurate to about 20% (63):

$$D_{\rm H_2O} = \frac{k_B \times T}{6 \times \pi \times \mu_{\rm PEI} \times r_{\rm H_2O}} \tag{5-17}$$

Where:

Table 29: Input for Einstein-Stokes equation to calculate the diffusion coefficient of H₂O in PEI

Symbol	Description	Value	Unit
k_B	Boltzmann's constant	1.3806x10 ⁻²³	[J/K]
T	Temperature	293	[K]
μ_{PEI}	80/20 PEI/H ₂ O wt% viscosity	4.076	[kg/(m*s)]
$d_{H_{2}O}$	H ₂ O kinematic diameter	2.65x10 ⁻¹⁰ (71)	[m]

The diffusion coefficient of H_2O in PEI obtained from the Einstein-Stokes equation is $4*10^{-13}$ m²/s. The diffusion coefficient obtained in Section 4.2.4, which only considered the layer thickness and the experimental time, was $7*10^{-11}$ m²/s which is two orders of magnitude higher.

If the diffusion coefficient of H_2O obtained from the Einstein-Stokes equation is used in the MATLAB model the correlation with experimental data (experiments done in the climate chamber at 70 % relative humidity and 20 °C) is very weak, like Figure 81 shows. This could be because Einstein-Stokes equation only considers viscosity, but not the molecular interactions.

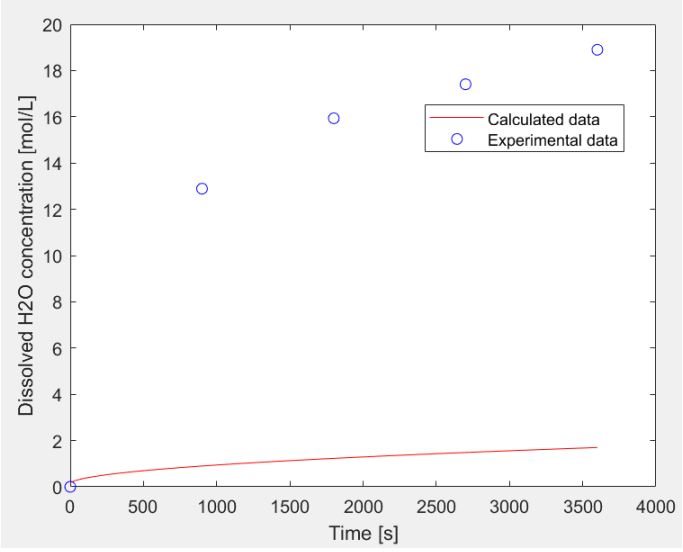
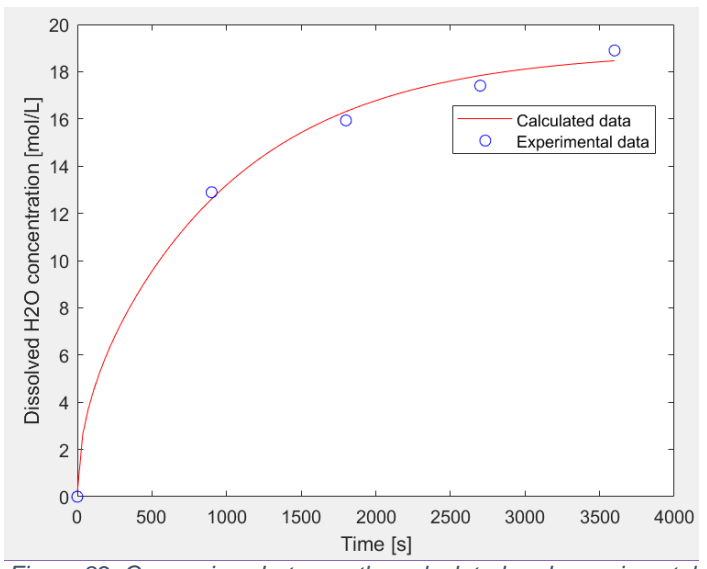


Figure 81: Experimental vs. calculated H2O loading using diffusion coefficient obtained from Einstein-Stokes equation

Figure 82 shows that if the diffusion coefficient of H_2O is found as explained before, by correlating the calculated H_2O loadings with the experimental H_2O loadings, the H_2O loadings follow the same trend. Figure 83 shows how the H_2O diffuses through the layer of polyamine



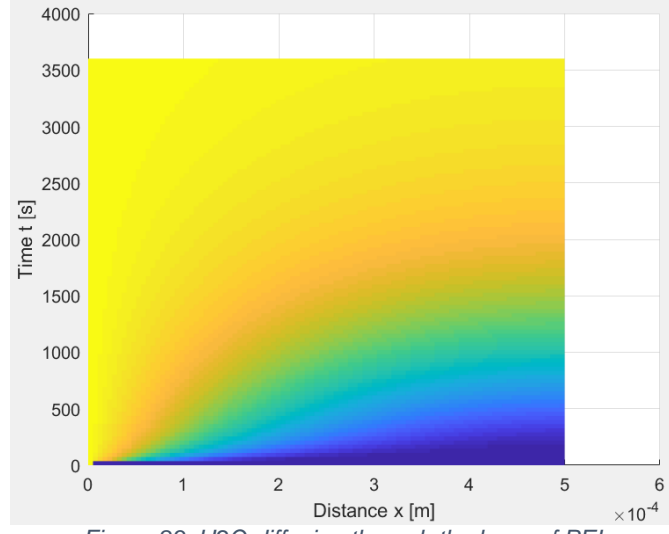


Figure 82: Comparison between the calculated and experimental (70% relative humidity and 20 °C) H2O loading in PEI

Figure 83: H2O diffusion through the layer of PEI

The diffusivity coefficients of H_2O in PEI obtained from the model are shown in Table 30.

Table 30: Calculated diffusivity coefficients of H₂O in PEI

	$D_{\rm H_2O}$ (m ² /s)	Relative humidity				
		35% 50% 70% 95%				
	10 °C	2*10 ⁻¹⁰	9*10 ⁻¹¹	6*10 ⁻¹¹	1*10 ⁻¹⁰	
Т	20 °C	8*10 ⁻¹¹	2*10 ⁻¹⁰	1*10 ⁻¹⁰	9*10 ⁻¹¹	
	30 °C	1*10 ⁻¹⁰	2*10 ⁻¹⁰	2*10 ⁻¹⁰	1*10 ⁻¹⁰	
	40 °C	3*10 ⁻¹⁰	1*10 ⁻¹⁰	2*10 ⁻¹⁰	1*10 ⁻¹⁰	

As explained before, two methodologies can be followed to obtain the diffusion coefficient of H2O, as explained before: Einstein-Stokes equation and the MATLAB model. It seems that the second methodology gives a more accurate correlation between calculated and experimental H₂O loadings. This is why the diffusion coefficients obtained via Equation (5-13) will be further studied in this thesis.

The average value of the diffusion coefficient of H₂O in PEI is 1*10⁻¹⁰ m²/s.

The diffusion coefficient of H_2O in PEI is dependent on the H_2O content in the air (Figure 84). Normally it would be expected that the diffusion coefficient of H_2O is independent on the H_2O content in the air. However, a different relative humidity will lead to different H_2O loadings which will change the viscosity of the sorbent. Moreover, the same phenomena can also influence the polyamine composition. These two circumstances can influence the diffusion coefficient of H_2O in the polyamine.

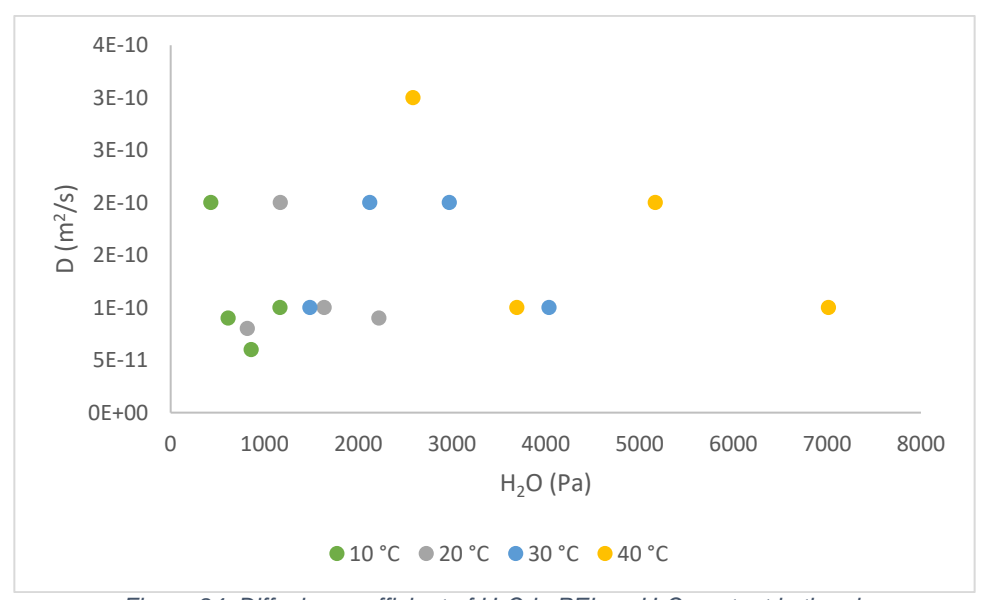


Figure 84: Diffusion coefficient of H_2O in PEI vs. H_2O content in the air

The diffusion coefficient should increase with higher temperature while keeping the same relative humidity. Figure 85 shows that the diffusion coefficients of H_2O at 95% relative humidity are quite stable whereas the diffusion coefficients of H_2O at 70% relative humidity follow the expected trend. The fact that the diffusion coefficient of H_2O at 50% relative humidity and 40 °C decreases could imply that it is an outlier. Finally, the diffusion coefficient at 35% relative humidity decreases for 20 and 30 °C but then it increases again.

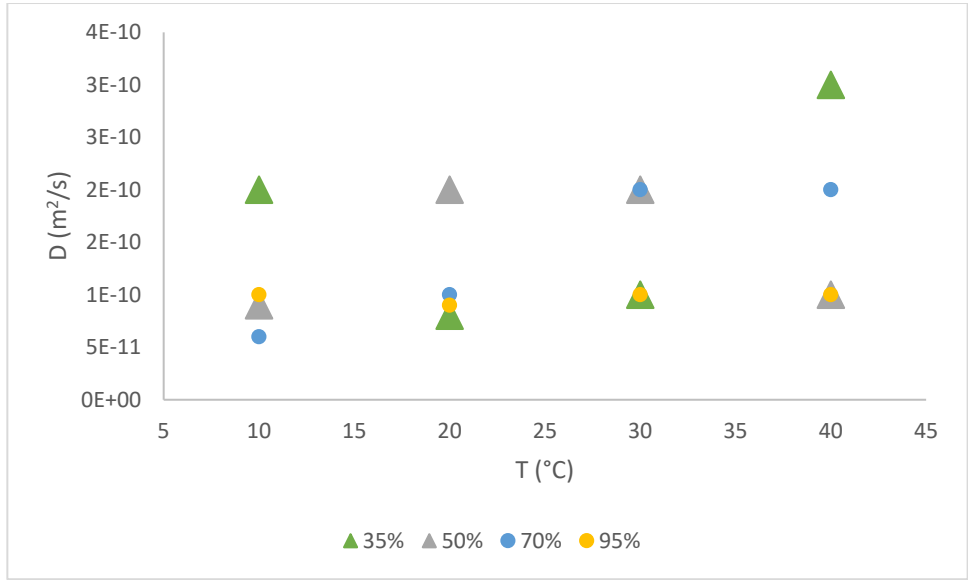


Figure 85: Diffusion coefficient of H₂O vs. temperature

Figure 86 shows the diffusion coefficient of H₂O versus the viscosity of PEI.

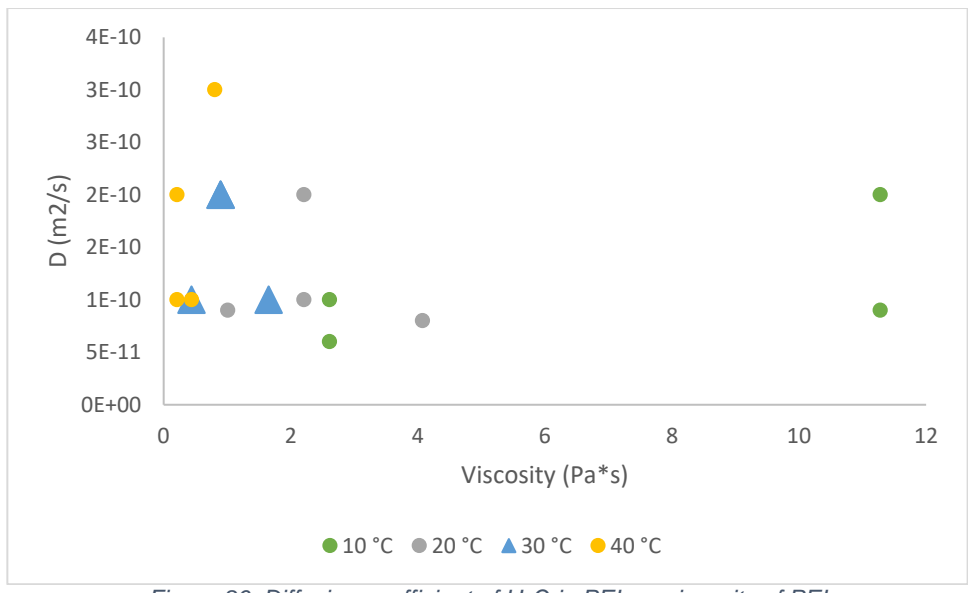
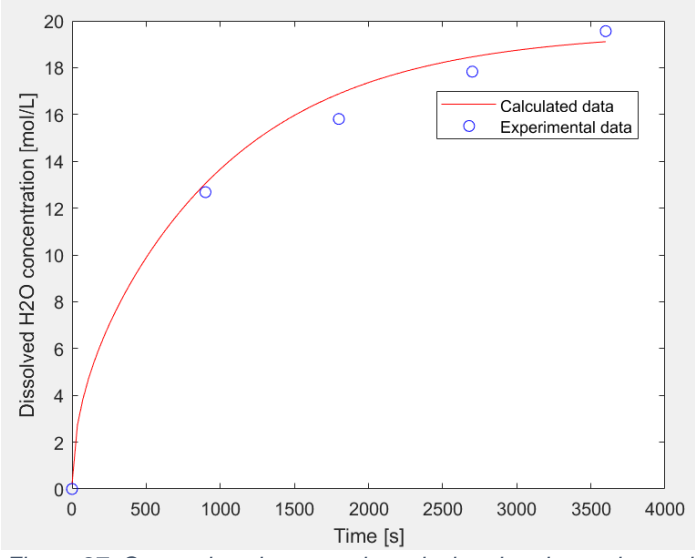


Figure 86: Diffusion coefficient of H_2O in PEI vs. viscosity of PEI

The procedure to calculate the diffusivity coefficients H_2O in TEPA is the same as the one for PEI. Figure 87 shows the correlation between the calculated and experimental H_2O loadings in TEPA. Figure 88 shows how the H_2O diffuses through the layer of polyamine



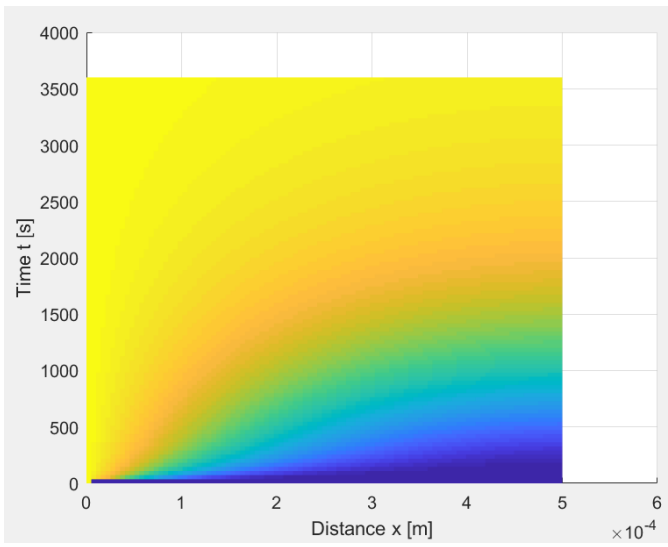


Figure 87: Comparison between the calculated and experimental H₂O loading in TEPA

Figure 88: H₂O diffusion through the layer of TEPA

The diffusivity coefficients of H₂O in TEPA obtained from the model are shown in Table 31.

Table 31: Calculated diffusion coefficients of H₂O in TEPA

Table 31: Galediated diffusion coefficients of Fig. 111 FEF 74			
Temperature	20 °C	$D_{\rm H_2O} \ ({\rm m^2/s})$	
	35%	2*10 ⁻¹⁰	
Relative humidity	50%	2*10 ⁻¹⁰	
	70%	1*10 ⁻¹⁰	
	95%	2*10 ⁻¹⁰	

The average diffusion coefficient of H_2O in TEPA is $2*10^{-10}$ m²/s.

Although these diffusion coefficients were obtained from Equations (5-15) to (5-18) and the experimental data, due to the difficulty of these measurements, it is to be expected that there is a significant margin of error of around 25% (36): the diffusion coefficient of PEI could be between 2.5*10⁻¹¹ and 1.25*10⁻¹⁰ m²/s. The diffusion coefficient of TEPA could be between 5*10⁻¹¹ and 2.5*10⁻¹⁰ m²/s.

This method might not be extremely accurate but it gives the order of magnitude of the diffusion coefficient of H₂O. The diffusion coefficient of CO₂ in PEI and TEPA impregnated on monoliths is 2*10⁻¹² m²/s (64). The order of magnitude is two times lower probably due to the tortuosity of the channels. The diffusion coefficient of CO₂ in NMC and SCC is between 3*10⁻¹³ and 9*10⁻¹² m²/s (72). The order of magnitude is two times lower probably because both NMC and SCC are materials with a higher viscosity than PEI and TEPA.

It can be concluded that the diffusion coefficient of H₂O in PEI and TEPA are extremely similar.

5.3. CO₂ absorption model

As explained before, the CO_2 absorption depends on two different phenomena: kinetics and diffusion. However, the absorption will be limited by the slowest process. The Hatta number is a dimensionless parameter that represents the ratio between the rate

of reaction and diffusion. Therefore, if the Hatta number is high the absorption will be diffusion limited. On the other hand, if the Hatta number is low the absorption will be reaction limited. Once the CO₂ absorption was determined to be diffusion or reaction limited the model was developed.

5.3.1. Equilibrium CO₂ loading of the polyamine

The equilibrium CO₂ loading of PEI and TEPA was not measured experimentally since the focus of the thesis was more related to residence times that could be realistic for flowing conditions, like 60 minutes.

Unveren et al. (73) calculated the maximum CO_2 adsorption capacities in amine impregnated silica supports. The adsorption experiments were performed in a 100% CO_2 flow at 75 $^{\circ}C$ for 5 hours. The results are shown in Tables 32 and 33 for TEPA and PEI respectively.

Table 32: Loadings of CO₂ in TEPA impregnated silica and polymeric support (73)

rable 62: Leadings of 6-62 in 121 / imprograted sinea and polyment eappoin (16)				
Sorbent type	47 wt% TEPA	52 wt% TEPA	50 wt% TEPA	50 wt% TEPA
	on MCM-41	on SBA-15	on KIT-6	on PMMA
CO ₂ adsorption	1.6	3.0	2.9	2.7
capacities (mol/				
kg adsorbent)				

Table 33: Loadings of CO₂ in PEI impregnated silica and polymeric support (73)

Sorbent type	50 wt%	50 wt%	52 wt%	50 wt% PEI	50 wt%
	PEI on	PEI on	PEI on	on PMMA	PEI on PS
	MCM-41	SBA-15	KIT-6		
CO ₂ adsorption	2.1	2.2	1.4	1.6	1.7
capacities (mol/					
kg adsorbent)					

CO₂ adsorption capacities of TEPA based adsorbents are higher than those based on PEI probably due to the high number of amine groups present in TEPA (73).

The CO_2 adsorption capacities changes depending on the support. This implies that the interaction of TEPA and PEI with the support changes the CO_2 adsorption capacities. The CO_2 adsorption capacity of TEPA on MCM-41 is lower than the others. Two CO_2 adsorption capacities can be observed in Table 39: on one hand, MCM-41 and SBA-15 and on the other hand KIT-6, PMMA and PS.

It is assumed that the average of these CO₂ loadings is the equilibrium CO₂ loading for bulk PEI and TEPA due to the lack of data (2.6 mol/kg and 1.8 mol/kg for TEPA and PEI respectively).

5.3.2. Diffusion coefficient of CO₂ assuming kinematic diameter relation

In this section, the diffusion coefficient of CO₂ is calculated by taking into account only the relation between the kinematic diameters of CO₂ and H₂O.

It was already shown before that the diffusion coefficient of H₂O obtained from the Einstein-Stokes equation is not in good agreement with the experimental results. This

is why the Einstein-Stokes equation will not be used to estimate the diffusion coefficient of CO₂.

It is possible to calculate the diffusion coefficient of CO_2 from the average diffusion coefficient of H_2O , obtained in Section 5.2, with the assumption that the molecular interactions of CO_2 and H_2O with PEI and TEPA (as well as the molecular interactions between H_2O and CO_2) are the same and then, the kinematic diameter of the particle can be taken into account.

$$D_{\text{CO}_2,\text{av,i}} = D_{\text{H}_2\text{O},\text{av,i}} \times \frac{d_{\text{H}_2\text{O}}}{d_{\text{CO}_2}}$$
 (5-18)

Where:

Table 34: Input to calculate the diffusion coefficient of CO₂ considering only the kinematic diameter influence

Symbol	Description	Value	Unit
$D_{\rm H_2O,av,PEI}$	Diffusion coefficient of H2O	1x10 ⁻¹⁰	[m²/s]
$D_{\rm H_2O,av,TEPA}$	Diffusion coefficient of H2O	2x10 ⁻¹⁰	[m ² /s]
$d_{ m H_2O}$	H₂O kinematic diameter	2.65x10 ⁻¹⁰ (71)	[m]
d_{CO_2}	CO ₂ kinematic diameter	3.30x10 ⁻¹⁰ (71)	[m]

The results are shown in Table 35:

Table 35: Diffusivity coefficients of CO₂ in TEPA and PEI considering only the kinematic diameter influence

Sorbent	D_{CO_2} (kinematic diameter influence)
TEPA	1*10 ⁻¹⁰
PEI	1*10 ⁻¹⁰

It is surprising that the diffusion coefficient of CO_2 in PEI has the same value as the diffusion coefficient of H_2O . The diffusion coefficient of CO_2 should be lower than the diffusion coefficient of H_2O because the CO_2 has a higher kinematic diameter.

Equation (5-18) only takes into account the kinematic diameter difference between CO₂ and H₂O. However, as mentioned before, it does not consider the molecular interactions between CO₂, H₂O, TEPA and PEI. This phenomenon might be relevant since all the CO₂ absorption experiments were performed in the presence of H2O.

In can be concluded that, according to the kinematic diameter relation, the diffusion coefficients of H_2O and CO_2 are similar. However, looking at the experimental results it seems that CO_2 requires more time to achieve equilibrium than H_2O .

5.3.3. Theoretical approach and discussion related to the Hatta number

The Hatta number is one of the key parameters of the CO₂ absorption, since it will determine if the process is diffusion or reaction limited. The discussion will be preceded by some theoretical background.

Theory related to the Hatta number

The CO₂ flux in the absence of reaction obtained from the film theory model (Appendix H) is (41):

$$N_{\text{CO}_2} = -D_{\text{CO}_2} \frac{\partial c_{\text{CO}_2}}{\partial x} \Big|_{x=0} = k_{\text{G}} \times (p_{\text{CO}_2} - p_{\text{CO}_{2,i}}) = k_{\text{L}} \times ([\text{CO}_2]_i - [\text{CO}_2])$$
 (5-19)

If the reaction is taken into account then (74):

$$N_{\text{CO}_2} = E \times k_{\text{L}}^0 \times ([\text{CO}_2]_i - [\text{CO}_2])$$
 (5-20)

The enhancement factor (E) represents the influence of a chemical reaction on the mass transfer rate. It is defined as the ratio between the absorption rate of a gas component in a liquid in the presence of a chemical reaction and the absorption rate in the absence of a reaction with the same concentration driving force (74). Then, by combining Eq (5-19) and (5-20) it is possible to see that E multiplies the physical liquid film mass transfer coefficient (k_I^0) (41).

$$k_L = E \times k_L^0 \tag{5-21}$$

E depends on the Hatta number and the enhancement factor of an infinitely fast reaction (E_{inf}) (74). As mentioned before, the Hatta number is a dimensionless parameter that compares the rate of reaction in a liquid film to the rate of diffusion through the film (75).

$$Ha = \frac{\sqrt{k_2 \times D_{\text{CO}_2} \times [\text{Amine}]}}{k_1^0}$$
 (5-22)

E_{inf} depends on the choice of the mass transfer model. In this case, for the film theory model (74):

$$E_{inf} = 1 + \frac{D_{\text{Amine}} \times [\text{Amine}]}{\lambda \times D_{\text{CO}_2} \times [\text{CO}_2]}$$
 (5-23)

Where:

Table 36: Input for dimensionless numbers

Symbol	Description	Value	Unit
k_2	Reaction rate constant	29	[m3*mol/s]
$D_{\mathrm{CO}_2}^-$	CO ₂ diffusion coefficient	1*10 ⁻¹⁰	[m²/s]
[Amine]	Amine concentration	4218	[mol/m³]
$k_{ m L}^0$	Physical liquid film mass transfer coefficient	1*10 ⁻¹⁰ (76)	[m/s]
$D_{ m Amine}$	Amine diffusion coefficient	1*10 ⁻⁹ (77)	[m²/s]
λ	Amine mol needed by CO ₂ to react	2	[-]
$[CO_2]$	CO ₂ concentration	0.003	[mol/m ³]
$k_{ m obs}$	Observed kinetic constant	45230	[1/s]

The pseudo-first order regime is achieved if the reaction is fast and the amine concentration is high. These conditions are fulfilled if (74):

$$2 < Ha \ll E_{inf}$$

Table 37 shows the values of the Hatta number and Einf. According to those values, the reaction takes place in the pseudo-first order regime.

Table 37: Values of Hatta number and enhancement factor for an infinitely fast reaction

Hatta number [-]	E _{inf} [-]
35	7*10 ⁶

In the pseudo-first order regime E is given by Eq. (5-24) (74):

$$E = \frac{Ha}{\tanh(Ha)} \tag{5-24}$$

Eq. (5-25) shows Ha in the pseudo-first order regime (41):

$$Ha = \frac{\sqrt{k_{\text{obs}} \times D_{\text{CO}_2}}}{k_L^0} \tag{5-25}$$

It can be concluded that the reaction takes place in the pseudo-first order regime. Due to the lack of data, the values of k_L^0 and $D_{\rm Amine}$ correspond to MEA solutions with H₂O. However, given the fact that the reaction constant is quite high (as mentioned in Section 4.2.3) it seems that the Hatta number will be high enough to ensure that the absorption process is diffusion limited, even though the values of k_L^0 and $D_{\rm Amine}$ do not correspond to TEPA solutions.

Discussion

As mentioned before, the equilibrium capacity of CO_2 in monoliths impregnated with PEI and TEPA is 2 and 3 mol CO_2 / kg sorbent respectively. The experimental data from this thesis shows an average CO_2 loading of 1 mol CO_2 / kg sorbent after 1 hour. This implies that the CO_2 capacities of this thesis are far from equilibrium.

On the other hand, experiments performed with polyamines preloaded with H_2O showed that H_2O goes to a specific value. For example, Table 12 showed that TEPA preloaded with 20 wt% of H_2O stabilizes around 13 mol H_2O / kg sorbent (for a relative humidity of 38% and a temperature of 19°C) whereas PEI preloaded with 30 wt% of H_2O stabilizes around 14 mol H_2O / kg sorbent (for a relative humidity of 44% and a temperature of 19°C). This means that H_2O reached equilibrium in one hour.

The driving force of H_2O changes in time because at a certain moment the polyamine will be full of H_2O since it does not react. Therefore, the diffusion of H_2O will be slower in time because the gradient becomes smaller.

The Hatta number compares the rate of reaction to the rate of diffusion (75). If the Hatta number is high, the reaction is relatively fast so the process is diffusion limited. Therefore, the CO_2 absorption process goes as fast as the diffusion. The CO_2 absorption has an infinitely driving force because it reacts and turns into carbamate. The value of the Hatta number is 70, as shown before, which is high enough to assume that the CO_2 absorption process is diffusion limited.

Diffusion coefficient of CO2 calculated assuming a high Hatta number

A new route can be followed to calculate the diffusion coefficient of CO_2 : by considering that the CO_2 absorption has a high Hatta number. This diffusion coefficient only considers the diffusion of the physical CO_2 , not the CO_2 turned into carbamate.

If the Hatta number is high the CO₂ model can be simplified since the reaction term is negligible:

$$\frac{\partial c_{\text{CO}_2}}{\partial t} = D_{\text{CO}_2} \times \frac{\partial c_{\text{CO}_2}^2}{\partial x}$$
 (5-26)

The left boundary conditions is:

$$c_{\text{CO}_2}(x=0,t) = c_{\text{eq}}$$
 (5-27)

The Henry constant is only needed for kinetics because kinetics depend on the physical concentration of CO_2 , which is a function of the Henry constant. The diffusion is related to the driving force. At equilibrium conditions, $4*10^{-4}$ atm of CO_2 is equal to 1.8 mol CO_2 / kg PEI or 2.6 mol CO_2 / kg TEPA according to the equilibrium data obtained from SAS (64).

The right boundary condition is:

$$c_{\text{CO}_2}(x = L, t) = 0 (5-28)$$

The reaction is assumed to be so fast that no CO₂ reaches the end of the layer thickness.

The initial condition is:

$$c_{\text{CO}_2}(x, t = 0) = 0 {(5-29)}$$

If the diffusion coefficient of CO₂ obtained from the kinematic diameter relation is used, the correlation between experimental and calculated CO₂ loadings is very weak (Figures 89 and 90). It seems that these diffusion coefficients are too high.

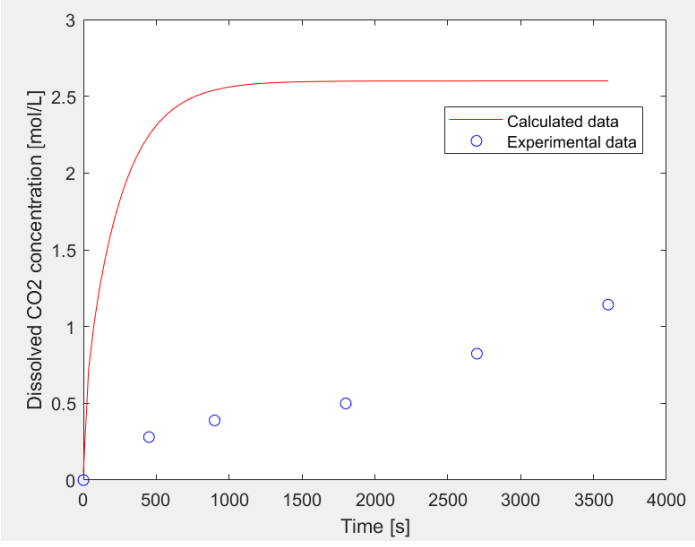


Figure 89: Correlation between experimental (TEPA 0.5 mm) and calculated CO₂ loadings using the diffusion coefficient of CO₂ from the kinematic relation

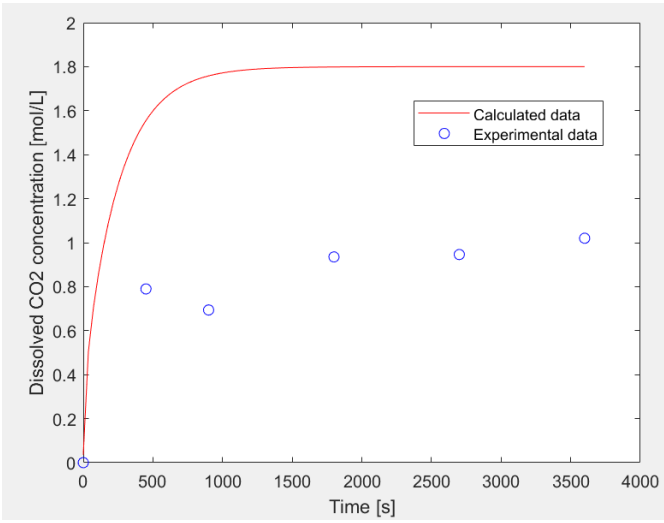


Figure 90: Correlation between experimental (PEI 0.5 mm) and calculated CO₂ loadings using the diffusion coefficient of CO₂ from the kinematic relation

Figure 91 shows that if the diffusion coefficient of CO_2 in TEPA is decreased until $3*10^{-12}$ m²/s the correlation between experimental and calculated CO_2 loadings is improved. Figure 92 shows that, according to the model, the equilibrium concentration of CO_2 in TEPA is achieved after around 9 hours. Figures 93 and 94 show the CO_2 diffusion process in the layer of 0.5 mm of TEPA.

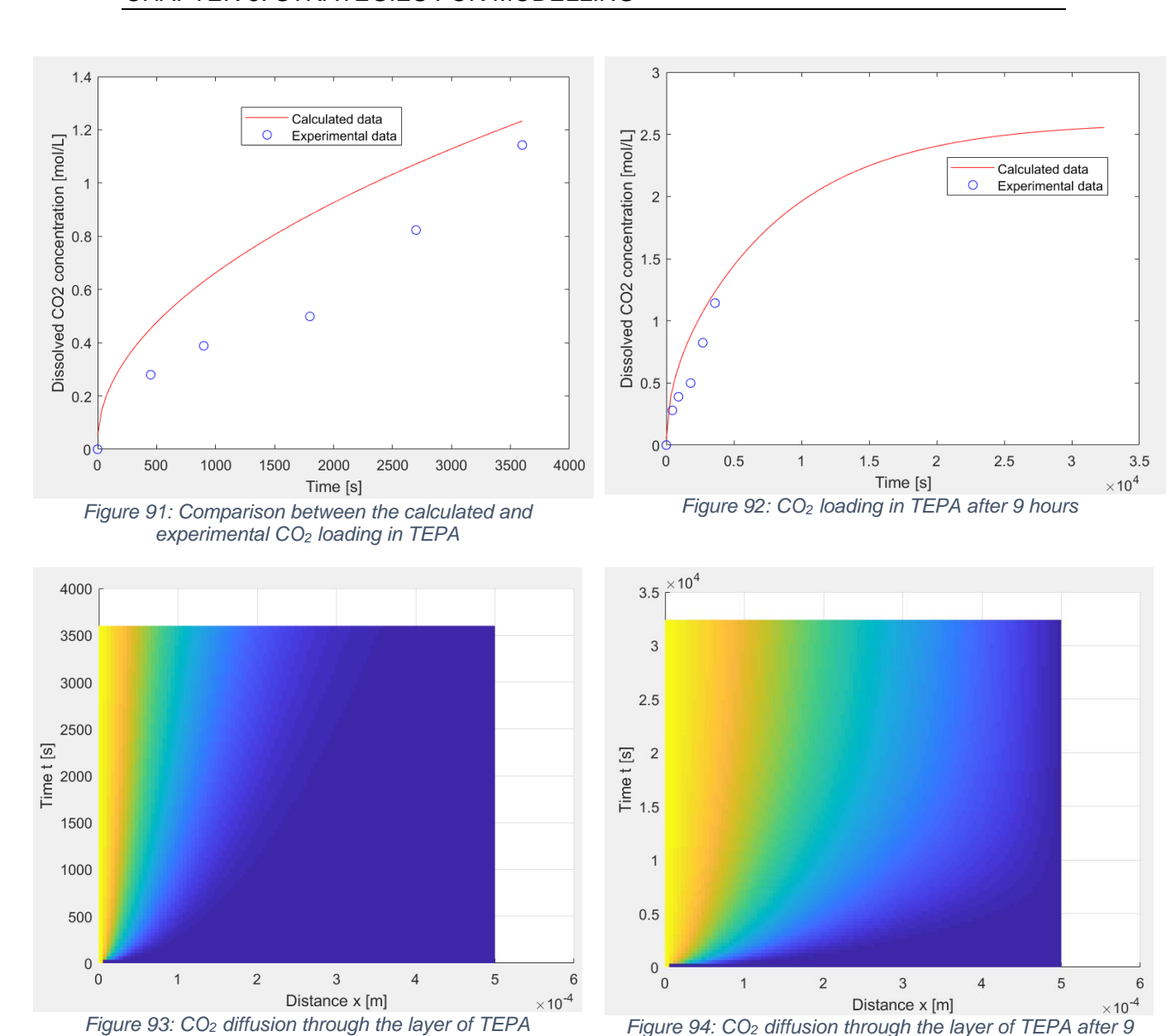


Figure 95 shows that if the diffusion coefficient of CO_2 in PEI is decreased until $4*10^{-12}$ m²/s the correlation between experimental and calculated CO_2 loadings is improved. Figure 96 shows that, according to the model, the equilibrium concentration of CO_2 in PEI is achieved after around 5 hours. Figures 97 and 98 show the CO_2 diffusion process in the layer of 0.5 mm of TEPA.

hours

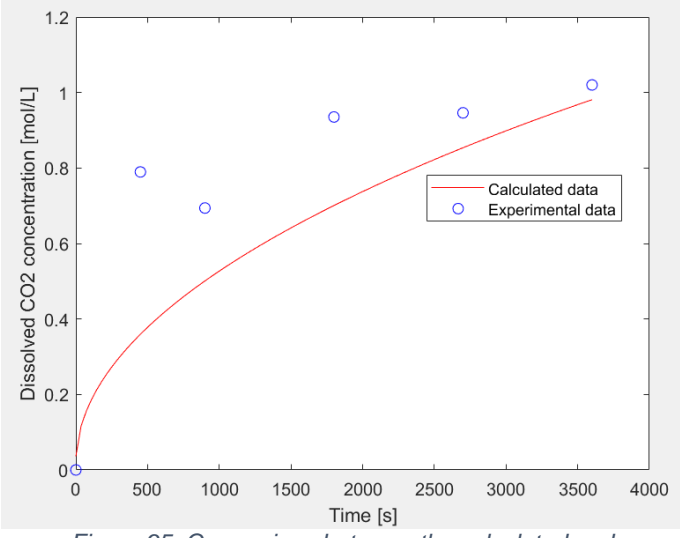


Figure 95: Comparison between the calculated and experimental CO₂ loading in PEI

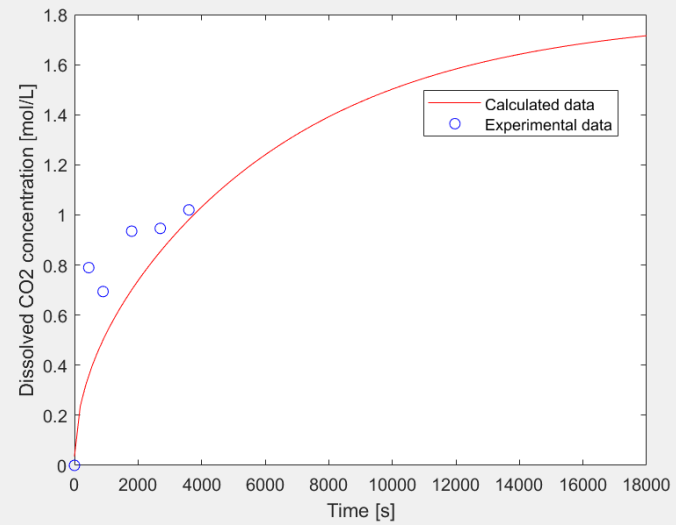


Figure 96: Calculated CO₂ loading in PEI achieving equilibrium after 5 hours

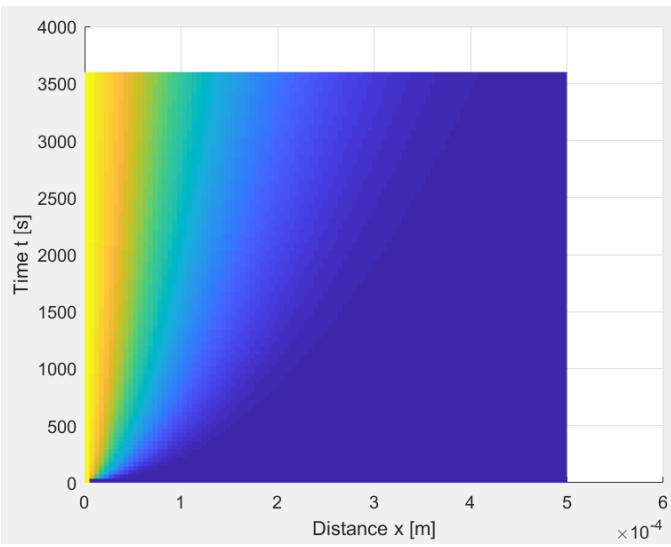


Figure 97: CO₂ diffusion through the layer of PEI

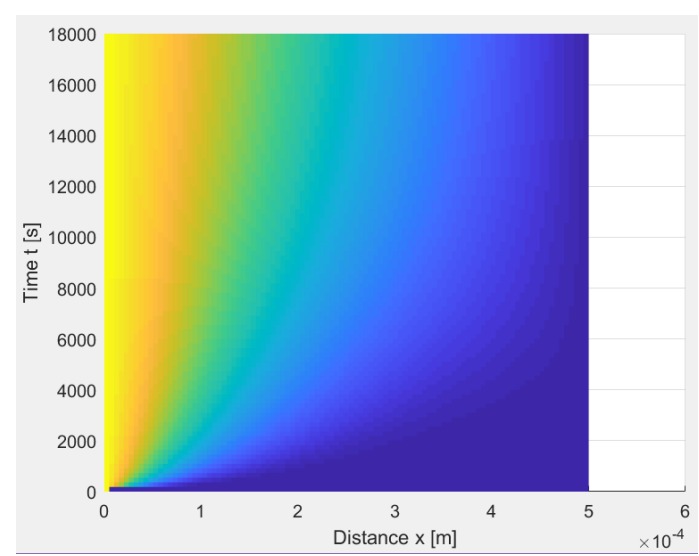


Figure 98: CO₂ diffusion through the layer of PEI after 5 hours

Table 38 shows that the diffusion coefficients of CO₂ obtained from the two different routes (kinematic diameters and high Hatta number) differ in two orders of magnitude.

Table 38: Comparison of diffusion coefficients of CO₂

Sorbent	D _{CO₂} (kinematic diameter)	D _{CO2} (high Hatta number)
TEPA	1*10 ⁻¹⁰ m ² /s	3*10 ⁻¹² m ² /s
PEI	1*10 ⁻¹⁰ m ² /s	4*10 ⁻¹² m ² /s

The difference between the diffusion coefficients calculated following the kinematic diameter methodology and the high Hatta number assumption can be due to the fact that CO_2 might have several molecular interactions with PEI and TEPA that H_2O does not have. The diffusion coefficient of CO_2 in monoliths impregnated with TEPA and PEI have a value of $2*10^{-12}$, slightly lower than the diffusion coefficients of CO_2 given by the high Hatta number assumption.

Figure 102 shows the absorption process if the Hatta number is high.

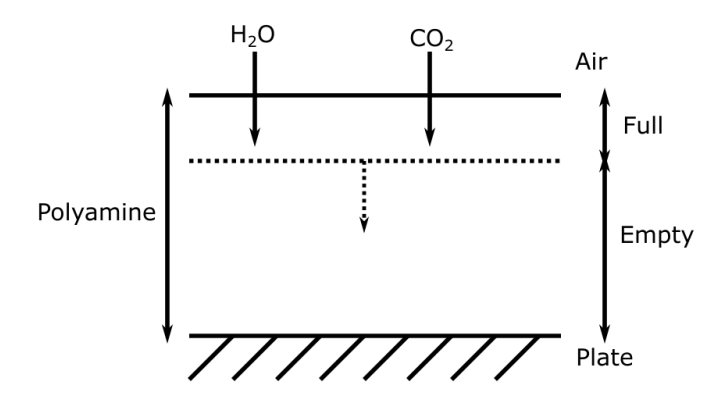


Figure 99: CO2 and H₂O diffusing into pure polyamine

The value of the Hatta number if, $3*10^{-12}$ m²/s is taken as the diffusion coefficient, is 6. Hence, the assumption of the first-pseudo regime for the reaction still holds. It can be concluded that the diffusion coefficients of CO₂ calculated following the route of assuming a high Hatta number are more realistic.

Polyamines will not be stagnant in ZEF's absorber. If the polyamine layer is stagnant there is no mixing so the effective diffusivity is much lower than in a flowing layer where there is mixing per definition, so the diffusion is faster (36). Therefore, it is expected that the diffusion coefficient of CO₂ in a flowing layer of polyamine will be higher, increasing the Hatta number value.

5.3.4. Hildebrand solubility parameter

The Hildebrand solubility parameter (δ) provides a numerical estimate of the degree of interaction between materials. Hence, it can be a good indicator of solubility.

Due to the high viscosity of the sorbents, it was not possible to perform the physisorption experiment with lower H₂O concentrations. This is because the stirrer that mixes the sorbent in the setup does not work for viscous fluids.

The cohesive energy density is the amount of energy required to separate a unit volume of molecules from their neighbours. The Hildebrand solubility parameter is the square root of the cohesive energy density (78):

$$\delta = \sqrt{\frac{\Delta H_{\nu,i} - RT}{V_{m,i}}} \tag{5-29}$$

The data used to calculate the Hildebrand solubility parameter is shown in Table 39. Unfortunately, the heat of vaporization of PEI could not be found.

Table 39: Input to calculate the Hildebrand solubility parameter

Symbol	Description	Value	Unit
$\Delta H_{v,H_2O}$	Heat of vaporization of water	44200 (79)	[J/mol]
$\Delta H_{v, \text{TEPA}}$	Heat of vaporization of TEPA	57902 (80)	[J/mol]
R	Ideal gas constant	8.314	[J/(K*mol)]
T	Temperature	293	[K]
$V_{m,\mathrm{H}_2\mathrm{O}}$	Molar volume of water	18	[cm³/mol]
$V_{m, \text{TEPA}}$	Molar volume of TEPA	190	[cm³/mol]

The larger the cohesive energy density of the solvent, the lower the solubility of non-polar compounds in that solvent.

Table 40 shows that the Hildebrand parameter of H₂O is almost three times higher than the Hildebrand parameter of TEPA.

Table 40: Hildebrand parameter for H₂O and TEPA

Component	$\delta (J^{1/2}/cm^{3/2})$
H_2O	48
TEPA	17

In this case, the cohesive energy density of H_2O is large, implying that the solubility of N_2O in H_2O , non-polar, is lower. Since the solubility constant was measured in a solution with 70 wt% of H_2O that solubility constant is lower than the actual one, since the H_2O content will be lower.

It can be concluded that the fact that the Henry constant was obtained from a solution of 30 wt% TEPA and 70 wt% H_2O has an influence, since the Hildebrand parameter of H_2O is lower than the Hildebrand parameter of TEPA. This could imply that if the physisorption experiment is repeated in a solution with lower H_2O content, the Henry constant will be different.

6 Strategies for designing

In this chapter lessons learned from the experiments and modelling are applied to give some guidelines regarding the design and scale-up of the absorber that fits ZEF requirements.

6.1. Effect of preloading H2O in polyamines in stagnant and flowing layers of polyamine

ZEF Team 4 focused its efforts on polyamines flowing vertically whereas this thesis is related to stagnant polyamines. In this Section, the differences regarding CO₂ loadings and kinetics in stagnant and flowing layers are briefly introduced.

ZEF Team 4 perceived that if the polyamine was not premixed with H_2O the CO_2 loading was lower, for both PEI and TEPA. However, this is in contrast with what was perceived in this thesis. Figure 100 shows that, in the case of PEI, PEI preloaded with H_2O has a lower ending CO_2 loading than pure PEI. Figure 101 shows that, in the case of TEPA, the kinetics and ending concentration of CO_2 are similar no matter if the polyamine is premixed or not with H_2O .

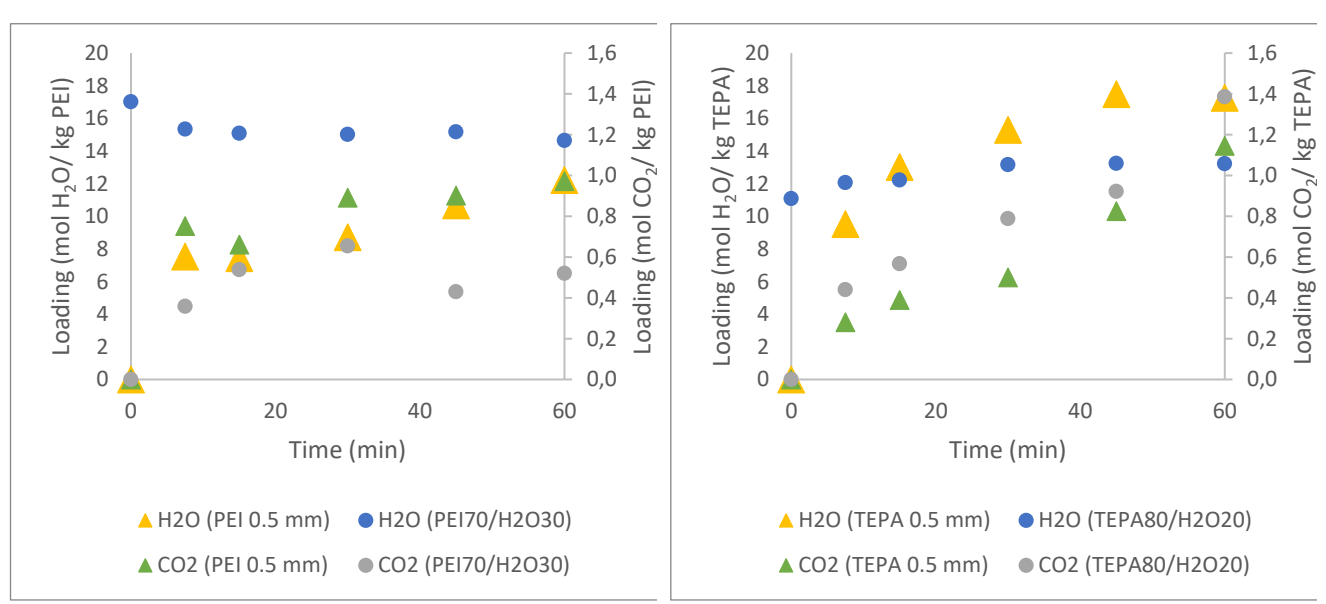


Figure 100: CO₂ and H₂O loadings of pure PEI and preloaded with H₂O

Figure 101: CO₂ and H₂O loadings of pure TEPA and preloaded with H₂O

This difference in kinetics between flowing and stagnant layers could be due to viscosity effects given the fact that viscosity changes if the polyamine is preloaded or not with H₂O.

Kinetics in flowing and stagnant layers are different because of viscosity effects. The layer of polyamine in touch with the wall has no velocity due to the maximum shear stress. The layer of polyamine in contact with the air absorbs H_2O which influences the

viscosity (Figure 102). Hence, this layer will flow slower than the layers under it (Figure 103).

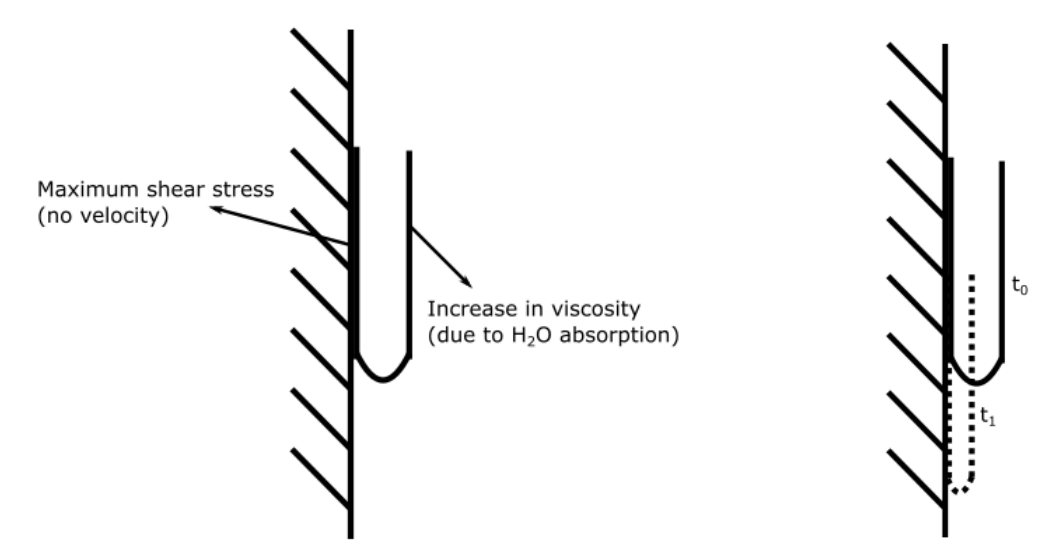


Figure 102: Flowing layer of polyamine at t=t₀

Figure 103: Flowing layer of polyamine at t=t1

Further research is needed regarding the effect of viscosity in the flowing behaviour of the polyamine.

6.2. Design of the absorber

A continuous absorber is designed using the experimental CO₂ loadings obtained in Chapter 4 and assuming a residence time of 60 minutes.

The lessons learned are:

- According to the data collected by ZEF Team 4, the polyamine has to be premixed with H₂O, otherwise less CO₂ is captured.
- Mixing patterns should be introduced in order to reduce the diffusion length since the process is diffusion limited. This is not considered in this design, since it is a first estimate.
- If the layer thickness is too low the velocity of the polyamine will be too slow, not allowing to perform many absorption-desorption cycles per day. On the other hand, if it is too high the flow will be too high, decreasing the residence time, leading to a low CO₂ loading.
- Experimental data from pure TEPA and PEI will be used. However, H₂O will be present in the polyamine after the desorption step, since not all the H₂O will be removed. Moreover, the composition of the sorbent changes while it flows on the plate due to the H₂O absorption. This will decrease the viscosity. This is not considered in this design, since it is a first estimate.

The data used for the design of the absorber is summarized in Table 41:

Table 41: Sorbents used in the absorber design

Sorbent	Layer thickness (mm)	CO ₂ loading (mol CO ₂ / kg sorbent)
PEI	0.50	1.0
TEPA	0.50	1.1

The whole ZEF complex would be powered by solar energy so the number of hours of sunlight is a key factor to be considered when choosing where to locate the ZEF plants (48). *Van den Berg* (48) suggested Spain as a potential candidate. Spain receives around 3000 annual hours of sunshine. Hence, in this base case, 8 hours are assumed as the average working hours per day.

Since the final design involves a continuous absorber the absorption time is assumed to be 60 minutes. The desorption time is assumed to be 30 minutes because the desorption step is faster than the absorption step (36).

ZEF has two criteria that have to be satisfied in the DAC unit: from the liquid side point of view, 293 g CO₂/ day should be captured whereas, from the gas phase point of view, 25% of the CO₂ coming in should be captured. The focus of the first design is the liquid phase. Hence, a maximum and constant driving force from the gas side is assumed.

6.2.1. Design of stagnant layer system

Firstly, a stagnant absorber is designed to gain some insight regarding the order of magnitude of the surface area. As mentioned before, if the polyamine layer is stagnant the diffusion coefficient will be lower than in a flowing layer, since there is no mixing. This is why the required absorption area is higher for stagnant than for flowing layers of polyamine.

1 cycle requires 90 minutes (60 of absorption and 30 of desorption respectively) so 5 cycles can be performed per day.

$$n_{\rm cycle} = \frac{t_{\rm sunlight}}{t_{\rm cycle}} \tag{6-1}$$

Since the amount of CO₂ absorbed per kg of sorbent is known, it is possible to calculate the amount of sorbent needed.

$$M_{\text{sorbent}} = \frac{Target\ yield}{Loading_{\text{CO}_2} \times n_{\text{cycle}}}$$
 (6-2)

The area can be easily calculated since the layer thickness and the sorbent volume are known.

$$V_{\text{sorbent}} = M_{\text{sorbent}} \times \rho_{\text{sorbent}}$$
 (6-3)

$$A = \frac{V_{\text{sorbent}}}{h} \tag{6-4}$$

The results are shown in Table 42:

Table 42: Area needed per sorbent to absorb the CO2 target yield

Sorbent	A (m ²)
PEI	2.54
TEPA	2.43

It can be concluded that the area needed to reach the ZEF's absorption goal of 293 g CO₂/ day is quite similar for both PEI and TEPA with a layer thickness of 0.5 mm.

6.2.2. Velocity calculation

The polyamine will flow in the continuous absorber. Hence, it is important to calculate the velocity at which the polyamine will flow on the plates.

Figure 104 shows the schematic drawing used to calculate the velocity distribution using Navier-Stokes equations.

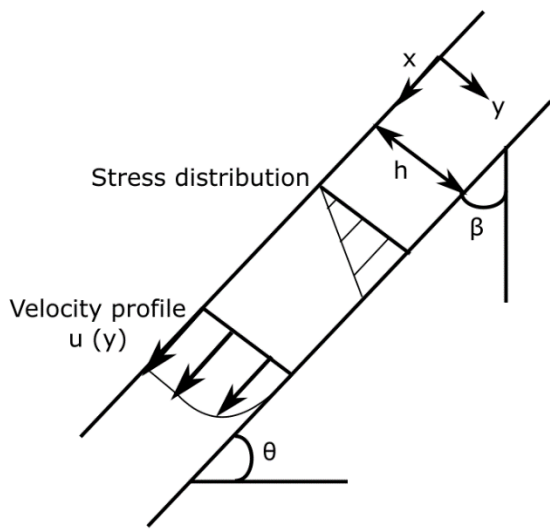


Figure 104: Laminar flow of a fluid layer falling down an inclined plate (81)

The velocity distribution can be obtained from the momentum equation along the x-direction. The flow is assumed to be steady (81):

$$0 = \rho g \cos \beta + \mu \frac{\partial^2 u}{\partial y^2} \tag{6-5}$$

Where:

Table 43: Input to calculate the velocity distribution

Symbol	Description	Unit
ρ	Density of sorbent	[kg/m³]
g	Gravity	[m/s ²]
μ	Viscosity of sorbent	[kg/(m*s)]
β	Angle of inclination	[°]
u	Velocity	[m/s]

Integrating twice gives:

$$u(y) = -\frac{\rho g \cos \beta}{2\mu} y^2 + Ay + B \tag{6-6}$$

Where A and B are constants. The boundary conditions allow to evaluate them.

The boundary condition on the liquid surface is zero shear stress,

$$y = 0, \mu \frac{du}{dy} = 0 \tag{6-7}$$

The boundary condition on the solid surface is zero velocity,

$$y = h, u = 0 \tag{6-8}$$

So, the velocity profile is

$$u(y) = \frac{\rho g \cos \beta}{2\mu} (h^2 - y^2)$$
 (6-9)

The average of the velocity is:

$$u_{avg} = \frac{\int_0^h u(y) \times dy}{h} = \frac{\rho g h^2 \cos \beta}{3\mu}$$
 (6-10)

Moreover, the velocity can be expressed as the plate length divided by the residence time:

$$u_{\text{avg}} = \frac{L}{RT} \tag{6-11}$$

It is assumed that the polyamine flows like an ideal plug flow and that there is no back mixing. Equations (6-10) and (6-11) will be used to design the absorber.

6.2.3. Design of flowing layer system

So far, the experimental data that belongs to stagnant layers has been used. The next step is to figure out how an absorber with flowing layers of polyamine would look like.

Figure 105 shows three possible distributions to fit the same area for the absorber. It seems that a compact design, option a, would require shorter plates.

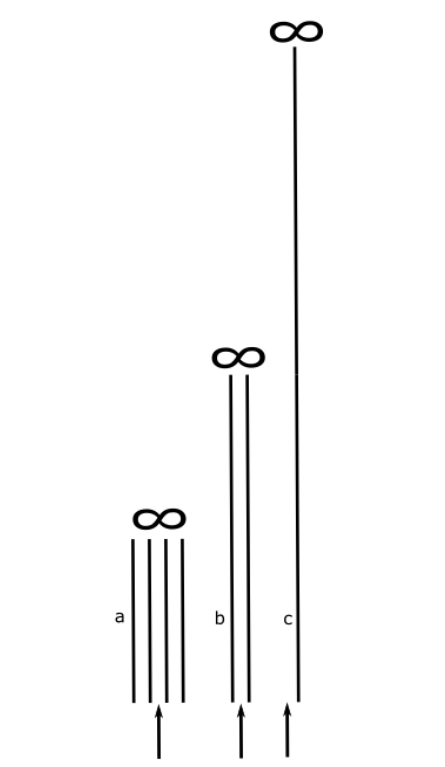


Figure 105: Possible designs of the absorber

The average velocity was calculated in Section 6.2.2:

$$u_{\text{avg}} = \frac{\rho g h^2 \cos \beta}{3\mu} \tag{6-12}$$

From Equation (6-11) it is possible to obtain the plate length:

$$L = u_{\text{avg}} \times RT \tag{6-13}$$

The average velocity depends on several parameters. The density and the viscosity depend on the sorbent whereas the layer thickness is fixed to be 0.5 mm. The angle of inclination depends on the orientation of the plates. Firstly, the plates are assumed to be vertical (β =0). Table 44 summarizes the average velocity and the length of the plates to achieve a residence time of 60 minutes.

Table 44: Average velocity and plate length per sorbent

Sorbent	Average velocity (m/s)	Plate length (m)
PEI	3.1*10 ⁻⁴	1.1
TEPA	8.7*10 ⁻³	31.24

Both plate lengths seem unrealistic, in terms of the size of ZEF's micro-plant. TEPA flows around 30 times faster than PEI, which explains why the plate is 30 times longer. The angle of inclination can be changed. This optimization will be studied in Section 6.3.

Since the total area required and the length are known, the width can be calculated:

$$w_{\text{total}} = \frac{A}{L} \tag{6-14}$$

However, if the polyamine flows vertically, two sides of each plate can be used. Then, the width is reduced by half.

$$w = \frac{w_{\text{total}}}{N_{\text{sides}}} \tag{6-15}$$

ZEF has already selected the fan SUNON (PMD1212PMB2-A) DC12V as the one suitable for the absorber unit (which was also used during the experiments). This fan has a cross-section area of 12x12 cm. Then, the width of the column of plates is assumed to be 10 cm longer (w_{plate}). In this way, the flow is slowed down (Figure 106)

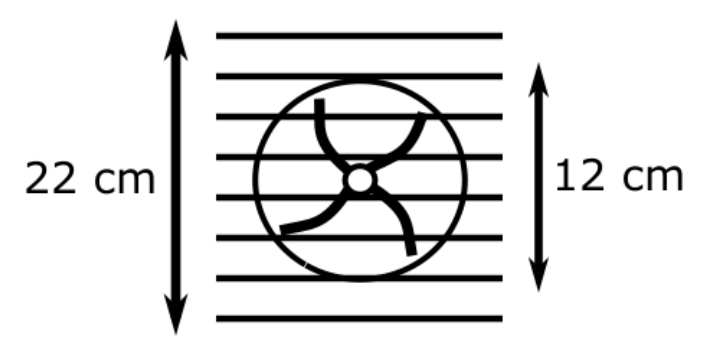


Figure 106: Width and height of absorber and fan

The minimum plate spacing (S_{plate}) is assumed to be 10 mm (Figure 107). If the plates are placed too close the flow will be disturbed and if they are too far the space will not be used efficiently. It is assumed that 10 mm is enough space for the air to flow. The

thickness of the plates is assumed to be 5 mm (th_{plate}) (Figure 107), just like the ones used in the experiments.

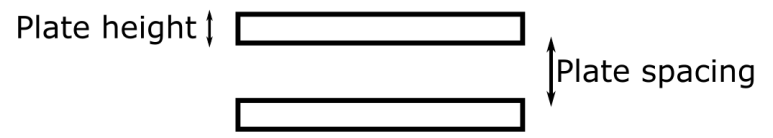


Figure 107: Plate height and spacing

The next step is to find out how many plates are required to achieve that area:

$$n_{\text{plate}} = \frac{w}{S_{\text{plate}} + th_{\text{plate}} + w_{\text{plate}}}$$
 (6-16)

Finally, a quick check is done:

$$A_{\rm plate} = N_{\rm plate} \times w_{\rm plate} \times L$$
 (6-17)

If the new calculated area is the same as the area calculated in Equation (6-4) the dimensions can be assumed as correct.

The dimensions to achieve a residence time of 60 minutes with a layer thickness of 0.5 mm of PEI and TEPA are shown in Table 45:

Table 45: Dimensions of the vertical absorber

Sorbent	β (°)	Plate width (m)	Plate length (m)	Number of plates (-)	A (m ²)
		\ /	\ /	plates (-)	
PEI	0	0.22	0.96	5	2.45
TEPA	0	0.22	31.24	1	13.74

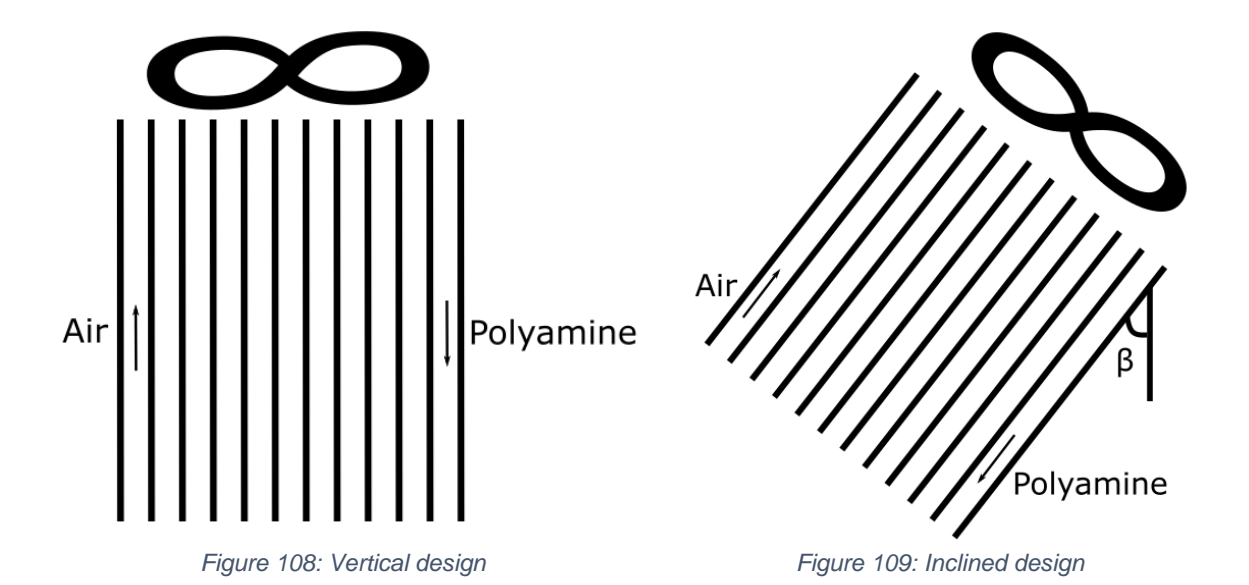
The area obtained if PEI is used as a sorbent is slightly lower than the required one, 2.54 m², whereas the area that corresponds to TEPA is surprisingly high. This is because the plate requires a huge length in order to keep the TEPA flowing for 60 minutes.

The main conclusion is that a vertical plate requires really long plates in order to keep the PEI and TEPA flowing for 60 minutes.

6.3. Optimization

The parameter that can be changed in order to make the dimensions more realistic, while keeping a residence time of 60 minutes, is the degree of inclination.

A vertical design has no β whereas an inclined design has a β different to zero (Figure 108 and 109).



If the plate is inclined then the sorbent will flow slower. Sinha (49) proposes a plate length of 0.3 m. This length will be used in this optimization.

$$\beta = \cos^{-1}(\frac{3 \times \mu \times L}{\rho \times g \times h^2 \times RT}) \tag{6-18}$$

Table 46 shows the absorber dimensions with different angles of inclination:

Sorbent β (°) Plate width Plate length Number of A (m²) (m) (m) plates (-) PEI 0.22 0.30 37 74 2.44 0.22 **TEPA** 89 0.30 35 2.31

Table 46: Dimensions of the inclined absorber

The angle of inclination of TEPA implies that the plates should be placed almost horizontally.

It can be concluded that the new angles of inclination reduce the plate length. The dimensions of the inclined absorber seem to fit better in the DAC unit of ZEF.

6.4. Cost of the sorbent

Another important factor is the cost of the sorbent since it is connected to the liquid inventory. The CO_2 loadings used in Sections 6.2 and 6.3 are not the net cycle capacity because not all the CO_2 (and H_2O) are fully desorbed. In a standard MEA desorption process, around 50% is desorbed (36). Then, the net cycle capacity is half:

$$\alpha_{net\ cycle} = \frac{Loading_{CO_2}}{2} \tag{6-19}$$

The mass of the sorbent is calculated like in Equation (6-2). However, in this case, the CO_2 loading is replaced by the net cycle capacity:

$$M_{sorbent} = \frac{Target \ yield}{\alpha_{net \ cycle} \times n_{cycle}}$$
 (6-20)

The cost of the sorbent can be calculated if the price of sorbent per kg is known.

$$C_{sorbent} = M_{sorbent} \times P_{sorbent} \tag{6-21}$$

The price of PEI and TEPA belong to the suppliers Polysciences and Sigma- Aldrich respectively (Table 47).

Table 47: Price of PEI and TEPA

Sorbent	Price (€/kg)	Reference
PEI	418	(82)
TEPA	78	(83)

Table 48 shows that PEI increases sharply the sorbent cost:

Table 48: Sorbents mass and cost

Sorbent	Mass (kg)	Cost (€)
PEI	1.33	557
TEPA	1.21	94

6.5. Final design

Due to the innovative nature of the system and that in this thesis is a first parametric study has been done, not enough data is available to make a full design. However, some guidelines can be made.

The dimensions of the inclined absorber are summarized in Table 50.

Table 49: Dimensions of the inclined absorber

Sorbent	B (°)	Plate width	Plate length	Number of	A (m ²)
		(m)	(m)	plates (-)	
PEI	74	0.22	0.30	37	2.44
TEPA	89	0.22	0.30	35	2.31

The proposed design is shown in Figure 110:

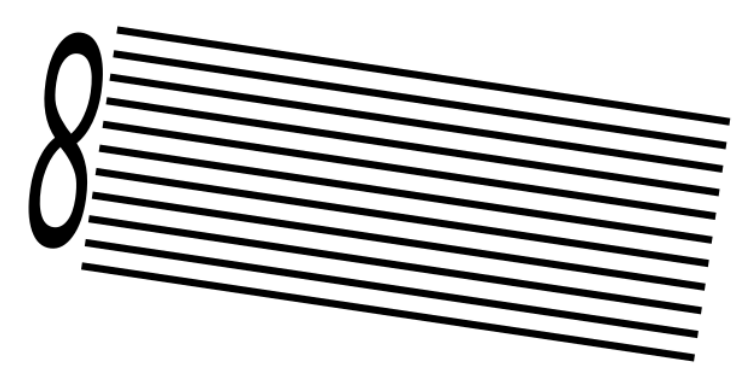


Figure 110: Inclined absorber design

7 Conclusions and recommendations

7.1. Conclusions

The objective of this thesis was to characterize, from the experimental and modelling point of view, the H_2O and CO_2 absorption on polyamines (PEI and TEPA). To that end, H_2O and CO_2 absorption experiments were done and the data collected from them was used to develop a model.

Firstly, absorption experiments were conducted in a climate chamber where only H_2O was present. From these experiments, it was concluded that the H_2O loading in the polyamine depends on the humidity of the air.

Secondly, CO_2 and H_2O were absorbed from the air at lab conditions. Several modifications were done in the sorbent: different type of polyamine, different layer thickness, blends of the polyamine, polyamines mixed with H_2O and higher CO_2 concentrations. Then, all the variations were compared using two parameters: CO_2 loading (mol CO_2 / kg sorbent) and H_2O loading (mol H_2O / kg sorbent). The first parameter is directly related to the CO_2 absorption capacity of the sorbent. Data from pure PEI and TEPA was used to design an absorber for the ZEF unit as a first estimate.

Thirdly, two models were developed in MATLAB in order to find the diffusion coefficients of H_2O and CO_2 in PEI and TEPA. It is important to mention that the CO_2 absorption process was identified to be diffusion limited. This was considered when developing the model. The main finding was to find out that the diffusion coefficient of CO_2 is two orders of magnitude lower than the diffusion coefficient of H_2O .

Finally, one inclined absorber design for the ZEF micro plant was proposed.

Three main questions were posed at the beginning of this thesis. Having studied the process, the questions can now be answered.

1) What is the effect of varying process conditions (type of polyamine, layer thickness, H₂O content, CO₂ ppm) in the air capture?

This question was answered performing air capture experiments at lab conditions.

- Pure TEPA captures more CO₂ than pure PEI.
- In general, the layer thickness plays an important role in the time frame considered, 60 minutes, which is assumed to be realistic for flowing systems.
 CO₂ loading and mass are highly influenced by the layer thickness before 60 minutes.
- Combining PEI and TEPA did not give higher CO₂ loadings than pure TEPA.
- In the case of TEPA, an increase in the H₂O content improved the loading of CO₂. The opposite happened in the case of PEI.
- The results of the experiments variation of CO₂ concentration in the air lead to high noise in the data set, making it difficult to come to a conclusion. However,

it is expected that when the CO₂ concentration is increased there would be a direct influence in the CO₂ loading.

2) What is the chemical process that drives the CO₂ absorption on polyamines?

The experimental results using FTIR suggested that the major pathway goes via the carbamate and less via the bicarbonate. This is of relevance for the desorption due to the higher amount of desorption energy needed to split the CO_2 from a carbamate than from a bicarbonate. However, due to the fact that CO_2 reacts forming carbamate, kinetics are faster. Carbamate formation has also been experimentally measured because the Hatta number is very high.

3) How should an absorber be designed in order to meet ZEF requirements?

When using the ZEF configuration H_2O will be present in the sorbent after the desorption step since not all the H_2O will be removed. Hence, designing an absorber for pure PEI and TEPA is not realistic due to the fact that H_2O will always be present. The design of the ZEF absorber is based on achieving enough residence time. For horizontal systems, in an order of 60 minutes, a loading of 1 mol CO_2 / kg sorbent is achieved. This is a key parameter for the design.

For the ZEF design, only the absorption has been taken into account, and not the net cycle capacity. The vertical design dimensions seem to be unrealistic since the plates are probably too long to fit in the ZEF micro-plant. If the absorption data is taken, to achieve a residence time of 60 minutes the plates should be inclined. Table 50 shows the dimensions for both PEI and TEPA.

Table 50: Dimensions of the inclined absorber (proposed design)

Sorbent	β (°)	Plate width	Plate length	Number of	A (m ²)
		(m)	(m)	plates (-)	
PEI	74	0.22	0.30	37	2.44
TEPA	89	0.22	0.30	35	2.31

For the first time, a flowing system of polyamine has been considered as an option to capture CO₂ from the air showing that loadings of 1 mol CO₂/ kg sorbent are feasible. However, viscosity and low diffusion coefficients can lead to very long time periods before reaching equilibrium loading levels. Therefore, it is important to optimize the flowing behaviour in order to reach equilibrium.

7.2. Recommendations

This thesis is divided in three parts: experiments, modelling and design. Therefore, the recommendations section will follow the same structure.

7.2.1. Experiments

During this thesis, the layer thickness of the polyamine was roughly estimated.
The layer thickness of the polyamine is one of the key parameters for the
design of the continuous absorber. Hence, the layer thickness should be
calculated more accurately.

- The effects of PEI and TEPA penetrating into the paper, placed on top of the
 plate, were not considered in this thesis. However, they should be studied
 because if the polyamine penetrates into the paper the layer thickness will
 change. As mentioned before, the layer thickness is extremely important when
 it comes to the design of the absorber. Otherwise, a different surface should be
 found.
- Due to the focus of the research, only experiments at 20 °C were performed for TEPA inside the climate chamber. It is recommended to perform experiments at 10, 30 and 40 °C in order to calculate the average diffusion coefficient of H₂O in TEPA more accurately.
- More data points should be collected at the beginning of the H₂O and CO₂ absorption in order to gain more knowledge about the transient part of the absorption process. This should not be too difficult to do for the air capture experiments. However, this is probably challenging to do in the climate chamber because the conditions inside the climate chamber will be influenced by the lab conditions.
- It would be interesting to perform experiments with different layer thicknesses of polyamine for more than 60 minutes (and collect at least one more point during the transient period) in order to check if the CO₂ loading and mass become independent of the layer thickness.
- The equilibrium loadings, and the time needed to achieve them, should be found experimentally in order to be able to estimate the driving force. Given the fact that the CO₂ absorption seems to be diffusion limited, it is important to obtain the driving force, since the diffusion depends on it.
- Before performing experiments where the CO₂ ppm in the air are varied, a homogeneous CO₂ ppm distribution should be obtained in order to obtain more accurate CO₂ loadings in the polyamines.
- It is recommended to repeat the experiments with different CO₂ ppm in the air for pure TEPA since the results obtained in this thesis are extremely noisy.
- Experiments with different CO₂ concentration in the air should be repeated for TEPA premixed with 20 wt% of H₂O.
- In this thesis, all the experiments that involved CO₂ absorption were done in the presence of H₂O. It would be interesting to study the behaviour of CO₂ when no H₂O is present.
- If more CO₂ and H₂O absorption experiments are done it is recommended to do them in an environment with controlled temperature and relative humidity, specially the second one, since it varied remarkably on different days. In addition to this, the CO₂ ppm should always be measured (and not only when the CO₂ ppm are varied).
- Stopped flow technique for kinetics and physisorption experiments should be used so the H₂O content in the polyamine is the same as in the real process, around 20 wt%, not 70 wt%, which was used in this thesis.

- The Hatta number is a key parameter of the CO₂ absorption, since depending on its value, the process will be limited by diffusion or reaction. The Hatta number was calculated in this thesis using the physical liquid film mass transfer coefficient and the diffusion coefficient of a solution of MEA. It is recommended to obtain these two parameters for polyamines. In this way, the Hatta number will be measured more accurately.
- It is recommended to collect kinetic data at different times, this is, loadings, in order to check if the Hatta number decreases until a point where the CO₂ absorption process becomes reaction limited instead of diffusion limited.

7.2.2. Modelling

- The diffusion coefficient of both H₂O and CO₂ was assumed to be a constant in the modelling part. However, during the experiments, it could be seen that it depends on temperature and on the composition of the sorbent (the H₂O concentration increased sharply when the polyamine was not preloaded with H₂O). Hence, the diffusion coefficient varies in time. It is advised that further work should consider the dependence of the diffusion coefficient with respect to the H₂O loading when the model is further developed.
- The effective diffusion coefficient of a flowing layer of polyamine is expected to be higher than the diffusion coefficient of a stagnant layer of polyamine since mixing is present in the first case. It would be interesting to obtain this effective diffusivity value if a model of the continuous absorber is developed in the future.

7.2.3. Design

- The net cycle loading, this is, how much H₂O and CO₂ will remain in the sorbent after the desorption step, should be calculated for PEI and TEPA. The net cycle loading is one of the key parameters in the design of the absorber, since different H₂O loadings in the polyamine have different viscosity values, and the viscosity will influence the flowing behaviour.
- Mixing patterns should be studied given the fact that the CO₂ absorption seems to be a diffusion limited process.
- Research is needed regarding the change of flowing behaviour of the
 polyamines in time. Once the polaymines are flowing they will absorb H₂O. Both
 PEI and TEPA have higher viscosities with low H₂O content. Hence, the flowing
 behaviour of the polyamine will change in time.

"I see now that the circumstances of one's birth are irrelevant. It is what you do with the gift of life that determines who you are." Takeshi Shudo

Appendices

A. Calculations of the stream volumes

The difference between the volume of flue gas and the volume of air required to capture the same amount of CO₂ is remarkable. This Appendix shows the calculations followed to obtain the volume of both streams.

In order to obtain the stream volume that needs to be handled (φ^i) , the CO₂ concentration $(\mathcal{C}_{\text{CO}_2}^i)$ is needed and it can be calculated with the CO₂ density (ρ_{CO_2}) .

 CO_2 density (ρ_{CO_2} in [kg/m³]) can be calculated according to the ideal gas law. To simplify, it is assumed that both the flue gas and ambient air are at the same temperature and pressure (normal conditions):

$$\rho_{\text{CO}_2} = \frac{P \times MW_{\text{CO}_2}}{RT} \tag{A-1}$$

Where:

Table 51: Input to calculate CO2 density

Symbol	Description	Value	Unit
P	Total pressure of the stream	101.325	[kPa]
MW_{CO_2}	CO ₂ molecular weight	44	[g/mol]
R	Universal gas constant	8.314	[(L*kPa)/(mol*K)]
T	Temperature	293.15	[K]

Using the values of P, $MW_{\rm CO_2}$, and T from Table 51, a value of 1.83 kg/m³ was obtained for the CO₂ density. Knowing the CO₂ density makes possible to find the concentrations of CO₂ in the flue gas and air streams ($c_{\rm CO_2}^i$ in [kg/m³]):

$$c_{\text{CO}_2}^i = y_{\text{CO}_2}^i \times \rho_{\text{CO}_2}$$
 (A-2)

Where:

Table 52: Input to calculate CO2 concentration in flue gas and air streams

Symbol	Description	Value	Unit
$y_{CO_2}^i$	CO ₂ volume fraction	Varies	[-]
ρ_{CO_2}	CO ₂ density	1.83	[kg/m³]

Knowing the concentration of CO₂ in each stream, the volume of stream that needs to be handled (φ^i in m³) is calculated with the following equation (A-3):

$$\varphi^i = \frac{{}^{M}_{CO_2}}{c^i_{CO_2}} \tag{A-3}$$

Where:

Table 53: Input to calculate the volume of flue gas and air streams needed to capture CO2

Symbol	Description	Value	Unit
$M_{\rm CO_2}$	CO ₂ mass that must be captured	1	[kg]
$c_{\mathrm{CO}_2}^i$	CO ₂ concentration	Varies	[kg/m³]

B. Calculation to obtain the layer thickness equation

Achieving a homogeneous layer thickness of polyamine is one of the key parameters, since the layer thickness of the polyamine plays an important role in the experimental residence time of this thesis (60 minutes), as it will be shown in Section 4.1.2.

A combination of Equations (B-1) and (B-2) is enough to estimate an average layer thickness.

$$V = l \times B \times h \tag{B-1}$$

$$V = \frac{M}{\rho_i} \tag{B-2}$$

Combining the right terms of Eq (B-1) and (B-2),

$$l \times B \times h = \frac{M}{\rho_i} \tag{B-3}$$

Where:

Table 54: Input to calculate average layer thickness

Symbol	Description	Value	Unit
V	Volume	-	[m ³]
$ ho_{TEPA}$	Density of TEPA	998	[kg/m³]
$ ho_{PEI}$	Density of PEI	1050	[kg/m³]
l	Length of the plate where the polyamine is spread	0.23	[m]
В	Width of the plate where the polyamine is spread	0.095	[m]

C. Arduino codes and wiring

The sensors are controlled with Arduino microcontrollers. The wiring between the different sensors and the Arduino is shown in Figures 111 and 112 using the software Fritzing. The codes shown, written in the Arduino software, record the data taken by the sensors.

Given the fact that the library of sensors of Fritzing is quite limited the sensors were replaced by similar ones:

- The Si7021 sensor was not available so in Figure 111 it was replaced by an SHT15.
- The DHT22 sensor was not available so in Figure 112 it was replaced by an RHT03.
- The Telaire 6703 sensor was not available so in Figure 112 it was replaced by a BME280 Breakout.

However, the wiring shown in Figures 111 and 112 is the same as the one used during the experiments.

Measurement of relative humidity and temperature

#include "Si7021.h"

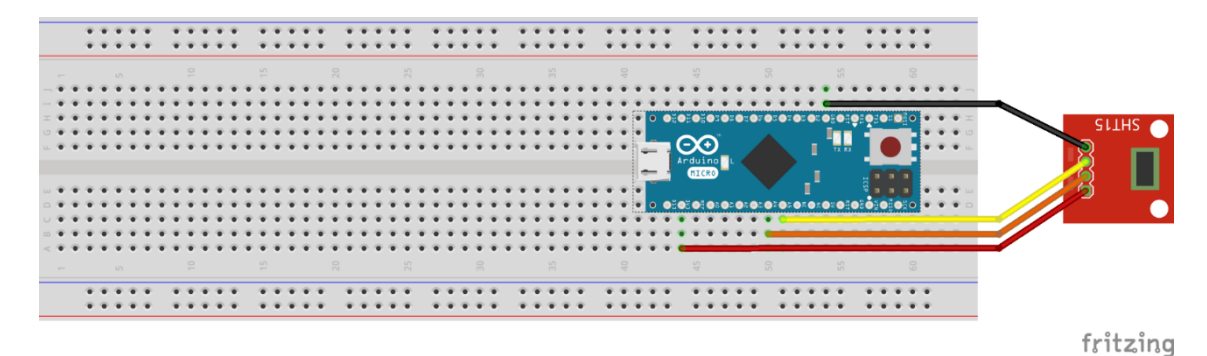


Figure 111: Wiring between RH & T sensor and Arduino

.....

```
Si7021 si7021;
void setup()
 uint64 t serialNumber = OULL;
  Serial.begin(115200);
  si7021.begin();
  serialNumber = si7021.getSerialNumber();
  Serial.print("Si7021 serial number: ");
  Serial.print((uint32_t) (serialNumber >> 32), HEX);
  Serial.println((uint32 t) (serialNumber), HEX);
  //Firware version
  Serial.print("Si7021 firmware version: ");
  Serial.println(si7021.getFirmwareVersion(), HEX);
void loop()
  Serial.print("Humidity: ");
  Serial.print(si7021.measureHumidity());
 Serial.print("% - Temperature: ");
Serial.print(si7021.getTemperatureFromPreviousHumidityMeasurement());
  Serial.println("C");
  delay(500);
```

Measurement of relative humidity, temperature and CO₂ concentration

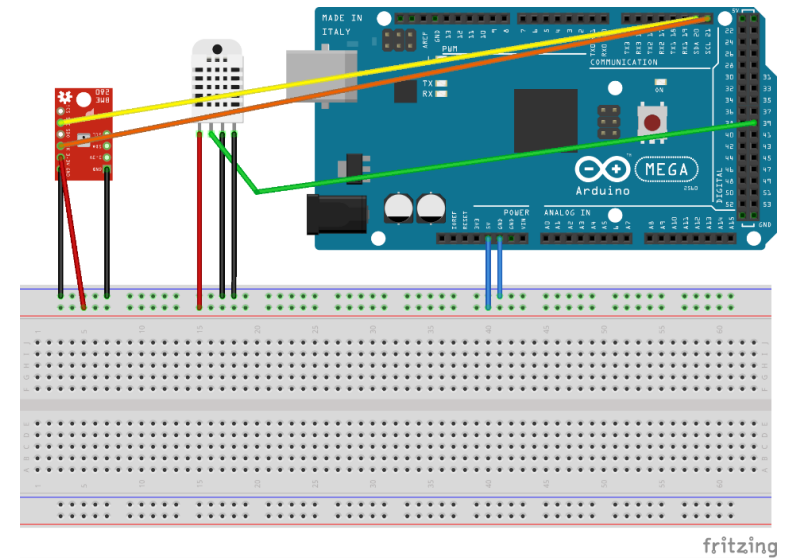


Figure 112: Wiring between RH & T sensor, CO2 sensor and Arduino

```
#include <Wire.h>
\#define ADDR 6713 0x15 // default I2C slave address (CO2 sensor)
int data [4];
int CO2ppmValue;
#include <dht.h> // RH T sensor
dht DHT;
#define DHT22 PIN 34
void setup()
  Wire.begin ();
  Serial.begin(9600);
  Serial.println("CO2 Value \t Temperature \t Humidity ");
int readC02() // C02 sensor
  Wire.beginTransmission(ADDR_6713);
  Wire.write(0x04); Wire.write(0x13); Wire.write(0x8B);
Wire.write(0x00); Wire.write(0x01);
  Wire.endTransmission();
  delay(2000);
  Wire.requestFrom(ADDR 6713, 4);
  data[0] = Wire.read();
  data[1] = Wire.read();
  data[2] = Wire.read();
  data[3] = Wire.read();
  CO2ppmValue = ((data[2] * 0xFF) + data[3]);
void loop()
  int co2Value =readC02(); // C02 sensor
    Serial.print(CO2ppmValue);
```

```
Serial.print("\t");
Serial.print("\t");
}

int chk = DHT.read22(DHT22_PIN); // RH & T sensor
{

   Serial.print(DHT.temperature);
   Serial.print("\t");
   Serial.print("\t");
   Serial.print(DHT.humidity);
   Serial.print("\t");
   Serial.print("\t");
   Serial.print("\t");
}

delay(2000);
```

D. H₂O duplos

Appendix D shows the H₂O mass measured twice for the same sample as well as the error between both measurements.

TNO asked to have 12 samples measured. Each sample was measured twice, as Table 55 shows. The error was calculated following Eq. (D-1). Then, the average error could be obtained using Eq. (D-2).

Table 55: Duplos of the H₂O measurements

	1 st measurement			2 nd measurement			
Number of the sample	Titrator in (g)	H ₂ O mass (mg)	g H₂O/ g sample	Titrator in (g)	H ₂ O mass (mg)	g H₂O/ g sample	Error (%)
1	0.2029	103.3875	0.5095	0.1648	81.1068	0.4922	3.53
2	0.1368	82.0445	0.5997	0.1756	105.1249	0.5987	0.18
3	0,1727	89.3339	0.5173	0.1675	87.2696	0.5210	0.72
4	0.1389	74.3575	0.5353	0.1293	70.4475	0.5448	1.74
5	0.1428	81.9494	0,5739	0.1636	95.8784	0.5861	2.08
6	0.1136	61.2648	0.5393	0.1895	108.6133	0.5732	5.91
7	0.1497	75.0913	0.5016	0.1370	68.9826	0.5035	0.38
8	0.2075	101.8992	0.4911	0.1172	58.6426	0.5004	1.86
9	0.1919	94.5360	0.4926	0.1686	83.6426	0.4961	0.70
10	0.1263	73.7415	0.5839	0.1536	91.4369	0.5953	1.92
11	0.1149	80.4560	0.7002	0.1634	115.4650	0.7066	0.91
12	0.1216	88.2272	0.7256	0.1328	95.9581	0.7226	0.42

$$Error (\%) = \left| \frac{\left(\frac{g_{H_2O}}{g_{sample}} \right)_{1st \ measurement} - \left(\frac{g_{H_2O}}{g_{sample}} \right)_{2nd \ measurement}}{\left(\frac{g_{H_2O}}{g_{sample}} \right)_{2nd \ measurement}} \right| \times 100$$
 (D-1)

Average error (%) =
$$\frac{\sum Error (\%)}{Number of samples}$$
 (D-2)

E. 756 coulometric FK titrator measurement error

Two different tests were done in order to check if the H₂O content measured by the 756 coulometric KF titrator was not correct.

The results given by the 756 coulometric KF titrator were not accurate since the H₂O content of the same sample varied dramatically for different measurements:

Table 56: H₂O contents of the same sample

	H ₂ O content (ppm)
Name of sample	70% 40°C 15 minutes
1st measurement	76244.5
2 nd measurement	96501.8
3 rd measurement	107004.8

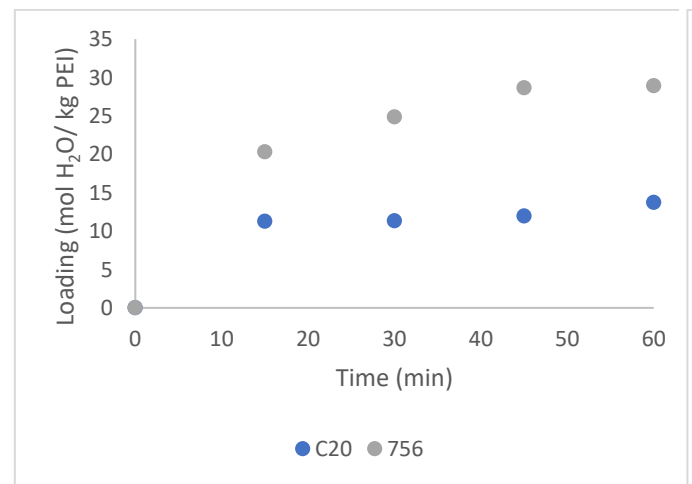
The final proof was that a sample, with known H_2O concentration of 52038 ppm, was analyzed in the 756 coulometric KF titrator:

Table 57: H₂O content of a sample, knowing its H₂O content, using the 756 coulometric KF titrator

	H₂O content (ppm)
1st measurement	75806.8
2 nd measurement	84989.5

Clearly, the results were completely off. This is why it was decided to use a different titrator. All the H_2O contents shown in this thesis were given by this titrator.

The error was possibly due to the fact that the wrong Hydranal was used. The 756 coulometric KF titrator uses a generator electrode with diaphragm. There were two hydranal solutions: Hydranal AG and AF. The first one requires an electrode with diaphragm whereas the second one does not. When the first solution was used the H_2O content measured by the 756 and C20 titrators was similar (Figure 114) while it was completely different in the other situation (Figure 113).



25 20 <u>%</u> Loading (mol H,O/ 15 10 5 0 0 20 40 60 80 100 120 Time (min) ● C20 ● 756

Figure 113: Comparison of water content in samples taken at 70% RH and 20 °C using Hydranal AG in both titrators

Figure 114: Comparison of water content in samples taken at 70% RH and 20 °C using Hydranal AF in both titrators

F. PEI is a Newtonian fluid

The fact that PEI could be a non- Newtonian fluid would add several difficulties in the modelling of the polyamine flow.

A liquid is non-Newtonian if its viscosity varies with shear rate. It was possible to check if PEI, a long branch polymer, was Newtonian or not using the Fuengilab SMART series SMART L. If using the same spindle and varying the rpm, the viscosity measurements do not vary remarkably then the fluid is Newtonian (84).

Table 58 shows that PEI is a Newtonian fluid since the viscosity is similar for different rotational speeds.

Table 58: Rotational speed vs. PEI viscosity

Rotational speed (rpm)	Viscosity (cP)
100	-
60	-
50	2060,9
30	2049,3

G. CO₂ duplos

Appendix G shows the error of the CO₂ loading measured twice for the same sample.

Some of the CO₂ measurements were measured twice, as Tables 78- 83 show. The error was calculated following Eq. (G-1). Then, the average error could be obtained using Eq. (G-2).

The CO₂ captured in the first round of experiments was measured twice:

Table 59: Error of CO₂ measurement (1st batch, PEI)

Sample		PEI (6	60 min)		PEI (120 min)			
Time (min)	15 30 45 60				30	60	90	120
Error (%)	2.02	1.20	0.73	2.30	0.49	0.79	2.84	0.60

Table 60: Error of CO₂ measurement (1st batch, TEPA)

Sample		TEPA	(60 min)	in) TEPA (120 min)					
Time (min)	15	30	45	60	30	90	120		
Error (%)	0.61	0.70	0.82	2.31	1.34	4.13	5.03		

The CO₂ captured in the second round of experiments was measured twice:

Table 61: Error of CO₂ measurement (2nd batch)

Sample		Т	EPA (60m	in)			
Time (min)	15	15 30 45 60					60
Error (%)	2.02	0.45	1.05	0.78	2.72	4.15	1.64

The CO₂ captured in the third round of experiments was measured twice:

Table 62: Error of CO₂ measurement (3rd batch, PEI)

Comple		חרו				DEL (0.50 mm)				,				
Sample	PEI (0.25 mm)				PEI (0.50 mm)				PEI (0.75 mm)					
Time (min)	7.5	15	30	45	60	7.5	30	45	60	7.5	15	30	45	60
Error (%)	0.74	0.53	0.26	0.68	0.18	1.31	0.97	0.77	1.72	0.57	0.73	0.20	0.93	1.01

Table 63: Error of CO₂ measurement (3rd batch, TEPA)

Sample	TEPA (0.50 mm)						TEPA (0.75 mm)				
Time (min)	7.5	7.5 15 30 45 60					15	30	45	60	
Error (%)	1.55	1.99	1.11	0.51	0.56	2.39	1.66	1.09	0.52	0.99	

The CO₂ captured in the fourth round of experiments was measured twice:

Table 64: Error of CO₂ measurement (4th batch)

Sample	25/ 75 wt% PEI/ TEPA 50/ 50 wt% PEI/ TEPA 75/ 25 wt% PEI/ TEPA							50/ 50 wt% PEI/ TE			A				
Time (min)	7.5	15	30	45	60	7.5	15	30	45	60	7.5	15	30	45	60
Error (%)	0.97	0.40	0.20	0.67	1.03	2.36	2.37	0.20	1.03	0.44	0.34	0.95	0.64	2.38	1.58

$$Error (\%) = \left| \frac{\left(\frac{g_{CO_2}}{g_{sample}} \right)_{1st \ measurement} - \left(\frac{g_{CO_2}}{g_{sample}} \right)_{2nd \ measurement}}{\left(\frac{g_{CO_2}}{g_{sample}} \right)_{2nd \ measurement}} \right| \times 100$$
 (G-1)

Average error (%) =
$$\frac{\sum Error (\%)}{Number of samples}$$
 (G-2)

H. Film theory

Before CO_2 can react, it must be absorbed by the liquid. Hence, mass transfer plays a determinant role in the capture process. Two different models can be used to explain the mass transfer of CO_2 into amine solutions: film theory and penetration theory. The reaction rate is calculated following the film theory.

In the film theory, the CO_2 is transferred from the bulk gas to the interface, where it is solubilised. Then, the CO_2 is transported to the bulk liquid. There are two key assumptions (41):

- The areas where the mass transfer resistance lies can be represented by two theoretical layers, one at each side of the interface.
- The mass transfer is assumed to be a steady state process.

The steady mass transfer equation without chemical reaction becomes (41):

$$0 = D_{\text{CO}_2} \frac{\partial^2 c_{\text{CO}_2}}{\partial x^2} \tag{H-1}$$

Where:

Table 65: Parameters of the steady mass transfer equation without chemical reaction

Symbol	Description	Unit
D_{CO_2}	CO ₂ diffusion coefficient	[m ² /s]
c_{CO_2}	CO ₂ concentration	[mol/m ³]
x	Direction where CO ₂ diffuses	[m]

The boundary conditions in the gas side are (41):

$$c_{\mathrm{CO}_2}\big|_{x=\delta_C} = p_{\mathrm{CO}_2} \tag{H-2}$$

$$c_{\text{CO}_2}\big|_{x=0} = p_{\text{CO}_{2,i}}$$
 (H-3)

The boundary conditions in the liquid side are (41):

$$c_{\text{CO}_2}\big|_{x=\delta_L} = [\text{CO}_2] \tag{H-4}$$

$$c_{\text{CO}_2}|_{x=0} = [\text{CO}_2]_i$$
 (H-5)

Where:

Table 66: Parameters of the boundary conditions

Symbol	Description	Unit
p_{CO_2}	CO ₂ partial pressure in the gas phase	[Pa]
$p_{\mathrm{CO}_{2.i}}$	CO ₂ partial pressure at the interface	[Pa]
δ_G	Thickness of the gas film	[m]
$[CO_2]$	CO ₂ concentration at the interface	[mol/m ³]
$[CO_2]_i$	CO ₂ concentration in the liquid phase	[mol/m ³]
δ_L	Thickness of the liquid film	[m]

The CO₂ flux at the interface is the same as the CO₂ flux from the bulk gas to the interface and from the interface to the bulk liquid due to continuity and the lack of reaction (41).

$$N_{\text{CO}_2} = -D_{\text{CO}_2} \frac{\partial c_{\text{CO}_2}}{\partial x} \Big|_{x=0} = k_{\text{G}} \times (p_{\text{CO}_2} - p_{\text{CO}_{2,i}}) = k_{\text{L}} \times ([\text{CO}_2]_i - [\text{CO}_2])$$
 (H-6)

Henry's law can be applied assuming that the interface is at equilibrium (41):

$$p_{\text{CO}_{2,i}} = H_{\text{CO}_2} \times [\text{CO}_2]_i$$
 (H-7)

Where:

Table 67: Parameters of CO₂ flux equation and Henry's law

Symbol	Description	Unit
$N_{\rm CO_2}$	CO ₂ flux	[mol/(m ² *s)]
$k_{\rm G} = \frac{D_{\rm CO_{2,G}}}{R \times T \times \delta_{\rm G}}$	Gas film mass transfer resistance	[mol/(m ² *Pa*s)]
$k_{\rm L} = \frac{R \times T \times \delta_{\rm G}}{\delta_{\rm I}}$	Liquid film mass transfer resistance	[m/s]
H_{CO_2}	Henry's constant for CO ₂	[Pa*m³/mol]

From Eq. (H-6) and (H-7):

$$N_{\text{CO}_2} = \frac{p_{\text{CO}_2} - H_{\text{CO}_2} \times [\text{CO}_2]}{\frac{1}{k_C} + \frac{H_{\text{CO}_2}}{k_1}}$$
(H-8)

Assuming that the amine solution is unloaded (41):

$$N_{\rm CO_2} = \frac{p_{\rm CO_2}}{\frac{1}{k_{\rm G}} + \frac{H_{\rm CO_2}}{k_{\rm L}}} \tag{H-9}$$

It is possible to obtain the overall mass transfer resistance (kov) from Eq. (H-9):

$$\frac{1}{k_{\rm ov}} = \frac{1}{k_{\rm G}} + \frac{H_{\rm CO_2}}{k_{\rm L}} \tag{H-10}$$

Where:

Table 68: Parameters of simplified CO2 flux in film theory

Symbol	Description	Unit
$N_{\rm CO_2}$	CO ₂ flux	[mol/(m ² *s)]
p_{CO_2}	CO ₂ partial pressure in the gas phase	[Pa]
k_{G}	Gas film mass transfer coefficient	[mol/(m ² *Pa*s)]
$k_{ m L}$	Liquid film mass transfer coefficient	[m/s]
H_{CO_2}	Henry's constant for CO ₂	[Pa*m³/mol]
$k_{ m ov}$	Overall mass transfer resistance	[mol/(m ² *Pa*s)]

In the pseudo-first order regime Eq. (H-9) simplifies to:

$$N_{\text{CO}_2} = \frac{p_{\text{CO}_2}}{\frac{1}{k_G} + \frac{H_{\text{CO}_2}}{\sqrt{k_{obs} \times D_{\text{CO}_2}}}}$$
(H-14)

Pure CO₂ is used in the kinetics setup so the gas film mass transfer resistance is neglected. Rearranging the terms in Eq. (H-14):

$$k_{obs} = \frac{H_{CO_2}^2}{D_{CO_2}} \times (\frac{1}{k_{ov}})^{-2}$$
 (H-15)

I. Other CO₂ and H₂O experiments from the air

This Appendix contains four different experiments. In the first one, the experimental time was increased from 60 to 120 minutes in order to find out when the CO_2 and H_2O would achieve equilibrium. In the second experiment, the air velocity was changed to check if the absorption process has limitations in the gas phase. The third and four experiments belong to TEPA in contact with different CO_2 ppm in the air. These last two experiments were moved to the Appendix since the CO_2 loading decreased while the CO_2 ppm increased. The reason is unknown.

Finding steady state of CO₂ and H₂O absorption

In this batch of experiments, the experimental time was varied from 60 till 120 minutes in order to figure out the time required to achieve steady state of CO₂ and H₂O absorption.

The air was blown over the layer of polyamine. Hence this configuration did not achieve a uniform flow since the fan created a conical flow, where the edges of the flow had a higher speed than the centre. However, this was not a big issue since the plate was located at the bottom edge. In addition to this, the flow decreased over the length of the plate.

- For the experiment with PEI the flow speed decreased from 5.69 m/s next to the fan to 1.58 m/s at the end of the plate.
- For the experiment with TEPA the flow speed decreased from 5.42 m/s next to the fan to 1.50 m/s at the end of the plate.

In order to find the equilibrium absorption of CO₂ and H₂O two experiments were done: one at 120 minutes and another one at 60 minutes, just like it was done before in the climate chamber. Figures 115- 118 show the experimental results:

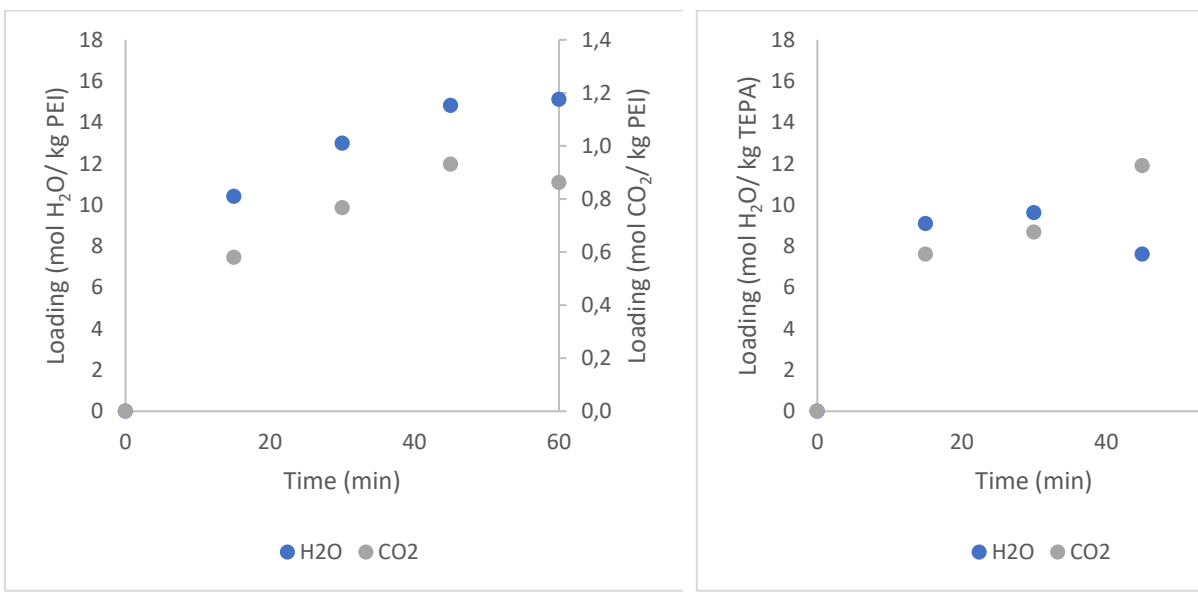


Figure 115: Loading of H₂O and CO₂ in PEI in contact with air for 60 min

Figure 116: Loading of H₂O and CO₂ in TEPA in contact with air for 60 min

1,4

1,2

1,0

0,8

0,6

0,2

0,0

60

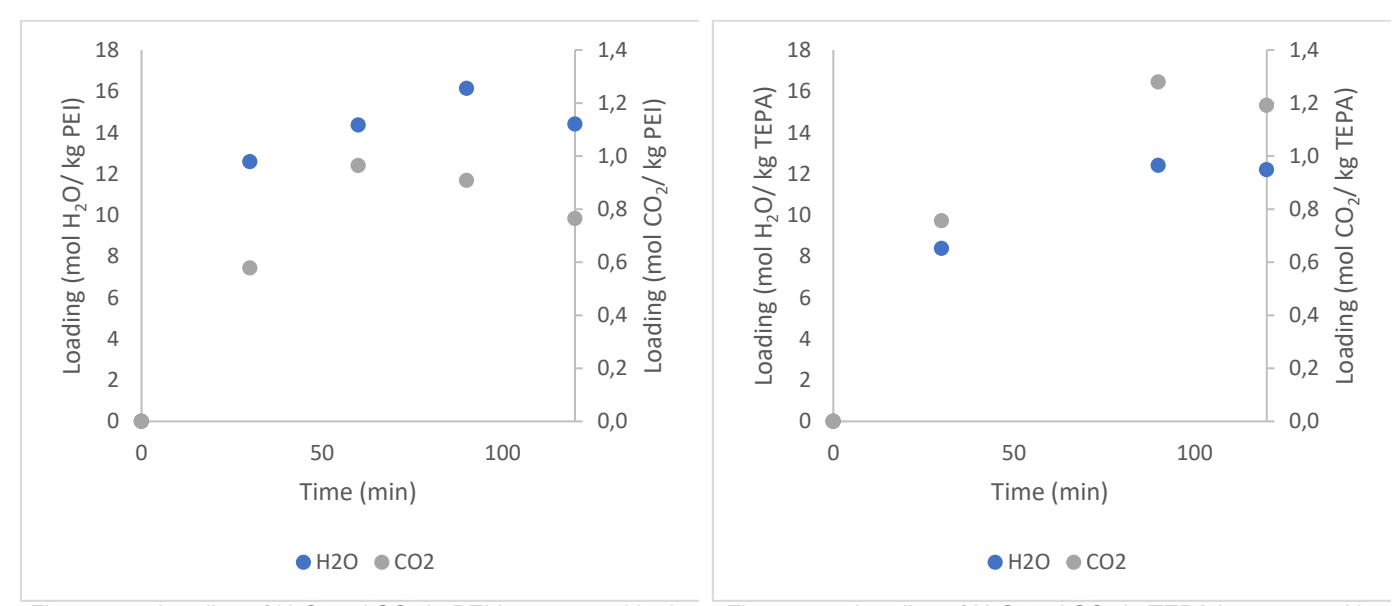


Figure 117: Loading of H₂O and CO₂ in PEI in contact with air for 120 min

Figure 118: Loading of H₂O and CO₂ in TEPA in contact with air for 120 min

On one hand, PEI results are surprising since both loadings are higher at 60 minutes than at 120. Since only one experiment was done, it cannot be stated which one is not correct. On the other hand, CO_2 and H_2O loadings of TEPA are higher at 120 minutes than at 60, which was the expected behaviour. 82% of the CO_2 absorption and 96% of the H_2O absorption take place before 60 minutes.

Table 69: Lab conditions and CO2 and H2O loadings of finding steady-state experiments

Time	60 min		120 min	
Sorbent	TEPA	PEI	TEPA	PEI
Relative humidity (%)	33	47	33	47
Temperature (°C)	19	18	19	18
CO ₂ loading (mol CO ₂ / kg sorbent)	1.0	0.9	1.2	0.8
H ₂ O loading (mol H ₂ O/ kg sorbent)	11.7	15.1	12.4	14.4

These experiments give some insight regarding the H_2O and CO_2 time to reach steady state. It is important to make a distinction between working and equilibrium capacity. The working capacity is measured when absorption takes place during a period of time that is lower than the one required to reach equilibrium. Working capacity may be more relevant because it may be better to shorten the length of the absorption cycle (38). In this case, the length of the experiments was shortened till 60 minutes, since almost all the CO_2 and H_2O were already captured. It might be interesting to find out the equilibrium capacity and the time needed to reach it. It can be said from this experiment that this time is more than 120 minutes in the case of CO_2 .

Changing the air velocity

In this batch of experiments, the air flow was varied in order to check if the process might have gas diffusion limitations. The way of doing this was to compare the CO₂ and H₂O loadings from two different air flows.

This round of experiments was done with a different configuration. The air was sucked by the fan, instead of blown, which created a more uniform flow. Also, the voltage was reduced to 4V which decreased the flow speed. The flow speed was 0.89 m/s at the center and 0.53 m/s at the edges of the plate.

Figures 119 and 120 show the experimental results:

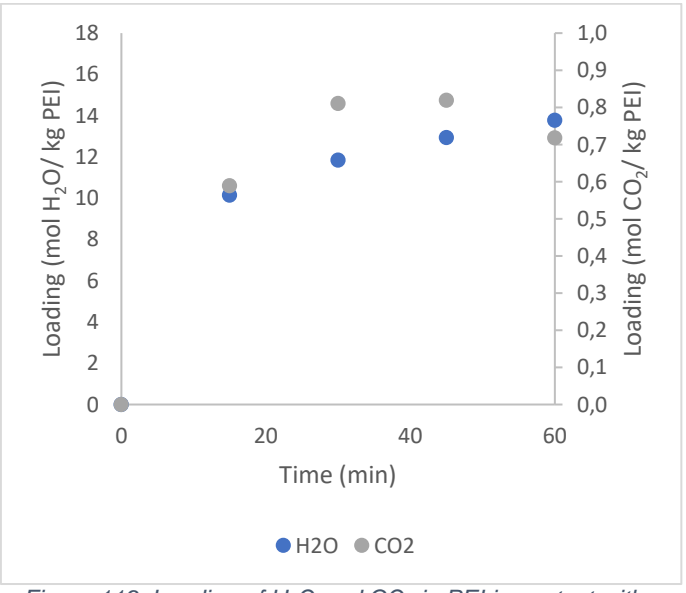


Figure 119: Loading of H₂O and CO₂ in PEI in contact with a uniform flow of air

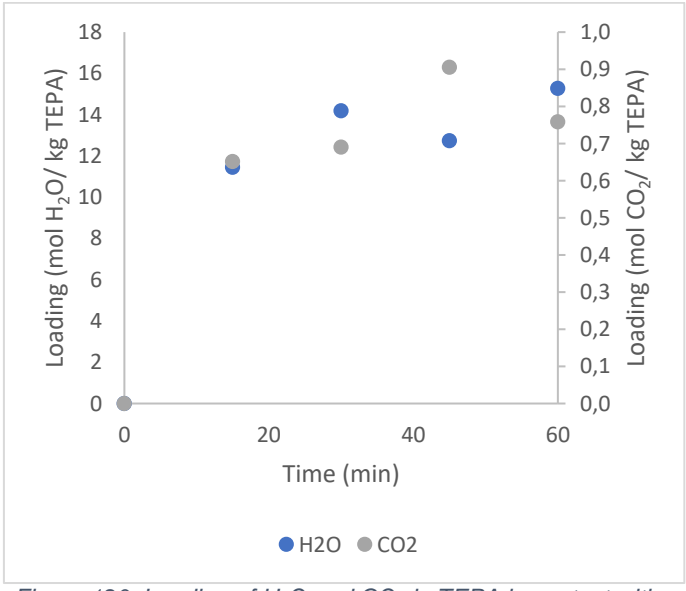
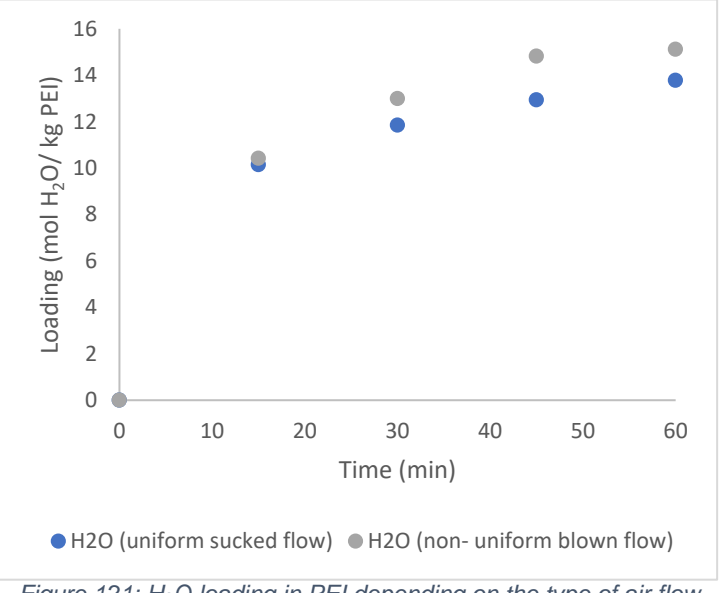


Figure 120: Loading of H₂O and CO₂ in TEPA in contact with a uniform flow of air

Figures 121- 124 show graphically the CO₂ and H₂O loading variation for the uniform and non-uniform flow situations. The uniform flow data is obtained from experiments done in this section whereas the non-uniform flow data belongs to the previous section (60 min long experiments). PEI results from the previous section might not be accurate, as explained before.



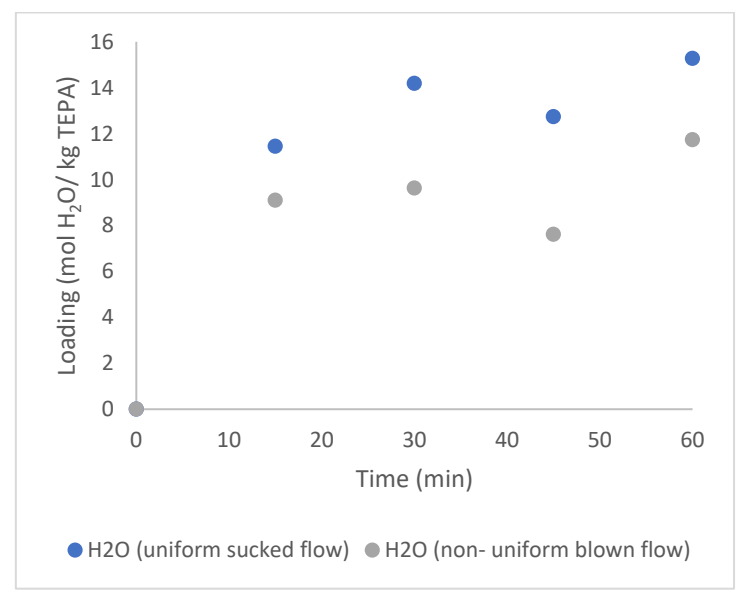
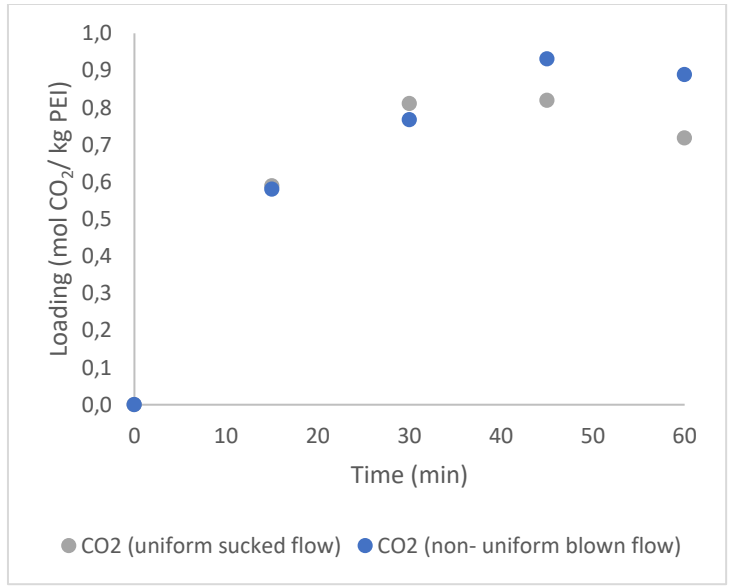


Figure 121: H₂O loading in PEI depending on the type of air flow

Figure 122: H₂O loading in TEPA depending on the type of air flow



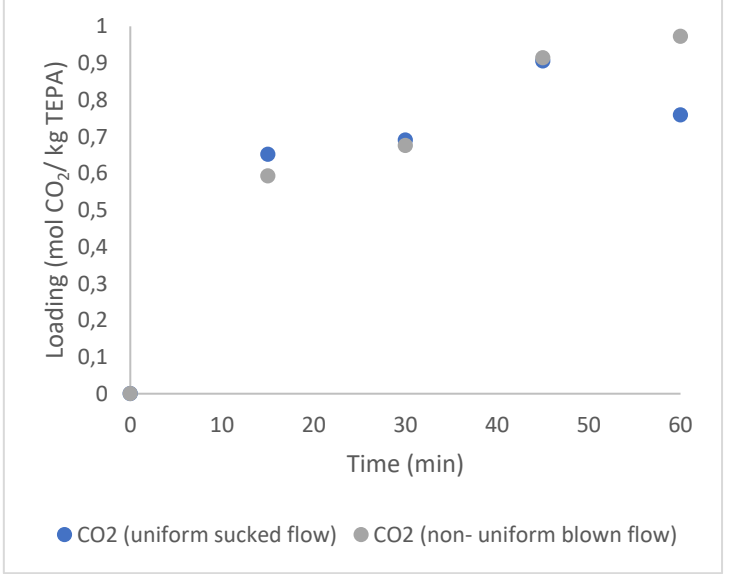


Figure 123: CO2 loading in PEI depending on the type of air flow

Figure 124: CO2 loading in TEPA depending on the type of air flow

It seems that the process is liquid-diffusion limited since changing the flow significantly (around 80% decrease) does not make a relevant change in the CO₂ loading (22% decrease for TEPA) or H₂O loading (23% increase), as Table 70 shows. It is surprising that the CO₂ loading decreases whereas the H₂O loading increases, specially when the relative humidity is lower.

Table 70: Lab conditions and CO₂ and H₂O loading for different air velocity experiments

Time	60 min		120 min	
Sorbent	TEPA	PEI	TEPA	PEI
Relative humidity (%)	33	47	33	47
Temperature (°C)	19	18	19	18
CO ₂ loading (mol CO ₂ / kg sorbent)	1.0	0.9	1.2	8.0
H ₂ O loading (mol H ₂ O/ kg sorbent)	11.7	15.1	12.4	14.4

CO₂ and H₂O absorption in polyamines seem to be liquid-diffusion limited and not gasdiffusion limited since changing the air flow significantly does not have the same significant effect in both H₂O and CO₂ loading.

TEPA in contact with air containing different concentrations of CO₂

As mentioned in Section 4.1.2, these experiments do not offer reliable results since the CO_2 loading decreased when the CO_2 concentration in the air increased.

Figures 125 and 126 show the H₂O and CO₂ loadings.

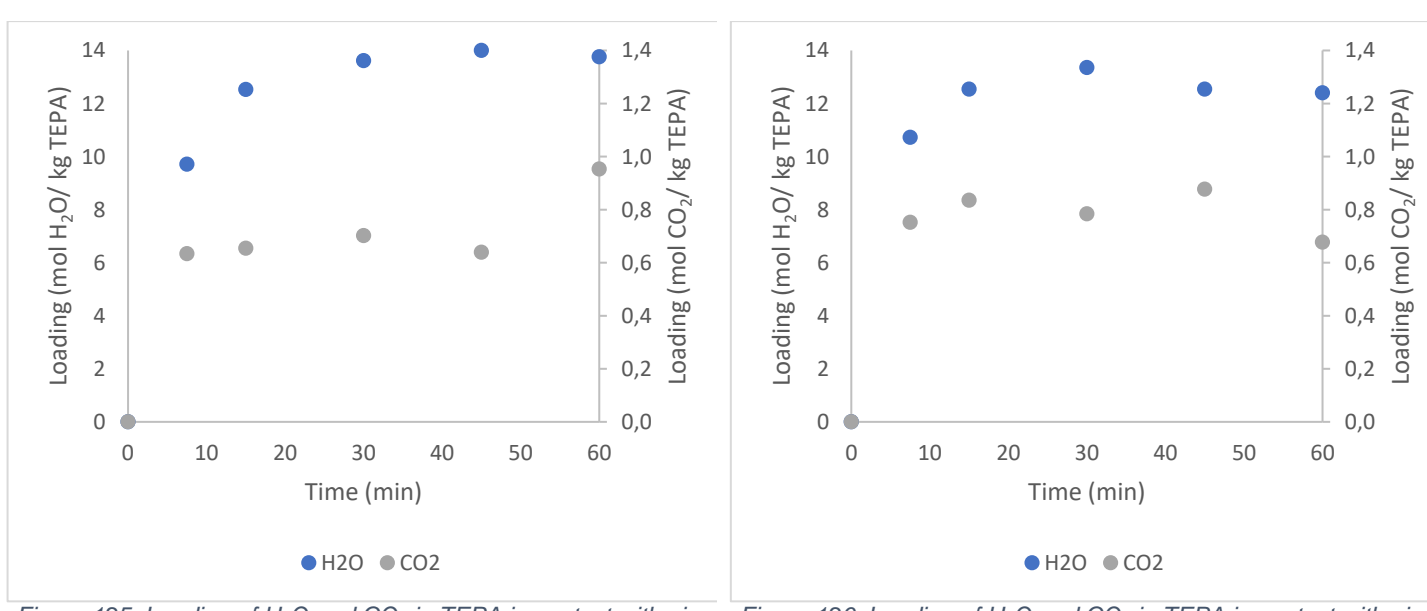


Figure 125: Loading of H₂O and CO₂ in TEPA in contact with air (800 ppm)

Figure 126: Loading of H₂O and CO₂ in TEPA in contact with air (1200 ppm)

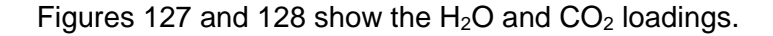
Table 71 shows that the CO_2 loading decreases from 0.95 mol CO_2 / kg sorbent to 0.68 mol CO_2 / kg sorbent for 800 and 1200 ppm of CO_2 respectively. The reason is still unknown.

Table 71: Lab conditions and CO₂ and H₂O loading of TEPA in contact with higher CO₂ concentrations

CO ₂ concentration in the air	800	1200
Sorbent	TEPA	
Relative humidity (%)	43	40
Temperature (°C)	19	19
CO ₂ ppm	844	1217
CO ₂ loading (mol CO ₂ / kg sorbent)	1.0	0.7
H ₂ O loading (mol H ₂ O/ kg sorbent)	13.8	12.4

TEPA premixed with H₂O in contact with air containing different concentrations of CO₂

As mentioned in Section 4.1.2, these experiments do not offer reliable results since the CO_2 loading decreased when the CO_2 concentration in the air increased.



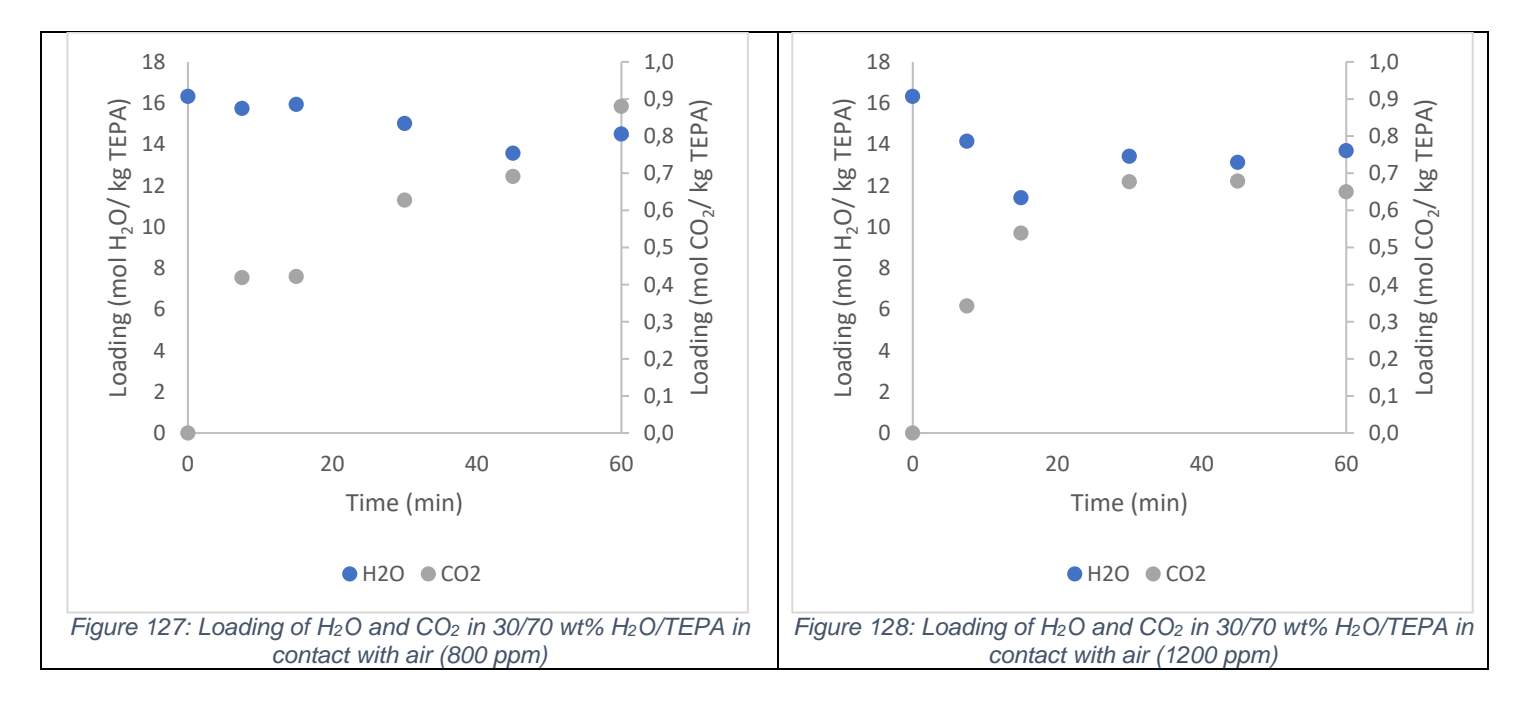


Table 72 shows that the CO_2 loading decreases from 0.88 mol CO_2 / kg sorbent to 0.65 mol CO_2 / kg sorbent for 800 and 1200 ppm of CO_2 respectively. The reason is still unknown.

Table 72: CO2 loading and ratio of TEPA mixed with water in contact with higher CO2 concentrations

CO ₂ concentration in the air	800	1200
Sorbent	TEPA	
Relative humidity (%)	40	39
Temperature (°C)	20	20
CO₂ ppm	856	1132
CO ₂ loading (mol CO ₂ / kg sorbent)	0.9	0.7
H ₂ O loading (mol H ₂ O/ kg sorbent)	14.5	13.7

J. Subtraction of the H₂O content in MeOH

The H_2O content in the MeOH used to dilute the samples of polyamine should be taken into account and subtracted from the H_2O content measured in the titrator. In this way, only the H_2O content from the H_2O absorbed by the polyamine is considered.

In order to do the H_2O measurement tests the samples were diluted with MeOH (as mentioned in Section 3.3.1), which also contains H_2O , so there might be a possibility of the H_2O contained in the MeOH affecting the measurement of H_2O in the polyamine. Therefore, a comparison between the H_2O content of a sample considering the H_2O content of MeOH and not considering it was done. The results show that the H_2O present in MeOH has a great influence.

However, before starting with this, it is required to obtain the H₂O loading of the polyamine from the H₂O content given by the titrator, which can be given in ppm or mg, with some calculations.

$$Loading_{\rm H_2O} = \frac{ppm_{\rm H_2O}}{1000 \times MW_{\rm H_2O}} \times DR \tag{J-1}$$

$$Loading_{H_2O} = \frac{M_{H_2O}}{M_{total,titrator} \times MW_{H_2O}} \times DR$$
 (J-2)

$$DR = \frac{M_{\text{MeOH}} + M_{\text{PEI/TEPA}}}{M_{\text{PEI/TEPA}}}$$
 (J-3)

However, the H_2O ppm and mass also contain the H_2O from the MeOH used to dilute each sample. This H_2O needs to be subtracted from the H_2O loading.

$$M_{\text{total}} = M_{\text{MeOH}} + M_{\text{PEI/TEPA}} \tag{J-4}$$

$$Ratio = \frac{M_{\text{MeOH}}}{M_{total}} \tag{J-5}$$

$$M_{\text{MeOH,titrator}} = Ratio \times M_{\text{total,titrator}}$$
 (J-6)

$$M_{\rm H_2O,MeOH} = \frac{ppm_{\rm H_2O,MeOH}}{1000} \times M_{\rm MeOH,titrator}$$
 (J-7)

$$M_{\rm H_2O,PEI/TEPA} = M_{\rm H_2O,titrator} - M_{\rm H_2O,MeOH}$$
 (J-8)

$$Loading_{H_2O} = \frac{M_{H_2O,PEI/TEPA}}{(M_{\text{total,titrator}} - M_{\text{MeOH,titrator}}) \times MW_{H_2O}}$$
(J-9)

Figure 129 shows the difference in H_2O loading if the H_2O from the MeOH is taken into account or not in the sample of TEPA with a layer thickness of 0.25 mm.

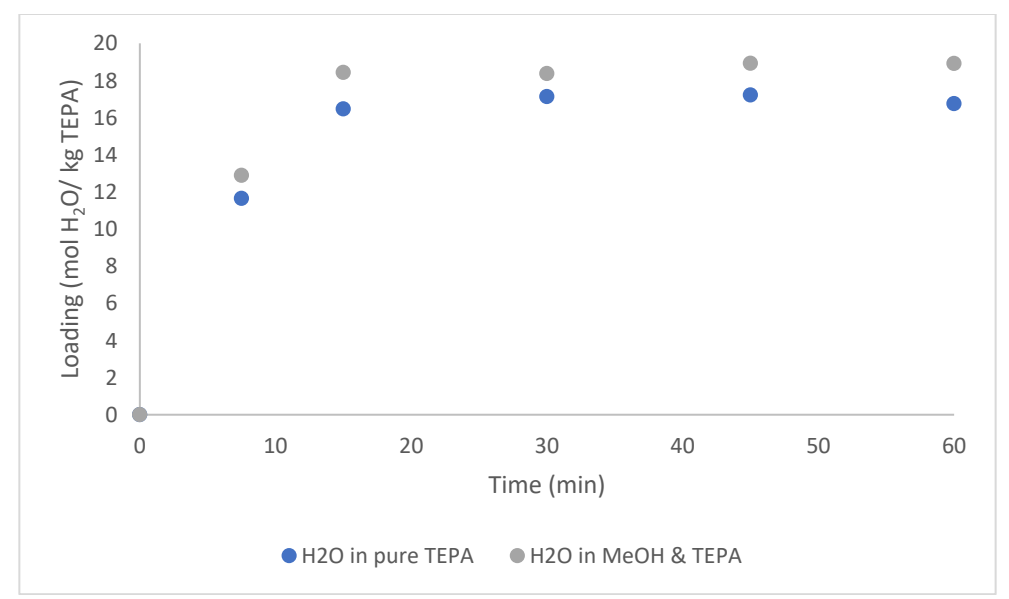


Figure 129: Comparison of water content in a sample considering the H₂O content of methanol (grey) and not considering it (blue)

It can be seen that the H_2O contained in the MeOH should be considered, and consequently removed from the H2O contained in the polyamine, since the error between both measurements is around 10.54%.

K. Calibration of CO₂ ppm

The main objective before starting the experiments, were the CO₂ ppm in the air were varied, is to achieve a uniform CO₂ distribution along the pipe. In order to do this, two fans were used instead of one.

The CO₂ sensor was placed in each position shown in Figure 130 in order to find out the CO₂ ppm in different points if the setup.

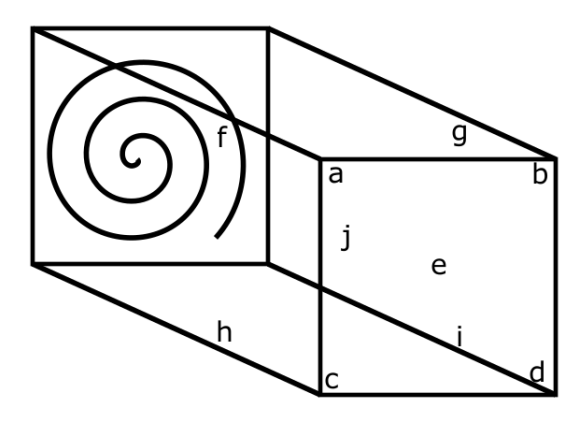


Figure 130: CO₂ ppm distribution

The values measured by the CO₂ sensor are shown in Tables 73 and 74 which show huge uncertainty in the data.

Table 73: CO₂ ppm distribution for 800 ppm

a	b	С	d	е
655	1503	756	1292	1275
f	g	h	i	j
580	2086	596	1013	1265

Table 74: CO₂ ppm distribution for 1200 ppm

Tamera i ii a az plani anamia mani i za plani					
а	b	С	d	е	
706	1024	759	1329	1074	
f	g	h	i	j	
567	1313	586	886	1055	

It can be seen that, despite all efforts, the CO2 concentration was far from homogeneous. This could be due to the fact that the cross section of both fans was way bigger than the cross-section of the CO2 pipe coming from the MFC and the CO2 bottle. It is recommended that, if this experiment is repeated in the future, a more uniform CO2 distribution along the pipe should be obtained.

The CO2 distribution shown in Tables 73 and 74 is not the same as the CO2 distribution of each of the experiments.

L. Spectrometers

The most relevant spectrometers were shown and analysed in Section 3. However, more spectrometers were done and they will be discussed here.

PEI

Figure 131 shows a huge drop between 3000 and 3500 cm $^{-1}$ which is due to the H₂O addition, since there is a huge decrease in that same area in the spectrometer of pure H₂O.

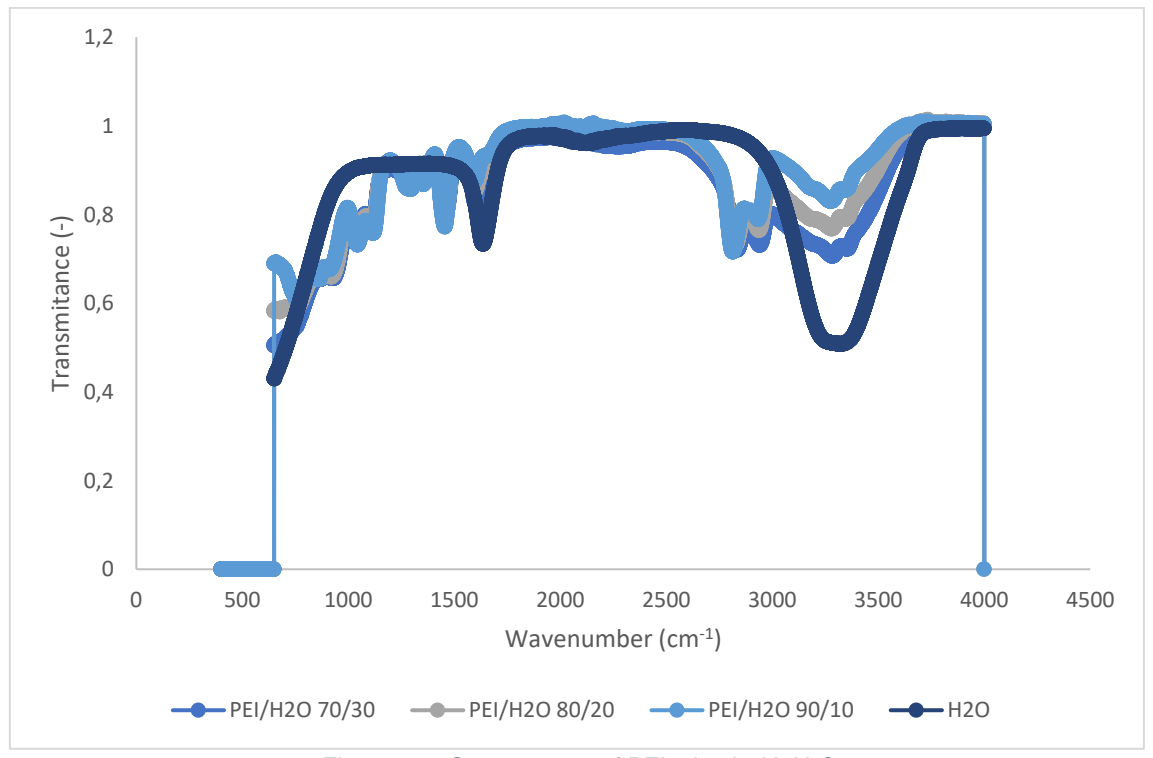


Figure 131: Spectrometer of PEI mixed with H₂O

Figure 132 shows that there is no relevant difference between the spectrometer of PEI blown by air with a CO₂ concentration of 800 and 1200 ppm. It seems that a difference of 0.20 mol CO₂/ kg PEI is not high enough to be identified in the spectrometers.

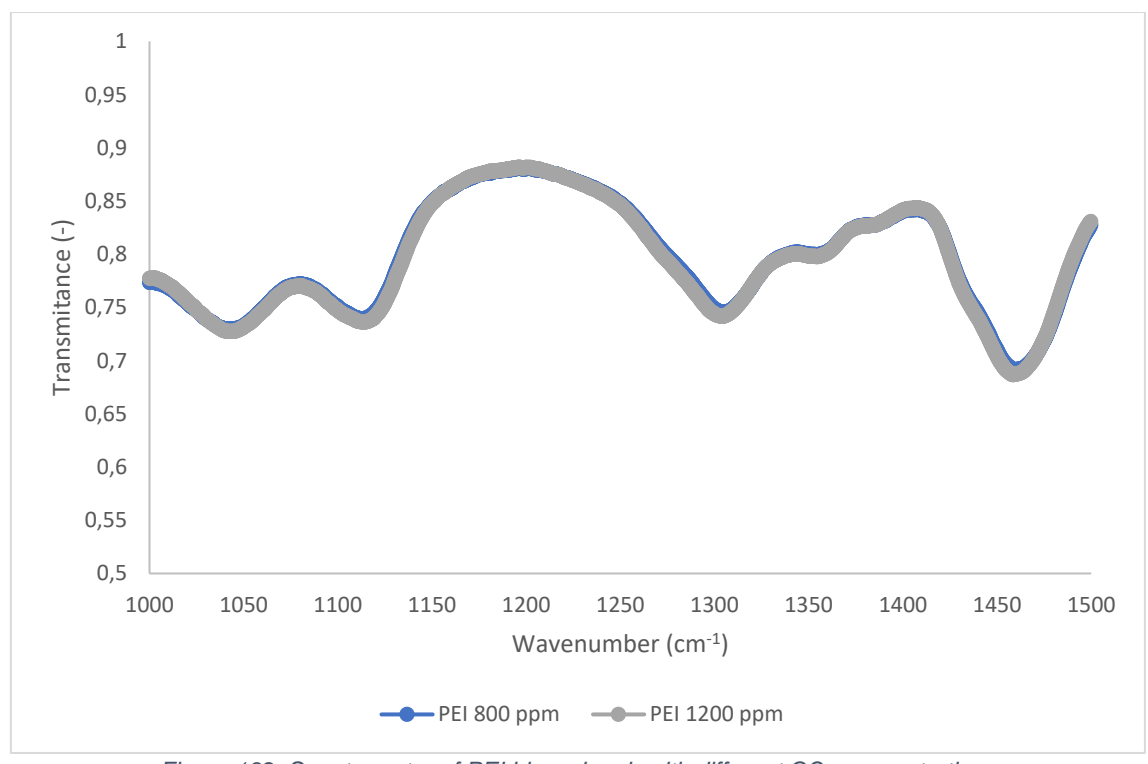


Figure 132: Spectrometer of PEI blown by air with different CO₂ concentrations

Figure 133 shows that there is a relevant difference between the spectrometer of a solution of PEI blown by air with a CO_2 concentration of 800 and 1200 ppm. It seems that a difference of 0.67 mol CO_2 / kg solution is high enough to be identified in the spectrometers.

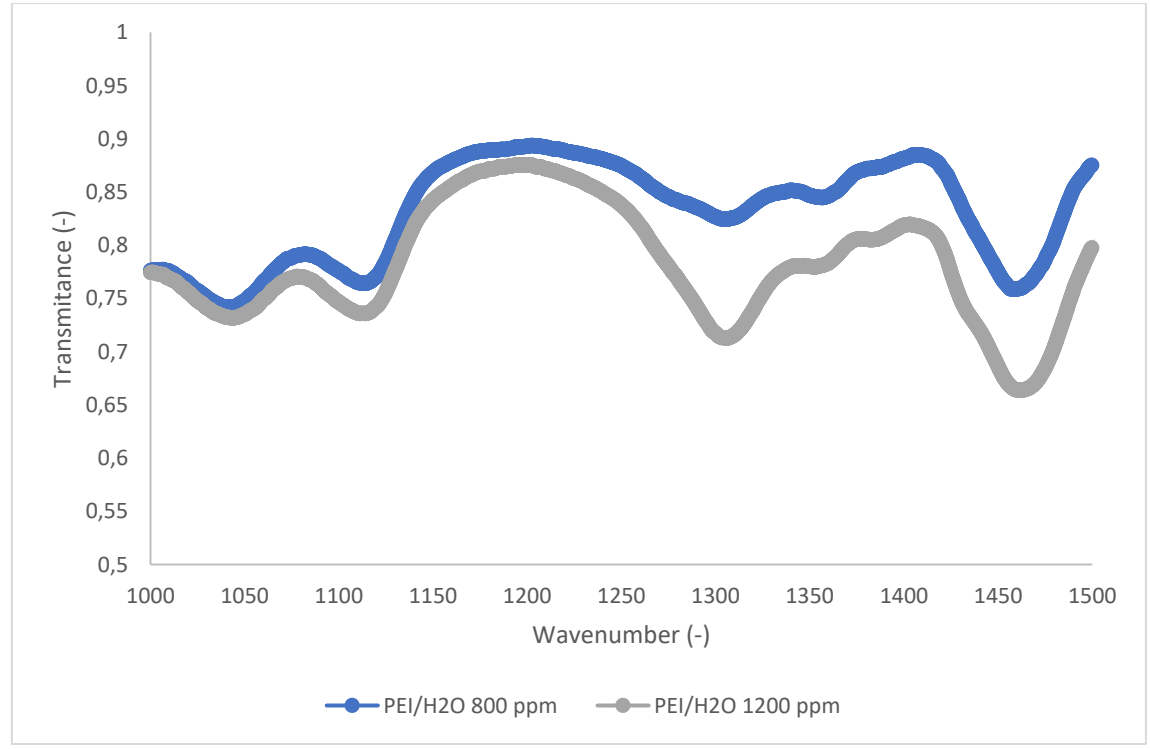


Figure 133: Spectrometer of PEI mixed with H₂O blown by air with different CO₂ concentrations

TEPA

Just like Figure 131, Figure 134 shows a huge drop between 3000 and 3500 cm $^{-1}$ due to the H_2O addition.

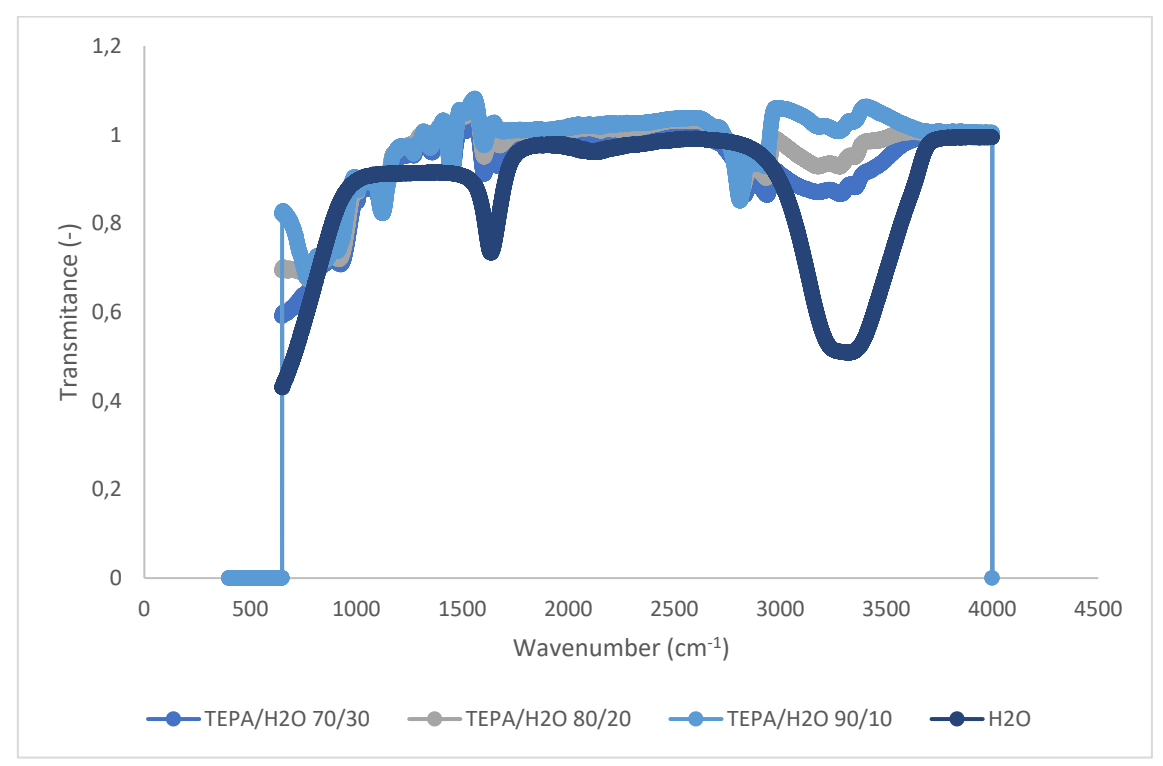


Figure 134: Spectrometer of TEPA mixed with H₂O

Just like Figure 132, there is no relevant difference between the spectrometer of TEPA blown by air with a CO₂ concentration of 800 and 1200 ppm. As explained before, the experiments gave incorrect results because the CO₂ loading was lower at 1200 than at 800 ppm. This difference can also be seen in this Figure, since the spectrometer that belongs to the experiment done at 1200 ppm has a slightly lower transmittance.

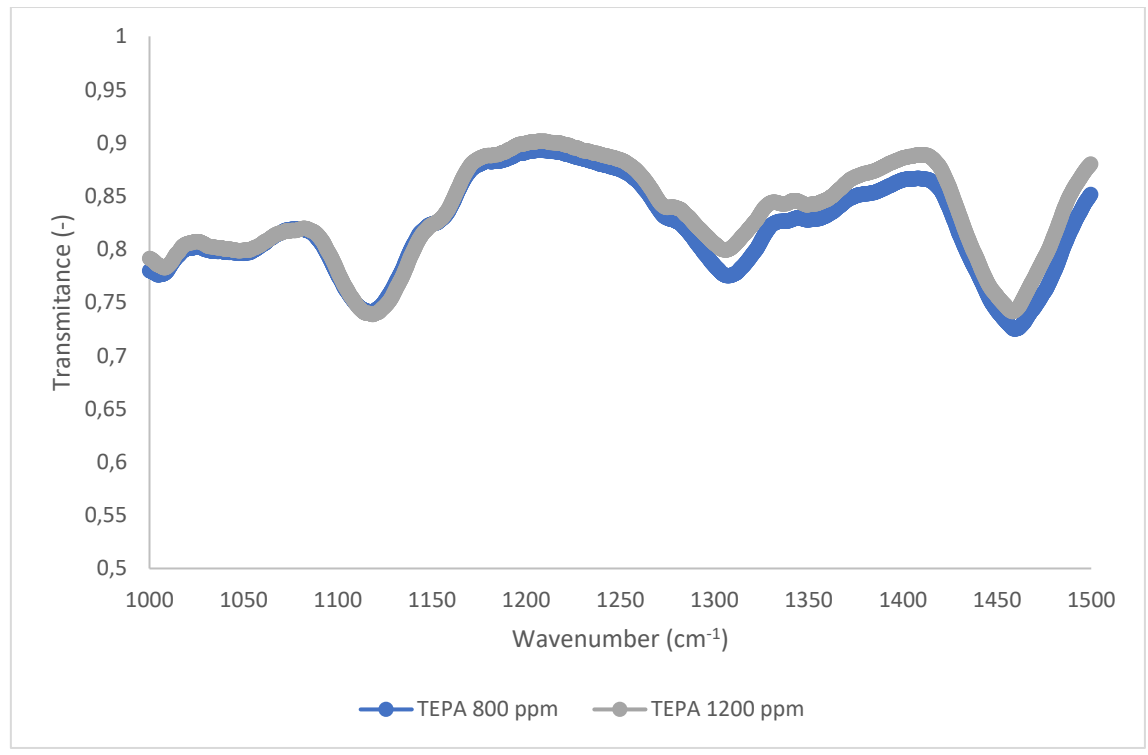


Figure 135: Spectrometer of TEPA blown by air with different CO₂ concentrations

As mentioned before, this batch of experiments gave not realistic results, since the CO_2 loading was lower at 1200 than at 800 ppm. However, according to the spectrometer the peaks that correspond to 1200 ppm are sharper. Hence, the spectrometer results are totally opposed to the CO_2 loadings obtained before. The reason is unknown.

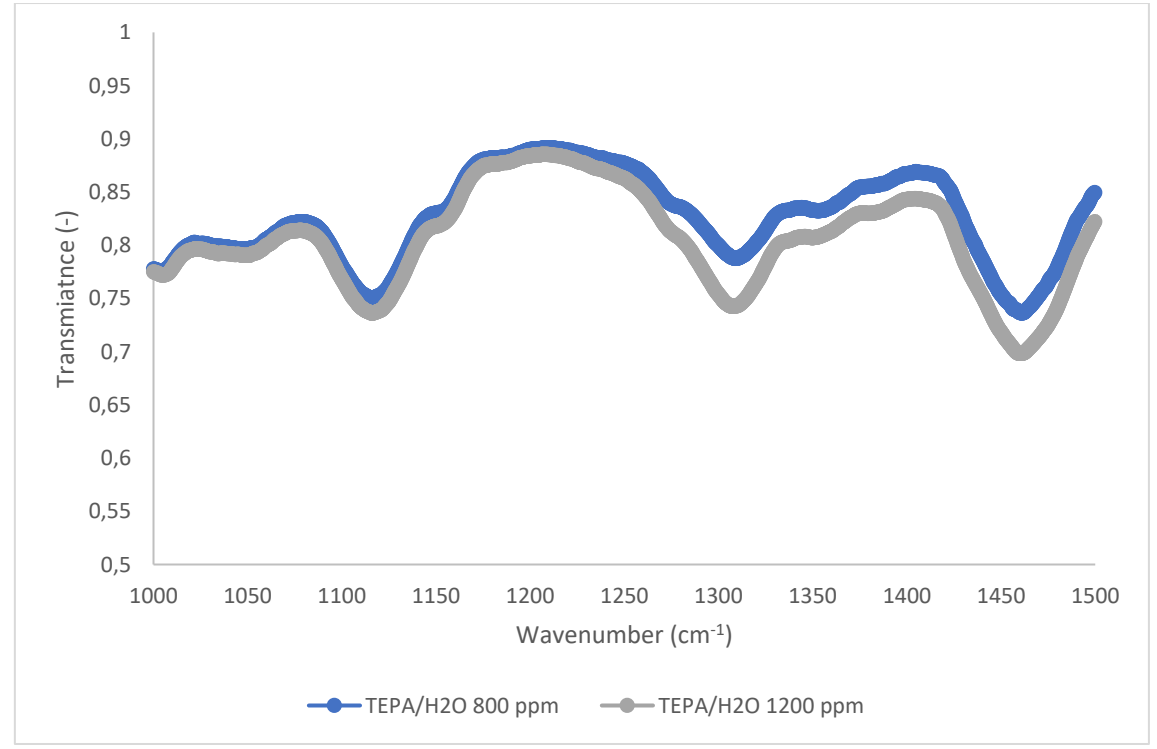


Figure 136: Spectrometer of TEPA mixed with H₂O blown by air with different CO₂ concentrations

M. MATLAB codes

This Appendix contains the two MATLAB codes used to estimate the diffusion coefficient of H₂O and CO₂ in PEI and TEPA.

H₂O model

```
close all
clear all
clc
numx = 100; % number of steps
numt = 100; % number of steps
xmax = 0.0005; % LT [m]
tmax = 3600; % Experimental time [s]
m = 0; % Slab (pdepe solver)
x = linspace(0,xmax,numx); % LT [m]
t = linspace(0,tmax,numt); % Time [s]
sol = pdepe(m,@pdex1pde,@pdex1ic,@pdex1bc,x,t);
u = sol(:,:,1);
% EXPERIMENTAL DATA
% Experimental time
Exp time old = [0; 15*60; 30*60; 45*60; 60*60]; % [s]
Exp time new = [0; 7.50*60; 15*60; 30*60; 45*60; 60*60]; % [s]
% Climate chamber
Exp data 70 20C = [0; 12892; 15936; 17406; 18898]/1000; % mol H2O/ L
Exp data 70 30C = [0; 16079; 18965; 17603; 19611]/1000; % mol H2O/ L
Exp data 70 40C = [0; 16614; 19386; 19278; 20892]/1000; % mol H2O/ L
Exp data 70 10C = [0; 12908; 16042; 20075; 24315]/1000; % mol H2O/ L
PEI
Exp data 50 20C = [0; 11836; 11905; 12543; 14411]/1000;
Exp data 50 30C = [0; 13294; 13943; 14868; 15364]/1000;
Exp_{data_50_40C} = [0; 12012; 13164; 17207; 17049]/1000;
Exp data 50\ 10C = [0; 7355; 10301; 11905; 12250]/1000;
Exp data 35 20C = [0; 6547; 8859; 9357; 10904]/1000;
Exp data 35 30C = [0; 9910; 10563; 11415; 12027]/1000;
Exp data 35\ 40C = [0; 10347; 11053; 10542; 8842]/1000;
Exp data 35\ 10C = [0; 12246; 12098; 11396; 13429]/1000;
Exp data 95 20C = [0; 14845; 18609; 21692; 23731]/1000;
Exp data 95\ 30C = [0; 16521; 21511; 23076; 25015]/1000;
Exp data 95\ 40C = [0; 15395; 17696; 19139; 20209]/1000;
Exp data 95 10C = [0; 10891; 15278; 16448; 21915]/1000;
TEPA 35 20C=[0;9971;10761;11429;11560]/1000;
```

```
TEPA 50 20C=[0;14670;16691;16736;16768]/1000;
TEPA 70 20C=[0;12681;15808;17830;19560]/1000;
TEPA 95 20C=[0;16436;19085;20277;20732]/1000;
% PLOTS
% Surface plot
figure1=figure;
s=surf(x,t,u);
s.EdgeColor = 'none';
% title('Numerical solution')
xlabel('Distance x [m]')
ylabel('Time t [s]')
zlabel('Dissolved H2O concentration [mol/L]');
figure2=figure;
avgU = sum(u, 2)/numx;
plot(t,avgU,'r')
% title('Model vs Experimental data')
xlabel('Time [s]');
ylabel('Dissolved H2O concentration [mol/L]');
hold on
plot(Exp time old, TEPA 70 20C, 'bo')
legend('Calculated data', 'Experimental data');
hold off
function [c,f,s] = pdex1pde(x,t,u,DuDx)
c = 1;
% D = 4e-13; (D of E-S equation)
D = 1e-10; % diffusion coefficient [m2/s]
f = D*DuDx;
s = 0;
end
8 -----
function u0 = pdex1ic(x)
u0 = 0; % if there is no water in the polyamine
end
% -----
function [pl,ql,pr,qr] = pdex1bc(xl,ul,xr,ur,t)
              35RH 50RH 70RH 95RH
u H2O lig 10C = [13429; 12250; 24315; 21915]/1000;
u H2O liq 20C = [10904; 14411; 18898; 23731]/1000;
u H2O lig 30C = [12027; 14868; 19611; 25015]/1000;
u H2O liq 40C = [11053; 17207; 20892; 20209]/1000;
u H2O liq TEPA 20C = [11560; 16768; 19560; 20732]/1000;
88888888888888888888888
% pl = ul - (u H2O lig 20C(3,1));
pl = ul - (u H2O liq TEPA 20C(3,1));
88888888888888888888888
ql = 0;
```

```
pr = 0;
qr = 1;
```

end

CO₂ model assuming a high Hatta number

```
close all
clear all
clc
numx = 100; % number of steps
numt = 100; % number of steps
xmax = 0.0005; % LT [m]
tmax = 3600*1; % Experimental time [s]
m = 0; % Slab (pdepe solver)
x = linspace(0, xmax, numx); % LT [m]
t = linspace(0,tmax,numt); % Time [s]
sol = pdepe(m,@pdex1pde,@pdex1ic,@pdex1bc,x,t);
u = sol(:,:,1);
% EXPERIMENTAL DATA
% Experimental time
Exp time = [0; 7.5*60; 15*60; 30*60; 45*60; 60*60]; % [s]
% Varying layer thickness
TEPA 050mm = [0; 280.08; 388.57; 498.97; 823.40; 1142.64]/1000; %
mol CO2/ L TEPA
PEI 050mm = [0; 789.56; 693.98; 935.18; 946.15; 1020.04]/1000;
% PLOTS
% Surface plot
figure1=figure;
s=surf(x,t,u);
s.EdgeColor = 'none';
xlabel('Distance x [m]');
ylabel('Time t [s]');
zlabel('Dissolved CO2 concentration [mol/L]');
figure2=figure;
avgU = sum(u, 2)/numx*2;
plot(t,avgU,'r');
xlabel('Time [s]');
ylabel('Dissolved CO2 concentration [mol/L]');
hold on
plot(Exp_time, TEPA_050mm, 'bo')
legend('Calculated data', 'Experimental data');
hold off
function [c,f,s] = pdex1pde(x,t,u,DuDx)
c = 1;
```

```
% D = 1e-10 (PEI), D = 3e-12 (TEPA)
D = 3e-12; % diffusion coefficient [m2/s]
f = D*DuDx;
s = 0;
% -----
function u0 = pdex1ic(x)
u0 = 0;
end
% -----
function [pl,ql,pr,qr] = pdex1bc(xl,ul,xr,ur,t)
c eq TEPA=2.6;
c_eq_PEI=1.8;
pl=ul-c_eq_TEPA;
ql=0;
pr = ur;
qr = 0;
end
```

Bibliography

- 1. U.S. National Climate Assessment. *Climate Change Impacts in the United States*. Washington: U.S. Government Printing Office, 2014. 9780160924026.
- 2. EPA. EPA: United States Environmental Protection Agency. *Greenhouse Gas Emissions*. [Online] 31 October 2018. [Cited: 15 October 2018.] https://www.epa.gov/ghgemissions/overview-greenhouse-gases.
- 3. Working Group III. *Climate Change 2014. Mitigation of Climate Change.* Cambridge: Cambridge University Press, 2014. 978-1-107-05821-7.
- 4. J.G.J. Olivier, K.M. Schure, J.A.H.W. Peters. *Trends in global CO2 and total greenhouse gas emissions*. The Hague: PBL Publishers, 2017.
- 5. National Academy of Science. *Advancing the Science of Climate Change*. Washington: The National academies press, 2010. 0-309-14589-9.
- 6. Food and Agriculture Organization of the United Nations. *FAOSTAT*. [Online] http://www.fao.org/faostat/en/?#data/EM.
- 7. Regenerable polyamine based solid adsorbents for CO2 capture from the air. Goeppert, Alain. Columbia: Loker Hydrocarbon Research Institute, 2014.
- 8. McMurry, John. *Fundamentals of Organic Chemistry:5th Edition.* s.l. : Brooks/Cole, 2002. 0534395732.
- 9. Use of monoethanolamine (MEA) for CO2 capture in a global scenario: Consequences and alternatives. Luis, Patricia. Louvain: Elsevier, 2016, Vol. Desalination 380.
- 10. Review: Room Temperature Ionic Liquids and System Designs for CO2 capture. Kathryn A. Mumford, Nouman R. Mirza, Geoffrey W. Stevens. Melbourne: Energy Procedia, 2017, Vol. 114.
- 11. Nielsen, Arthur Kohl and Richard. *Gas purification*. Houston: Gulf Publishing Company, 1960. 0-88415-220-0.
- 12. Siloxane removal from landfill and digester gas A technology overview. M. Ajhar, M. Travesset, S. Yüce, T. Melin. 2913–2923, s.l.: Elsevier, 2010, Vol. Bioresource Technology 101.
- 13. Ruthven, Douglas M. *Principles of adsorption and adsorption processes.* Fredericton: Wiley- Interscience, 1984. 0-471-86606-7.
- 14. P. Bernardo, J.C. Jansen. Polymeric membranes for the purification of hydrogen. [book auth.] Angelo Basile, T. Nejat Veziroğlu Velu Subramani. *Compendium of Hydrogen Energy.* s.l.: Woodhead Publishing, 2015.
- 15. Zhao, Guozhao Ji and Ming. Membrane Separation Technology in Carbon Capture. [book auth.] Yongseung Yun. *Recent Advances in Carbon Capture and Storage*. Beijing: IntechOpen, 2017.
- 16. Air as the renewable carbon source of the future: an overview of CO2 capture from the atmosphere. Alain Goeppert, Miklos Czaun, G. K. Surya Prakash, George A. Olah. 7833, s.l.: Energy Environ. Sci., 2012, Vol. 5.
- 17. Flart, Stijn de. Capturing Carbon Dioxide directly from the air. Delft: s.n., 2016.
- 18. Carbon A List. *Insight into innovations to close the carbon cycle*. [Online] 29 June 2017. [Cited: 15 June 2018.] http://carbonalist.com/2017/06/what-is-direct-air-capture-pt-3/.
- 19. Carbon Engineering. *History and Trajectory*. [Online] 2019. [Cited: 21 October 2018.] http://carbonengineering.com/history-and-trajectory/.

- 20. Climeworks. *Climeworks launches DAC-3 plant in Italy.* [Online] 1 October 2018. [Cited: 21 October 2018.] http://www.climeworks.com/climeworks-launches-dac-3-plant-in-italy/.
- 21. Infinitree. [Online] [Cited: 21 October 2018.] http://www.infinitreellc.com/.
- 22. CNCE. [Online] [Cited: 21 October 2018.] https://cnce.engineering.asu.edu/.
- 23. Skytree. [Online] [Cited: 21 October 2018.] https://www.skytree.eu/.
- 24. Global Thermostat. *The GT Solution*. [Online] [Cited: 21 October 2018.] https://globalthermostat.com/the-gt-solution/.
- 25. Aresta, Michele. *Carbon dioxide as chemical feedstock.* Weinheim: Wiley-VCH, 2010. 978-3-527-32475-0.
- 26. Shah, Nafi. TexasVox. *Direct Air Capture of CO2: A Climate Solution with Limitations.* [Online] 26 July 2018. [Cited: 08 April 2019.]
- http://www.texasvox.org/direct-air-capture-co2-climate-solution-limitations/.
- 27. David W. Keith, Geoffrey Holmes, David St. Angelo, Kenton Heidel. *A process for capturing CO2 from the atmosphere.* s.l.: Elsevier, 2018.
- 28. Cost and performance of fossil fuel power plants with CO2 capture and storage. Edward S. Rubin, Chao Chen, Anand B. Rao. 4444–4454, Pittsburgh: Energy Policy, 2007, Vol. 35.
- 29. Kranendonk, Jan van. Solar fuel from air. Delft: s.n., 2017.
- 30. Neri, Guillermo Enrique Gutiérrez. *Modeling of a natural circulation flow reactor for methanol synthesis from renewable sources.* Delft: s.n., 2018.
- 31. Veneman, Rens. *Adsorptive systems for post-combustion CO2 capture.* Twente: Ipskamp Drukkers BV, 2015. 978-90-365-3926-5.
- 32. Ron Zevenhoven, Pia Kilpinen. *Control of pollutants in flue gases and fuel gases.* Helsinki: Helsinki University of Technology, 2001. 951-22-5527-8.
- 33. Engineering ToolBox. *Air Composition and Molecular Weight.* [Online] 2003. [Cited: 30 November 2018.] https://www.engineeringtoolbox.com/air-composition-d_212.html.
- 34. Economic and energetic analysis of capturing CO2 from ambient air. Kurt Zenz House, Antonio C. Baclig, Manya Ranjan, Ernst A. van Nierop Jennifer Wilcox and Howard J. Herzog. 51, Pittsburgh: PNAS, 2011, Vol. 108.
- 35. Climate strategy with CO2 capture from the air. David Keith, Minh Ha-Duong, Joshua Stolarof. 17-45, s.l.: Climatic Change, Springer Verlag, 2006, Vol. 74.
- 36. Goetheer, Earl. Private conversation. 2019.
- 37. Absorption and Reaction Kinetics of Amines and Ammonia Solutions with Carbon Dioxide in Flue Gas. Chia Hao Hsu, Hsin Chu & Chorng Ming Cho. 246-252, s.l.: Journal of the Air & Waste Management Association, 2012, Vol. 53. 2162-2906.
- 38. Adosrben materials for carbon dioxide capture from large anthropogenic point sources. Sunho Choi, Jeffrey H. Dresse, Christopher W. Jones. 796-854, Weinheim: ChemSusChem, 2009, Vol. 2. 10.1002/cssc.200900036.
- 39. CAPTURING CARBON DIOXIDE DIRECTLY FROM THE ATMOSPHERE. Lackner, Frank S. Zeman and Klaus S. 2, New York: World Resource Review, 2004, Vol. 16.
- 40. McMurry, John E. *Organic Chemistry (3rd edition)*. Belmont : s.n., 1992. 0-534-16218-5.
- 41. Monteiro, Juliana Garcia Moretz-Sohn. Contributions to kinetics and equilibrium of CO2 absorption into N,N,-diethylethanolamine (DEEA), N-Methyl-

- 1,3-propane-diamine (MAPA) and their blends. Trondheim: NTNU, 2014. 978-82-326-0331-2.
- 42. Oxtoby, David W. and Gillis, Pat. *Principles of Modern Chemistry (8 ed.).* Boston: Cengage Learning, 2015. 978-1305079113.
- 43. Venemans, Rens. Informative e-mail.
- 44. Goeppert, Alain. Inormative e-mail.
- 45. *J. Am.* J. C. Hicks, J. H. Drese, D. J. Fauth, M. L. Gray, G. G. Qi, C. W. Jones. 130, s.l.: Chem. Soc., 2008. 2902.
- 46. Sotiris Giannoulidis, Sjors Wagenaar. *Experimental testing and design of a direct air capture unit for methanol production.* Delft : s.n., 2017.
- 47. Laake, Daniel van. Characterization of a sorbent for a small scale direct air capture system. Delft: s.n., 2018.
- 48. Berg, R. W. van den. *Designing a direct air capture unit for methanol synthesis*. Delft : s.n., 2018.
- 49. Sinha, Mrigank. Experimental study of absorption and desorption in a continuous direct air capture system to build a concept model. Delft: s.n., 2019.
- 50. ESPEC CORP. Temperature (& Humidity) Chambers Platinous® K Series Chambers. Osaka: s.n., 2005.
- 51. Silicon Labs. I2C HUmidity and Temperature sensor.
- 52. HobbyElectronica. *Electronica, Arduino, Componenten, Modules en Sensors.* [Online] [Cited: 10 03 2019.]
- https://www.hobbyelectronica.nl/product/dht22/?gclid=CjwKCAjwvuzkBRAhEiw A9E3FUo5OefUXP08gagB_yA7fZPr-
- _n4lNTj3svhpZpDl2GNZKabzbY_grxoCq80QAvD_BwE.
- 53. Telaire. Telaire 6703 Series CO2 Module. 2019.
- 54. Sinha, Mrigank. THESIS. ASK FOR TITLE. Delft: s.n., 2019.
- 55. Aqueous amine solution characterization for post-combustion CO2 capture process. Nabil El Hadri, Dang Viet Quang, Earl L.V. Goetheer, Mohammad R.M. Abu Zahra. s.l.: Applied Energy, 2017, Vol. 185.
- 56. Absorption of CO2by Amine Blends Solution: An Experimental Evaluation. Adewale Adeosun, Nabil El Hadri, Earl Goetheer, Mohammad R.M. Abu-Zahra. 9, s.l.: Research Inventy, 2013, Vol. 3. 2278-4721.
- 57. The reaction of CO2 with ethanolamines. Danckwerts, P.V. 443-446, Cambridge: Chemical Engineering Science, 1979, Vol. 34.
- 58. Kinetics of carbon dioxide reaction with diethylaminoethanol in aqueous solutions. C.J. Kim, D.W. Savage. 6, Annandale: Chemical Engineering Science, 1987, Vol. 42.
- 59. ON THE KINETICS BETWEEN CO2 AND ALKANOLAMINES BOTH IN AQUEOUS AND NON-AQUEOUS SOLUTIONS. AN OVERVIEW. G. F.
- VERSTEEG, L. A. J. VAN DUCK and W. P. M. VAN SWAAU. 113-158, Enschede: Chem. Eng. Comm, 1996, Vol. 144.
- 60. Ova, Bart. THESIS TITLE. Delft: s.n., 2019.
- 61. ToolBox, Engineering. Engineering ToolBox. *Water- Saturation pressure.* [Online] 2014. [Cited: 1 March 2019.]
- https://www.engineeringtoolbox.com/water-vapor-saturation-pressured 599.html.
- 62. Monteiro, Juliana Garcia Moretz-Sohn. *TNO. Confidential report.* Delft : s.n., 2018.
- 63. Cussler, E. L. Diffusion. Mass transfer in fluid systems. Cambridge: Cambridge University Press, 2009. 978-0-511-47892-5.

- 64. Mechanism and Kinetics of CO2 Adsorption on Surface Bonded Amines. Maximilian W. Hahn, Matthias Steib, Andreas Jentys and Johannes A. Lercher. 4126–4135, Munich: J. Phys. Chem. C, 2015, Vol. 119. DOI: 10.1021/jp512001t.
- 65. Clark, Jim. Chemistry. LibreTexts. *The fingerprint region.* [Online] 31 December 2013. [Cited: 3 May 2019.]
- https://chem.libretexts.org/Bookshelves/Physical_and_Theoretical_Chemistry_Textbook_Maps/Supplemental_Modules_(Physical_and_Theoretical_Chemistry)/Spectroscopy/Vibrational_Spectroscopy/Infrared_Spectroscopy/The_Fingerprint_Region.
- 66. Organic Chemistry at CU Boulder. [Online] University of Colorado. [Cited:
- 2019 April 15.] https://orgchemboulder.com/Spectroscopy/irtutor/aminesir.shtml.
- 67. University of Puget Sound. [Online] [Cited: 15 April 2019.]
- http://www2.ups.edu/faculty/hanson/Spectroscopy/IR/IRfrequencies.html.
- 68. In situ Fourier Transform-Infrared (FT-IR) analysis of carbon dioxide absorption and desorption in amine solutions. P. Jackson, K. Robinson, G. Puxty and M. Attalla. 985–994, s.l.: Energy Procedia, 2009, Vol. 1.
- 69. Stocker, Thomas. *Introduction to Climate Modelling*. Bern: Springer, 2011. 978-3-642-00772-9.
- 70. Levenspiel, Octave. *Chemical Reaction Engineering*. Oregon: John Wiley & Sons, 1999. 0-471-25424-X.
- 71. Ahmad Fauzi Ismail, Kailash Chandra Khulbe, Takeshi Matsuura. *Gas Separation Membranes: Polymeric and Inorganic.* s.l.: Springer, 2015. 3319010956.
- 72. Solubility and Diffusivity of CO2 in Natural Methyl Cellulose and Sodium Carboxymethyl Cellulose. Tina Perko, Elena Markocic, Zeljko Knez, and Mojca Skerget. 56, Maribor: J. Chem. Eng. Data, 2011. 4040-4044.
- 73. Solid amine sorbents for CO2 capture by chemical adsorption: A review. Elif Erdal Ünveren, Bahar Ozmen Monkul, Serife Sarıoglan, Nesrin Karademir, Erdogan Alper. 37- 50, s.l.: Petroleum, 2017, Vol. 3.
- 74. Determination of kinetics in gas-liquid reaction systems. An overivew. Kierzkowska-Pawlak, Hanna. 2, Lodz: ECOL CHEM ENG S., 2012, Vol. 19.
- 75. R. Byron Bird, Warren E. Stewart, Edwin N. Lightfoot. *Transport Phenomena*. s.l.: John Wiley & Sons, 2007. 978-0-470-11539-8.
- 76. Modelling of the reactive absorption of CO2 using mono-ethanolamine. Chinmay Kale, Andrzej Gorak, Hartmut Schoenmakers. 294-308, Dortmund: International Journal of Greenhouse Gas Control, 2013, Vol. 17.
- 77. Effect of Temperature on Diffusivity of Monoethanolamine (MEA) on Absorption Process for CO2 Capture. E. E. Masiren, N. Harun, W. H. W. Ibrahim and F. Adam. 1, Kuantan: INTERNATIONAL JOURNAL OF ENGINEERING TECHNOLOGY AND SCIENCES, 2016, Vol. 5.
- 78. Burke, John. Conservation online. *Solubility Parameters: Theory and Application.* [Online] Foundation of the American Institute for Conservation of Historic and Artistic Works, 23 November 2008. [Cited: 1 May 2019.] http://www.cool.conservation-us.org/byauth/burke/solpar/solpar2.html.
- 79. The Engineering ToolBox. *Water Heat of Vaporization*. [Online] 2010. [Cited: 1 May 2019.] https://www.engineeringtoolbox.com/water-properties-d_1573.html.
- 80. Huntsman. Technical bulleting: TEPA. The Woodlands: s.n., 2008.

- 81. Pijush Kundu, Ira Cohen, David Dowling. *Fluid Mechanics*. 2015. 9780124059351.
- 82. Polysciences, Inc. *Polyethylenimine, Branched, Mw 600 (bPEI 600).* [Online] Polysciences, Inc. [Cited: 1 May 2019.]
- http://www.polysciences.com/default/catalog-products/polyethylenimine-branched-bpei-600/.
- 83. Sigma- Aldrich. *Tetraethylenepentamine*. [Online] Sigma- Aldrich. [Cited: 1 May 2019.]
- https://www.sigmaaldrich.com/catalog/product/aldrich/t11509?lang=en®ion= NL.
- 84. Navarro, David. Private conversation. [E-mail] Barcelona: s.n., 2019.